

THE EFFECTS OF REALISTIC IRRIGATION ON THE GREAT PLAINS LOW-LEVEL JET

By

Samuel E Arcand

A THESIS

Submitted to  
Michigan State University  
in partial fulfillment of the requirements  
for the degree of

Geography – Master of Science

2017

## **ABSTRACT**

### **THE EFFECTS OF REALISTIC IRRIGATION ON THE GREAT PLAINS LOW-LEVEL JET**

By

Samuel E Arcand

Low-level jets (LLJs) are relatively fast-moving streams of air that form in the lower troposphere and are a common phenomenon across the Great Plains. LLJs play an important role in moisture transport and development of nocturnal convection in the spring and summer. Alterations to surface moisture and energy fluxes can influence the planetary boundary layer (PBL) development and thus LLJs. One important anthropogenic process that has been shown to affect the surface energy budget is irrigation. In this study, we investigate the effects of irrigation on LLJ development across the Great Plains by incorporating a dynamic and realistic irrigation scheme into the Weather Research and Forecasting (WRF) model. Two WRF simulations were conducted with and without the irrigation scheme over the exceptionally dry summer of 2012 over the Great Plains. The results show changes to LLJ features both over and downstream of the most heavily irrigated regions in the Great Plains. There were statistically significant increases to LLJ speeds in the irrigated simulations. Decreases to the mean jet core height on the order of 50 m during the overnight hours were also simulated. The overall frequency of jet occurrences increased over the irrigated regions by 5-10%, however, these differences are not statistically significant. These changes are weaker than what had been reported in earlier studies based on simple representations of irrigation that unrealistically saturate the soil columns over large areas over a long period of time, which highlights the importance and necessity to represent human activity more accurately in modeling studies.

This thesis is dedicated to all of my friends, family, and mentors who have offered their continued support throughout this journey.

Thank you.

## ACKNOWLEDGMENTS

I cannot thank my co-advisor's Dr. Lifeng Luo and Dr. Shiyuan Zhong enough for all of their help and support while finishing this stage of my education. They provided exceptional technical guidance, as well as enlightening personal advice. Both of which helped me get through this research. I would also like to thank the rest of my committee consisting of Dr. Julie Winkler, for her willingness and patience to help me through to the end. I would also like to acknowledge Xindi Bian for his aid in processing some of the data used in this study. I would also like to thank all of the friends I've made in East Lansing who've offered their advice and insightful conversation over the past few years.

I would like to acknowledge all of the financial support that made this work possible. This study was largely supported by the NOAA grant NA12OAR4310081, and the NASA grant NNX13AI44G. This study was also supported partially by the USDA National Institute of Food and Agriculture, Hatch project 1010691, and by the U.S. National Science Foundation (CRWater Sustainability and Climate 1039180).

Of course, I need to thank all of my family back home in Wisconsin, my mom, dad, and all of my brothers and sisters. I am extremely fortunate to have such a large group of caring people behind me. And, a very big thanks to my ultimate supporter, my wife, Jamie Arcand. Without her constant support and affirmation, I surely would not be where I am today.

## TABLE OF CONTENTS

<b>LIST OF FIGURES</b> .....	vii
<b>KEY TO ABBREVIATIONS</b> .....	xv
<b>CHAPTER I – INTRODUCTION</b> .....	1
<b>CHAPTER II - LITERATURE REVIEW</b> .....	5
<b>Low-Level Jets</b> .....	5
<i>Theory</i> .....	5
<i>Observational Studies</i> .....	7
<i>Modeling Studies</i> .....	9
<i>Climatology</i> .....	11
<b>Irrigation</b> .....	12
<b>Summary</b> .....	16
<b>CHAPTER III - THE EFFECTS OF REALISTIC IRRIGATION ON THE GREAT PLAINS LOW-LEVEL JET</b> .....	18
<b>Introduction</b> .....	18
<b>Methods</b> .....	20
<i>Model Setup</i> .....	20
<i>Irrigation Scheme</i> .....	20
<i>Experimental Setup</i> .....	21
<i>Data &amp; Analysis</i> .....	22
<b>Results</b> .....	23
<i>Simulations vs. NARR</i> .....	23
<i>GPLLJ Model Validation</i> .....	26
<i>Vertical Profiles</i> .....	26
<i>IRR &amp; NOIR Comparison</i> .....	27
<b>Discussion</b> .....	31
<b>Conclusion</b> .....	32
<b>CHAPTER IV - SUPPLEMENTARY RESULTS</b> .....	34
<b>NA LLJ Climatology</b> .....	35
<b>Irrigation vs. No Irrigation</b> .....	37
<i>Great Plains, California Central Valley &amp; Lower Mississippi Valley</i> .....	37
<i>Surface Moisture and Energy Budget</i> .....	40
<i>Great Plains Circulations</i> .....	56
<i>Great Plains Low-Level Jet Differences</i> .....	90
<b>APPENDIX</b> .....	112
<b>CHAPTER V - DISCUSSION AND CONCLUSION</b> .....	131

**BIBLIOGRAPHY.....134**

## LIST OF FIGURES

Figure 1. WRF model domain showing the total amount of added irrigation ( $\text{Kg/m}^2$ ) as black contours. The 3-month mean difference (IRR-NOIR) in surface temperature (color shading) between the simulations (Celsius). Station locations used for verification (white dots).....22

Figure 2. JJA 2012 LLJ features between the IRR simulation and the NARR.....25

Figure 3. U, v and wind speed (12 UTC) profiles for the three verification sites and times. Dodge City, KS (DDC) on 19 June 2012, Topeka, KS (TOP) on 4 July 2012, and Norman, OK (OUN) on 25 July 2012.....27

Figure 4. JJA mean and difference of GPLLJ core speed (m/s), height (m), and frequency (%) for the IRR and NOIR simulations. Shaded areas for the speed and height represent grid cells where the difference is statistically significant.....28

Figure 5. JJA mean 12 UTC temperature (Celsius) difference and vector wind (m/s) difference (IRR -NOIR). Increases in geopotential height (solid black lines) and decreases in geopotential height (dashed black lines) are plotted for each layer (m).....30

Figure 6. Comparison of LLJ speed, height, and frequency between the NARR, IRR and NOIR simulations for the Contiguous United States.....36

Figure 7. Accumulated irrigation throughout the entire irrigated simulation (JJA) for the Great Plains. Black contours show irrigation in  $\text{kg/m}^2$ . Color shading shows the JJA mean surface temperature difference (Celsius).....37

Figure 8. As in Figure 7, but over California’s Central Valley.....39

Figure 9. As in Figure 7, but over the Lower Mississippi River Valley.....40

Figure 10. Mean diurnal distribution of June surface (0-10 cm) soil moisture ( $\text{m}^3/\text{m}^3$ ) differences (IRR-NOIR).....41

Figure 11. Mean diurnal distribution of July surface (0-10 cm) soil moisture ( $\text{m}^3/\text{m}^3$ ) differences (IRR-NOIR).....42

Figure 12. Mean diurnal distribution of August surface (0-10 cm) soil moisture ( $\text{m}^3/\text{m}^3$ ) differences (IRR-NOIR).....43

Figure 13. June, July, and August mean diurnal distribution of surface (0-10 cm) soil moisture ( $\text{m}^3/\text{m}^3$ ) differences (IRR-NOIR).....44

Figure 14. Mean differences (IRR-NOIR) of June diurnal surface sensible heat flux ( $\text{W/m}^2$ )....45

Figure 15. Mean differences (IRR-NOIR) of July diurnal surface sensible heat flux ( $W/m^2$ ).....	46
Figure 16. Mean differences (IRR-NOIR) of August diurnal surface sensible heat flux ( $W/m^2$ ).....	47
Figure 17. June, July, and August mean differences (IRR-NOIR) of diurnal surface sensible heat flux ( $W/m^2$ ).....	48
Figure 18. Mean June diurnal surface latent heat flux ( $W/m^2$ ) differences (IRR-NOIR).....	49
Figure 19. Mean July diurnal surface latent heat flux ( $W/m^2$ ) differences (IRR-NOIR).....	50
Figure 20. Mean August diurnal surface latent heat flux ( $W/m^2$ ) differences (IRR-NOIR).....	51
Figure 21. June, July, and August mean diurnal surface latent heat flux ( $W/m^2$ ) differences (IRR-NOIR).....	52
Figure 22. Mean diurnal June surface skin temperature (Celsius) differences (IRR-NOIR).....	53
Figure 23. Mean diurnal July surface skin temperature (Celsius) differences (IRR-NOIR).....	54
Figure 24. Mean diurnal August surface skin temperature (Celsius) differences (IRR-NOIR).....	55
Figure 25. June, July, and August mean diurnal surface skin temperature (Celsius) differences (IRR-NOIR).....	56
Figure 26. Mean diurnal planetary boundary layer height (PBLH) differences (IRR-NOIR) for June (meters).....	57
Figure 27. Mean diurnal planetary boundary layer height (PBLH) differences (IRR-NOIR) for July (meters).....	58
Figure 28. Mean diurnal planetary boundary layer height (PBLH) differences (IRR-NOIR) for August (meters).....	59
Figure 29. Mean diurnal planetary boundary layer height (PBLH) differences (IRR-NOIR) for June, July, and August (meters).....	60
Figure 30. June, July, and August mean geopotential height difference in meters (IRR-NOIR) at 925 hPa.....	61
Figure 31. June, July, and August mean geopotential height difference in meters (IRR-NOIR) at 850 hPa.....	62
Figure 32. June, July, and August mean geopotential height difference in meters (IRR-NOIR) at 700 hPa.....	63

Figure 33. June, July, and August mean geopotential height difference in meters (IRR-NOIR) at 500 hPa.....	64
Figure 34. June, July, and August total precipitation difference in mm (IRR-NOIR).....	65
Figure 35. June mean vertical wind speed (m/s) cross-section differences (IRR-NOIR) Cross-section centered on latitude 37.5°N spanning longitudes 105°W-94°W.....	66
Figure 36. July mean vertical wind speed (m/s) cross-section differences (IRR-NOIR). Cross-section centered on latitude 37.5°N spanning longitudes 105°W-94°W.....	67
Figure 37. August mean vertical wind speed (m/s) cross-section differences (IRR-NOIR). Cross-section centered on latitude 37.5°N spanning longitudes 105°W-94°W.....	68
Figure 38. June, July, and August mean vertical wind speed (m/s) cross-section differences (IRR-NOIR). Cross-section centered on latitude 37.5°N spanning longitudes 105°W-94°W.....	69
Figure 39. June mean u-wind component (m/s) vertical cross-section difference (IRR-NOIR). Cross-section centered on latitude 37.5°N spanning longitudes 105°W-94°W.....	70
Figure 40. July mean u-wind component (m/s) vertical cross-section difference (IRR-NOIR). Cross-section centered on latitude 37.5°N spanning longitudes 105°W-94°W.....	71
Figure 41. August mean u-wind component (m/s) vertical cross-section difference (IRR-NOIR). Cross-section centered on latitude 37.5°N spanning longitudes 105°W-94°W.....	72
Figure 42. June, July, and August mean u-wind component (m/s) vertical cross-section difference (IRR-NOIR). Cross-section centered on latitude 37.5°N spanning longitudes 105°W-94°W.....	73
Figure 43. June mean v-wind component (m/s) vertical cross-section difference (IRR-NOIR). Cross-section centered on latitude 37.5°N spanning longitudes 105°W-94°W.....	74
Figure 44. July mean v-wind component (m/s) vertical cross-section difference (IRR-NOIR). Cross-section centered on latitude 37.5°N spanning longitudes 105°W-94°W.....	75
Figure 45. August mean v-wind component (m/s) vertical cross-section difference (IRR-NOIR). Cross-section centered on latitude 37.5°N spanning longitudes 105°W-94°W.....	76
Figure 46. June, July, and August mean v-wind component (m/s) vertical cross-section difference (IRR-NOIR). Cross-section centered on latitude 37.5°N spanning longitudes 105°W-94°W.....	77
Figure 47. June mean w-wind component (m/s) vertical cross-section difference (IRR-NOIR). Cross-section centered on latitude 37.5°N spanning longitudes 105°W-94°W.....	78

Figure 48. July mean w-wind component (m/s) vertical cross-section difference (IRR-NOIR). Cross-section centered on latitude 37.5°N spanning longitudes 105°W-94°W.....	79
Figure 49. August mean w-wind component (m/s) vertical cross-section difference (IRR-NOIR). Cross-section centered on latitude 37.5°N spanning longitudes 105°W-94°W.....	80
Figure 50. June, July, and August mean w-wind component (m/s) vertical cross-section difference (IRR-NOIR). Cross-section centered on latitude 37.5°N spanning longitudes 105°W-94°W.....	81
Figure 51. June mean water vapor mixing ratio (kg/kg) vertical cross-section difference (IRR-NOIR). Cross-section centered on latitude 37.5°N spanning longitudes 105°W-94°W.....	82
Figure 52. July mean water vapor mixing ratio (kg/kg) vertical cross-section difference (IRR-NOIR). Cross-section centered on latitude 37.5°N spanning longitudes 105°W-94°W.....	83
Figure 53. August mean water vapor mixing ratio (kg/kg) vertical cross-section difference (IRR-NOIR). Cross-section centered on latitude 37.5°N spanning longitudes 105°W-94°W.....	84
Figure 54. June, July, and August mean water vapor mixing ratio (kg/kg) vertical cross-section difference (IRR-NOIR). Cross-section centered on latitude 37.5°N spanning longitudes 105°W-94°W.....	85
Figure 55. Mean vertical diurnal profiles of the u-wind component (m/s) difference (IRR-NOIR) over the Great Plains. Averaged for a box bounded between 105°W–94°W and 30°N–45°N.....	87
Figure 56. Mean vertical diurnal profiles of the v-wind component (m/s) difference (IRR-NOIR) over the Great Plains. Averaged for a box bounded between 105°W–94°W and 30°N–45°N.....	88
Figure 57. Mean vertical diurnal profiles of the w-wind component (m/s) difference (IRR-NOIR) over the Great Plains. Averaged for a box bounded between 105°W–94°W and 30°N–45°N.....	89
Figure 58. Mean vertical diurnal profiles of the overall wind speed (m/s) difference (IRR-NOIR) over the Great Plains. Averaged for a box bounded between 105°W–94°W and 30°N–45°N.....	90
Figure 59. JUNE 00 UTC Jet Heights and differences (IRR-NOIR). The gray shading depicts statistical significance at the 95% confidence interval.....	92
Figure 60. JUNE 06 UTC Jet Heights and differences (IRR-NOIR). The gray shading depicts statistical significance at the 95% confidence interval.....	92
Figure 61. JUNE 12 UTC Jet Heights and differences (IRR-NOIR). The gray shading depicts statistical significance at the 95% confidence interval.....	93
Figure 62. June 18 UTC Jet Heights and differences (IRR-NOIR). The gray shading depicts statistical significance at the 95% confidence interval.....	93

Figure 63. June LLJ All Hours Height and differences (IRR-NOIR). The gray shading depicts statistical significance at the 95% confidence interval.....94

Figure 64. June 00 UTC Jet speed and differences (IRR-NOIR). The gray shading depicts statistical significance at the 95% confidence interval.....94

Figure 65. June 06 UTC Jet speed and differences (IRR-NOIR). The gray shading depicts statistical significance at the 95% confidence interval.....95

Figure 66. June 12 UTC Jet speed and differences (IRR-NOIR). The gray shading depicts statistical significance at the 95% confidence interval.....95

Figure 67. June 18 UTC LLJ speed and differences (IRR-NOIR). The gray shading depicts statistical significance at the 95% confidence interval.....96

Figure 68. June all hours LLJ speed and differences (IRR-NOIR). The gray shading depicts statistical significance at the 95% confidence interval.....96

Figure 69. July 00 UTC LLJ height and differences (IRR-NOIR). The gray shading depicts statistical significance at the 95% confidence interval.....97

Figure 70. July 06 UTC LLJ height and differences (IRR-NOIR). The gray shading depicts statistical significance at the 95% confidence interval.....97

Figure 71. July 12 UTC LLJ height and differences (IRR-NOIR). The gray shading depicts statistical significance at the 95% confidence interval.....98

Figure 72. July 18 UTC LLJ height and differences (IRR-NOIR). The gray shading depicts statistical significance at the 95% confidence interval.....98

Figure 73. July all hours LLJ height and differences (IRR-NOIR). The gray shading depicts statistical significance at the 95% confidence interval.....99

Figure 74. July 00 UTC LLJ speed and differences (IRR-NOIR). The gray shading depicts statistical significance at the 95% confidence interval.....99

Figure 75. July 06 UTC LLJ speed and differences (IRR-NOIR). The gray shading depicts statistical significance at the 95% confidence interval.....100

Figure 76. July 12 UTC LLJ speed and differences (IRR-NOIR). The gray shading depicts statistical significance at the 95% confidence interval.....100

Figure 77. July 18 UTC LLJ speeds and differences (IRR-NOIR). The gray shading depicts statistical significance at the 95% confidence interval.....101

Figure 78. July all hours LLJ speed and differences (IRR-NOIR). The gray shading depicts statistical significance at the 95% confidence interval.....101

Figure 79. August 00 UTC LLJ height and differences (IRR-NOIR). The gray shading depicts statistical significance at the 95% confidence interval.....102

Figure 80. August 06 UTC LLJ height and differences (IRR-NOIR). The gray shading depicts statistical significance at the 95% confidence interval.....102

Figure 81. August 12 UTC LLJ height and differences (IRR-NOIR). The gray shading depicts statistical significance at the 95% confidence interval.....103

Figure 82. August 18 UTC LLJ height and differences (IRR-NOIR). The gray shading depicts statistical significance at the 95% confidence interval.....103

Figure 83. August all hours LLJ height and differences (IRR-NOIR). The gray shading depicts statistical significance at the 95% confidence interval.....104

Figure 84. August 00 UTC LLJ speed and differences (IRR-NOIR). The gray shading depicts statistical significance at the 95% confidence interval.....104

Figure 85. August 06 UTC LLJ speed and differences (IRR-NOIR). The gray shading depicts statistical significance at the 95% confidence interval.....105

Figure 86. August 12 UTC LLJ speed and differences (IRR-NOIR). The gray shading depicts statistical significance at the 95% confidence interval.....105

Figure 87. August 18 UTC LLJ speed and differences (IRR-NOIR). The gray shading depicts statistical significance at the 95% confidence interval.....106

Figure 88. August all hours LLJ speed and differences (IRR-NOIR). The gray shading depicts statistical significance at the 95% confidence interval.....106

Figure 89. JJA 00 UTC LLJ height and differences (IRR-NOIR). The gray shading depicts statistical significance at the 95% confidence interval.....107

Figure 90. JJA 06 UTC LLJ height and differences (IRR-NOIR). The gray shading depicts statistical significance at the 95% confidence interval.....107

Figure 91. JJA 12 UTC LLJ height and differences (IRR-NOIR). The gray shading depicts statistical significance at the 95% confidence interval.....108

Figure 92. JJA 18 UTC LLJ height and differences (IRR-NOIR). The gray shading depicts statistical significance at the 95% confidence interval.....108

Figure 93. JJA 00 UTC LLJ speed and differences (IRR-NOIR). The gray shading depicts statistical significance at the 95% confidence interval.....	109
Figure 94. JJA 06 UTC LLJ speed and differences (IRR-NOIR). The gray shading depicts statistical significance at the 95% confidence interval.....	109
Figure 95. JJA 12 UTC LLJ speed and differences (IRR-NOIR). The gray shading depicts statistical significance at the 95% confidence interval.....	110
Figure 96. JJA 18 UTC LLJ speed and differences (IRR-NOIR). The gray shading depicts statistical significance at the 95% confidence interval.....	110
Figure 97. JJA all hours LLJ speed and differences (IRR-NOIR). The gray shading depicts statistical significance at the 95% confidence interval.....	111
Figure 98. June LLJ height for 00, 06, 12, and 18 UTC. Averages are for a box between approximately 100°W – 90°W and 30°N – 43°N.....	113
Figure 99. June LLJ speed for 00, 06, 12, and 18 UTC. Averages are for a box between approximately 100°W – 90°W and 30°N – 43°N.....	114
Figure 100. July LLJ height for 00, 06, 12, and 18 UTC. Averages are for a box between approximately 100°W – 90°W and 30°N – 43°N.....	115
Figure 101. July LLJ speed for 00, 06, 12, and 18 UTC. Averages are for a box between approximately 100°W – 90°W and 30°N – 43°N.....	116
Figure 102. August LLJ height for 00, 06, 12, and 18 UTC. Averages are for a box between approximately 100°W – 90°W and 30°N – 43°N.....	117
Figure 103. August LLJ speed for 00, 06, 12, and 18 UTC. Averages are for a box between approximately 100°W – 90°W and 30°N – 43°N.....	118
Figure 104. June, July, and August LLJ height for 00, 06, 12, and 18 UTC. Averages are for a box between approximately 100°W – 90°W and 30°N – 43°N.....	119
Figure 105. June, July, and August LLJ speed for 00, 06, 12, and 18 UTC. Averages are for a box between approximately 100°W – 90°W and 30°N – 43°N.....	120
Figure 106. (Blue line) June, July, and August timeseries of daily mean LLJ height averaged across 06 and 12 UTC for the IRR simulation, and averaged for a box between approximately 100°W – 90°W and 30°N – 43°N. (Red line) 8 day moving average of LLJ height.....	121
Figure 107. (Blue line) June, July, and August timeseries of daily mean LLJ height averaged across 06 and 12 UTC for the NOIR simulation, and averaged for a box between approximately 100°W – 90°W and 30°N – 43°N. (Red line) 8 day moving average of LLJ height.....	122

Figure 108. (Blue line) June, July, and August timeseries of daily mean LLJ speed averaged across 06 and 12 UTC for the IRR simulation, and averaged for a box between approximately 100°W – 90°W and 30°N – 43°N. (Red line) 8 day moving average of LLJ height.....123

Figure 109. (Blue line) June, July, and August timeseries of daily mean LLJ speed averaged across 06 and 12 UTC for the NOIR simulation, and averaged for a box between approximately 100°W – 90°W and 30°N – 43°N. (Red line) 8 day moving average of LLJ height.....124

Figure 110. Skew-T Log-P diagram at 00 UTC, 19 June 2012 for Dodge City, KS. Shown are the IRR (red solid line), NOIR (red dashed line), and observed (black dot-dash line) temperature and mixing ratio profiles. The wind profiles from left to right are for the IRR, NOIR and observations.....125

Figure 111. Skew-T Log-P diagram at 12 UTC, 19 June 2012 for Dodge City, KS. Shown are the IRR (red solid line), NOIR (red dashed line), and observed (black dot-dash line) temperature and mixing ratio profiles. The wind profiles from left to right are for the IRR, NOIR and observations.....126

Figure 112. Skew-T Log-P diagram at 00 UTC, 4 July 2012 for Topeka, KS. Shown are the IRR (red solid line), NOIR (red dashed line), and observed (black dot-dash line) temperature and mixing ratio profiles. The wind profiles from left to right are for the IRR, NOIR and observations.....127

Figure 113. Skew-T Log-P diagram at 12 UTC, 4 July 2012 for Topeka, KS. Shown are the IRR (red solid line), NOIR (red dashed line), and observed (black dot-dash line) temperature and mixing ratio profiles. The wind profiles from left to right are for the IRR, NOIR and observations.....128

Figure 114. Skew-T Log-P diagram at 00 UTC, 25 July 2012 for Norman, OK. Shown are the IRR (red solid line), NOIR (red dashed line), and observed (black dot-dash line) temperature and mixing ratio profiles. The wind profiles from left to right are for the IRR, NOIR and observations.....129

Figure 115. Skew-T Log-P diagram at 12 UTC, 25 July 2012 for Norman, OK. Shown are the IRR (red solid line), NOIR (red dashed line), and observed (black dot-dash line) temperature and mixing ratio profiles. The wind profiles from left to right are for the IRR, NOIR and observations.....130

## KEY TO ABBREVIATIONS

° - degrees

AGL - above ground level

CCV - California's Central Valley

CONUS - contiguous United States

EOF – empirical orthogonal function

GP - Great Plains

GPLLJ - Great Plains low-level jet

hPa - hectopascal(s)

IO - inertial oscillation

IRR - irrigation

JJA - June, July, and August

kg - kilogram(s)

LLJ - low-level jet

LMV - Lower Mississippi River Valley

m - meter(s)

mm - millimeter(s)

m/s - meters per second

NA - North America

NARR - North American Regional Reanalysis

NOIR - no irrigation

PBL - planetary boundary layer

PBLH - planetary boundary layer height

TKE – turbulent kinetic energy

US - United States

UTC - Coordinated Universal Time

W/m<sup>2</sup> - watts per square meter

WRF - Weather Research and Forecasting

## CHAPTER I - INTRODUCTION

Low-level jets (LLJs) are defined as relatively fast streams of air that occur in the lower troposphere. LLJs occur on every continent and can occur at any time of day, although, in the United States (US) they predominantly occur at night and are most frequent across the Great Plains (Bonner 1968; Whiteman et al. 1997). LLJs are linked to moisture transport and thunderstorm development across the central United States. For these reasons, perhaps the most extensively studied LLJ is the Great Plains low-level jet (GPLLJ).

LLJs contribute significantly to nocturnal storm initiation and maintenance. Means (1952) was one of the first to recognize the importance of the LLJ for thunderstorm forecasting. Since LLJs tend to peak in intensity overnight the associated convection does as well (Higgins et al. 1997). These nocturnal mesoscale convective systems are the main source of precipitation for crops throughout the central and Midwestern US. The water vapor which feeds these large complexes of storms originates in the Gulf of Mexico and the LLJ helps to transport it northward (Higgins et al. 1997). One particularly persistent and strong LLJ event aided in the production of widespread precipitation and flooding in the upper Mississippi River Basin during the warm season of 1993 (Arritt et al. 1996). Another unique feature described in this article was the contamination of their wind profiler data due to the presence of migrating birds. This is another important feature of LLJs and their importance to the migration of multiple species (Liechti 2006; La Sorte et al. 2014). In addition, as the search for renewable energy continues wind energy has become increasingly prevalent. Given the nature of the wind energy business, correctly forecasting LLJs is a very important factor (Storm et al 2009; Nunalee and Basu 2014)

The physical mechanisms responsible for LLJ development have been disputed since the first theory describing their formation came out. Blackadar (1957) offered what has become a widely accepted theory on LLJ development. His research points out an inertial oscillation is mainly responsible, which results during boundary stabilization after sunset. Holton (1967) offered a supplementary theory that thermal forcing due to uneven heating over sloped terrain contributes to the observed super-geostrophic flow. Since then, multiple studies have been done to try and determine which mechanisms and variables are the most important. Studies such as those done by Zhong et al. (1996) and Parish and Oolman (2010) agree that a primary mechanism is Blackadar's inertial oscillation, however, it must be in tandem with some other forcing to better match observations.

Given the vertical placement of LLJs their development is sensitive to processes within the planetary boundary layer (PBL). Klein et al. (2015) determined that the strongest LLJ events relative to the convective boundary layer wind speeds during the afternoon occurred on days with deep mixing followed by a strong inversion overnight. So, understanding the development of the boundary layer will be important to account for any changes to the structure and formation of LLJs. Surface and soil moisture values significantly impact the surface energy budget by altering the ratios of latent and sensible heat fluxes (Harding and Snyder 2012a; Basara and Crawford 2002). Because irrigation is a direct contributor to soil moisture it can potentially have a significant effect on the magnitude of surface and soil moisture, and therefore may influence the surface energy budget (Cook et al. 2014), thus ultimately affecting the development of LLJs. And, one primary driver of surface soil moisture change is anthropogenic irrigation used for agriculture throughout the Great Plains.

A new trend in recent research is the attempt to model anthropogenic effects on the atmosphere and boundary layer. Irrigation is possibly the most influential anthropogenic activities that directly affect the surface fluxes to the atmosphere and the water cycle especially throughout the Great Plains. There have been many studies on how irrigation affects regional climate (e.g., Harding and Snyder 2012a, b; Cook et al. 2014). However, there hasn't been many attempts to determine exactly how irrigation practices in the US have affected the GPLLJ. McCorcle (1988) was the first to examine soil moisture's effects on the GPLLJ, however, he was limited by computational resources at the time. Some of the issues he faced were the insufficient representation of land surfaces as well as an idealized application of irrigation. The idea was also picked up more recently by Huber et al. (2014) who used a higher resolution land surface model. However, irrigation was still applied in a highly idealized fashion which did not capture a realistic absolute amount of irrigated water.

This study aims to determine how irrigation will impact the GPLLJ. Specifically, the changes to maximum jet speed, jet height, and jet frequency will be compared between simulations with and without irrigation. A brief breakdown of the 2012 summer season via analysis of the North American Regional Reanalysis (NARR) dataset will be provided along with comparisons between the NARR and each Weather Research and Forecasting (WRF) simulation. Finally, the two WRF simulations will be compared against one another, highlighting changes to the LLJ variables listed above.

A dynamic and realistic irrigation scheme (Pei et al. 2016) added to the Noah land surface model inside WRF v3.6 provided the data used in this study. Past studies have used idealized irrigation schemes (McCorcle 1988; Huber 2014) where soil and subsurface layers are essentially either dry or completely saturated. The irrigation scheme for this study was developed

to dynamically add irrigation in such a way to as closely as possible mirror real-life. Specifically, the scheme was calibrated to best match the magnitude of irrigation practices across the Great Plains.

The goal of this study is to determine the effects that changes in soil moisture through irrigation have on the GPLLJ. This research utilizes a dynamic irrigation scheme to realistically represent irrigation practices throughout the Great Plains. LLJs especially the GPLLJ are important for many different processes. From moisture transport, to severe weather with implications stretching from air pollution and human health to the migration of birds and insects the LLJ is an important atmospheric phenomenon which has earned its place the literature.

## CHAPTER II - LITERATURE REVIEW

As mentioned in Chapter I, the focus of this study is to examine the impact realistic irrigation has on the GPLLJ. This means it will be important to establish foundations in both areas of research. An examination of the LLJ literature as well as irrigation and its impact on weather and climate is presented in this chapter.

### **Low-Level Jets**

#### *Theory*

The first reference of the phenomena was in a study by Wagner (1939) where he stated the fluctuations of surface temperature and pressure fields give rise to three large scale circulations which are responsible for the observed wind maximum and general wind patterns across the central United States. Later, Means (1952) was the one of the first to use the term low-level jet in a study on thunderstorm forecasting. Means (1952) noted that the importance of LLJs for the development and maintenance of thunderstorms was at that time being underrated. Since then, there has been and continues to be extensive work done on LLJs around the globe. It is widely accepted that the LLJ is important for many atmospheric and natural processes. However, theories surrounding the mechanisms that explain LLJ formation and location continue to be debated especially over the Great Plains LLJ.

There are two central questions which arise in the attempts to explain the GPLLJ. First and more generally, what accounts for the diurnal tendencies of the super-geostrophic winds observed within LLJs? Second, what accounts for the increased frequency of LLJs across the central United States. Obviously, the answers to these questions are by no means straight forward, else the literature on LLJs would not be nearly as extensive.

There are two generally recognized theories for the diurnal tendency and magnitude of LLJs across the Great Plains of North America. They are the inertial oscillation (IO) theory proposed by Blackadar (1957), and the differential surface heating over sloped terrain proposed by Holton (1967). However, it should be noted that the relative contribution of these theories is still debated. The general consensus is that neither theory alone can account for the observed diurnal trend and velocity, but that a combination of the two is a more accurate representation.

The IO theory states that as boundary-layer stabilization begins at sunset due to radiative surface cooling a force imbalance occurs as the free atmosphere becomes freed from the effects of daytime mixing with the formation of a surface inversion. Thus, allowing a relative wind maximum to form in the lower troposphere. Holton (1967) goes further building upon work done by Bleeker and Andre (1951) arguing that the lack of friction alone cannot account for the frequency and magnitude of LLJs observed over the Great Plains. Holton argues that a reversal in horizontal temperature gradients near the surface due to the sloped terrain across the central United States contributes a thermal wind enhancement to the low-level wind profile. Holton attributes much importance to the IO theory proposed by Blackadar (1957), in that it is crucial in explaining the diurnal phase. However, the IO theory alone cannot account for the observed tendency of formation over the Great Plains.

Buajitti and Blackadar (1957) looked at the diurnal wind structure within the boundary layer in Wichita, KS and Oklahoma City, OK in 1951. They used 29 days' worth of 6 hourly pilot-balloon observations, and compared them to algebraic and computer solutions of the equations of motion with varying degrees of eddy viscosity in both time and height. What they found is that rapidly decreasing values of average eddy viscosity and decreases in the amplitude of variation with height match the observations best.

A more recent study by Van de Wiel et al. (2010) extends the IO theory of Blackadar. Blackadar's initial work neglects the effects of friction within the boundary layer. The effects of friction within the nocturnal boundary layer are added to the IO model. Note that this friction is height dependent but not time dependent. This study describes the oscillation which occurs around the equilibrium wind vector at night instead of the geostrophic wind as advocated by Blackadar (1957). An interesting added finding from this paper was the detection of a backward oscillation. The backward oscillation seems to be like the oscillation which produces super-geostrophic winds above the inversion. Instead it works in the complete opposite fashion on the near surface winds. The authors suggest this may explain the slowing of surface winds within a stably stratified boundary layer at night.

#### *Observational Studies*

An observational study done by Frisch et al. (1991) examined a nocturnal jet event in North Dakota in June 1989. Data was collected remotely via a Doppler radar in clear air mode. The observations were taken while a strong pressure gradient was over the radar site but no frontal boundaries were observed. The observations show the intensification and veering of winds as the boundary layer stabilized and vertical mixing ceased, consistent with Blackadar's (1957) IO theory. The utility of this study is in the data collection method wherein the radar could take observations nearly continuously and provide a high temporal resolution of the development of the LLJ.

Parish et al. (1987) used airborne radar altimetry to analyze horizontal components of the geostrophic wind during a LLJ event. The data was collected on 23 July 1983 during a field project in north central Oklahoma by the University of Wyoming Beechcraft Super King Air aircraft. The focus of this study was on the kinematics of the LLJ as well as an analysis of the

surface heating and cooling over sloping terrain to lend support to the previous theory mentioned above. Their results indicated support of the previous mechanisms thought to be important for LLJ development. Contributions were made from both the IO theory and the differential heating over sloped terrain with the IO appearing the dominant mechanism.

Looking at the synoptic environment associated with LLJs Chen and Kpaeyeh (1993) examined 64 LLJ cases over 11 spring seasons (1979-89). The drive for this study was the lack of large scale circulation associations being made with LLJs with most research dedicated to the boundary layer processes. They determine that upper level divergence associated with a cyclogenesis in the lee of the Rockies and subsequent low level convergence act as a trigger for the formation of LLJs. This theme is a continuation of work done by Uccellini (Uccellini and Johnson 1979; Uccellini 1980) separating the LLJs between those forced by boundary layer processes i.e. IO and Holton's (1967) theories and those forced by larger synoptic scale circulations. Uccellini (1980) examined 15 previously studied LLJ cases with respect to the synoptic scale flow. His results support those found by Uccellini and Johnson (1979) and determined that 12 of the 15 LLJ cases were associated with an approaching upper-tropospheric jet streaks, and that unlike purely boundary layer forced LLJs the speed and coherence of jet continued into the afternoon. He also noted that although it appeared the synoptic flow regime was important, on average the fastest winds were still in the early morning, suggesting boundary layer process were still relevant. Thus, it is difficult to isolate the primary drivers of LLJs in some cases.

Zhong et al. (1996) conducted a case study of the GPLLJ using high spatial and temporal resolution data collected from the NOAA wind profiler network. The network consisted of 31 individual stations spread throughout the Great Plains in the south and central states. To add

robustness to the study the Regional Atmospheric Modeling System (RAMS) mesoscale model was used to supplement thermodynamic and other dynamical data which would be absent if only the profiler data was used. The results offered insight to the relative importance of the IO, as well as the significance of the base flow around the Bermuda High for development of strong LLJs. They also examined the role of soil moisture by forcing the soil to various levels of saturation. When compared with their control simulation they found that the low-level jet speeds trended weaker with some slight dependence on the horizontal distribution of the soil moisture.

### *Modeling Studies*

Many modeling studies have been done in order to quantify the importance of various mechanisms contributing to LLJ development and location. A study by Parish and Oolman (2010) utilized the Weather Research and Forecasting Nonhydrostatic Mesoscale Model run at 12 km horizontal resolution. They discredited the enhancement contributed by Holton's (1967) theory arguing such a thermal enhancement would be out of phase with the LLJs diurnal tendency. The authors instead offered an alternate explanation for the importance of the local topography. They argued the heating over the sloping terrain is important for the location of the observed jets. The location, as a result of the heating is due to enhanced background geostrophic flow around the Bermuda High which sets up a stronger base flow for the IO to act upon.

Fast and McCorcle (1990) ran a two-dimensional atmospheric model to simulate the GPLLJ. The model was coupled with a soil hydrology model to simulate changes in surface energy and moisture. The goal was to determine the sensitivity of the LLJ to changes in these surface fluxes in two-dimensions over three to exaggerate the impacts of surface variables, effects that would be masked within a three-dimensional model. In addition to changing surface forcing, their study also looked at the impact of including the slope of the Great Plains within the

model. What they found was that the addition of the sloped terrain added significantly to producing a realistic LLJ by contributing an enhanced buoyancy component. They also found decreases to jet speed when soil moisture was increased due to a relaxed temperature gradient from evaporational cooling.

To combine Blackadar's IO mechanism with Holton's mechanism Bonner and Paegle (1970) attempt to describe the observed diurnal variations using the model developed by Paegle (1970). Their observations came from 11 years of summertime rawinsonde data collected over Fort Worth Texas. The observation noted a regular diurnal variation of about  $3 \text{ ms}^{-1}$  at an average height of 600 m. To assess the contribution of the two mechanisms they modeled variations in eddy viscosity as well as geostrophic winds. Their results show a major contributor to the development of the GPLLJ is the oscillation of the thermal wind within the lowest 2 km arising over the sloped terrain, a similar conclusion as described by Holton (1967).

Combing the IO mechanism and Holton's mechanism for LLJ development Du and Rotunno (2014) constructed a simple analytical model to simulate LLJ formation and better understand the relative importance of each mechanism. The simulations attempted to answer three questions. The relative importance of Holton's mechanism? The relative importance of the IO mechanism? And, the contributions from their combination? Their results show that the Holton mechanism alone produces a weaker jet which peaks in speed slightly earlier than observations. Blackadar's IO mechanism shows a latitudinal jet max dependency, with timing sensitivity to the coefficient of daytime friction and sensitivity of magnitude on the coefficient of nighttime friction. In combination, the simulated LLJs show more consistent timing and magnitude when compared to the observations.

In a more recent study Shapiro et al. (2016) builds upon past studies to combine or unify the dominating mechanisms of LLJ development. Unlike past studies the authors here combine Blackadar's IO mechanism with Holton's mechanism via the addition of a thermal energy equation supplementing the equation of motion. The addition of the thermal energy equation allows the buoyancy terms to evolve with the governing equations. As with previous studies experiments were conducted which represented the individual mechanisms of Blackadar (1957) and Holton (1967) as well as their combination. This study does a good job of itemizing several different variables and how changes to each impact the LLJ. Some of their major findings include increased maximum jet speeds with increases in the background geostrophic flow and increases in maximum buoyancy. Decreased jet speeds were associated with increase to the Brunt- Väisälä frequency and warmer nighttime temperatures.

### *Climatology*

Acknowledging that a thorough classification and summarization of LLJ events would be useful Bonner (1968) conducted an intensive climatology over the United States to quantify the relative frequency, magnitude, and location of LLJs. He included an in-depth analysis specifically on the synoptic scale structure of the LLJ in the Great Plains region. Bonner used data collected from 47 rawinsonde observation sites throughout the United States over a period of two years. He concluded that most cases involved southerly flow with a nocturnal maximum agreeing to an extent with the inertial oscillation proposed by Blackadar.

A climatological study done by Whiteman et al. (1997) using 2 years of enhanced rawinsonde data from a site in north central Oklahoma found that the GPLLJ wind maximum typically occurs about 500 m above ground level, somewhat lower than previous studies. With wind speeds between 15 and 21  $\text{ms}^{-1}$ . The study also had set itself apart by breaking up LLJs

into categories based upon mean direction. The authors noted marked differences in climatologies between southerly-LLJs and northerly-LLJs. In the summer southerly-LLJs are most prominent with northerly-LLJs tending to form behind cold fronts. However, the authors noted that in the winter the relative frequencies are much closer together between the two classes of LLJ.

Noticing an apparent lack of research done on northerly-LLJs, Doubler et al. (2015) describes climatological differences between southerly and northerly LLJs. The North American Regional Reanalysis (NARR) was used to develop the LLJ climatology and it matches well with other case studies and climatologies. This article focused mainly on jet maximum speed, jet nose height, and jet frequency. Descriptions of LLJs from the Gulf of California and Mid-Atlantic Coast are included as well as four other minor regions of notable jet frequencies consisting of the Hudson Bay, the northeast coast of Hispaniola, the coast of British Columbia, and Tennessee and Kentucky. The authors note the need for further research to better understand these other LLJ regions.

## **Irrigation**

Irrigation through changes to soil moisture affects boundary layer energy and mass partitioning (Pielke 2001). Early studies on the weather impacted by irrigation ranges from increased precipitation (Schickedanz 1976) to increased tornadic activity (Beebe 1974). Barnston and Schickedanz (1984) examined the synoptic structure during periods of statistically increased irrigation-induced rainfall. The area of interest for their study was the region around the panhandle of Texas where they analyzed 40 years of rainfall data. They conducted an empirical orthogonal functions (EOF) analysis to identify those areas where precipitation was most likely to have been influenced by irrigation. Next, they analyzed the synoptic-scale flow patterns, what

they found is that irrigation was most likely to enhance precipitation when synoptic conditions were already conducive for rainfall, i.e., the presence of low-level convergence which allows the atmosphere to tap into the increased low-level moisture. Their results also showed a decrease in surface temperature of around 2 °C. The temperature change, when combined with increased dew point temperatures resulted in an average decrease in the Lifted Index by ~1 °C. Thus, leading to the potential for an increased chance of convection.

A climatological study done by Cook et al. (2014) examines the role irrigation has played as an historical climate forcing. According to Cook et al. (2014) irrigation is the single largest use of water anthropogenically and it has significant impacts to the surface energy budget thereby making it an important piece of the water cycle and the climate. This study runs two 5-member ensemble general circulation models (GCM) with irrigation added in addition to other anthropogenic and natural forcings. The model used for this study is the ModelE2-R run at  $2 \times 2.5$ -degree latitude and longitude resolution run from 1850 to 2000. The module used for irrigation is a reconstruction of 0.5-degree resolution twentieth century irrigation rates. The results indicate that irrigation causes cooling globally, however, the differences are only significant when restricted to the land. And, the large-scale differences and climate response are due mainly from the portioning of sensible heat into latent heat expressed by shifts in the Bowen ratio.

Adegoke et al. (2002) looked at the impact of irrigation on the surface energy budget for a region comprised mostly of the state of Nebraska. They conducted four simulations with the RAMS model. The four simulations were made up of three different schemes for representing the land surface. The lower boundary conditions for the RAMS model used here consisted of a 1997 satellite-derived estimate of irrigated land, wet and dry simulations using the Olson Global

Ecosystem (OGE) vegetation dataset, and the last used the Kuchler vegetation dataset. When irrigation was added (to the control and wet OGE) it was done so at 00 UTC each day by saturating the top 0.2 m of topsoil. When compared to the control the dry runs showed a 36% decrease in latent heat as well as a 2.6°C decrease in dew point temperatures. When compared to the natural vegetation of the Kuchler dataset the cooling and energy difference was even stronger. This study also included a brief statistical climate analysis looking at temperature trends between an historically irrigated region and one that isn't. They report the trends for York, NE (irrigated) and Halsey, NE (not irrigated). They found that trends in mean monthly temperatures decreased for York and increased for Halsey over the growing season.

Harding and Snyder (2012a & b) carried out an extensive study on the atmospheric response to irrigation in the Great Plains. Their motivation for the study had to do with the large increase in irrigated land post World War II and the subsequent depletion of the Ogallala Aquifer. The main goal of this study was to examine how changes in the surface energy budget due to irrigation impact precipitation. They used the WRF model to simulate the effects of irrigation by using a satellite derived irrigation dataset to determine which grid cells would be irrigated, then those grid cells were held at saturation. The simulations were run over nine April-October periods sub-divided equally into three year periods of dry, normal and wet conditions. On average their results showed ~0.91% increase in precipitation with some isolated areas increasing as much as 20%. Increases in precipitation were simulated for the normal and wet years, with decreases during the drought years. The authors suggested this may imply a soil moisture threshold exists which acts to suppress precipitation over relatively drier soil conditions.

At a Norman Mesonet site Basara and Crawford (2002) examined the relationship between soil moisture and atmospheric processes. Data was collected during an intensive observing period in 1999 from 1 June to 12 August. 13 days with clear skies and weak wind shear in the lower troposphere were identified and termed Ideal Days and constituted a wide range of soil and atmospheric conditions. These Ideal Days were used to better assess the four main components of the surface energy budget consisting of: latent heat, sensible heat, ground heat, and net radiation. The results showed a significant linear correlation relationships between maximum daily values of sensible heat and latent heat. Similar correlations were found between root-zone soil moisture and daily temperature and mixing ratio as well.

Although not technically an examination of irrigation, given the focus of the study and model domain McCorcle (1988) provided a first look at how simulated changes in soil moisture influences the GPLLJ. The main goal of this study was to determine how the LLJ is impacted by changes to the spatial distribution of soil moisture. A secondary focus is examining how the changes to the GPLLJ feedback to changes in Great Plains convection. Simulations were initialized with varying degrees of saturation and saturation location. Homogenous soil moisture simulations were conducted with increasingly saturated soils over all land areas. The results of these experiments showed a weakening of the LLJ through decreased buoyancy driven circulations, and a decrease in vertical velocities by up to 40%. Two heterogeneous simulations were run with soil saturated either in the plains or in higher elevation nearer to the Rockies. The results show a spatial dependence with respect to the impacts soil moisture has on the LLJ. When the soil moisture was added to lower elevations increased vertical motions were noted with the opposite being true when soil moisture was added to the higher elevations.

A pair of simulations (Irrigated and Control) were conducted with the Advanced Research WRF(ARW) in a study by Huber et al. (2014) to assess the impact of irrigation on the surface energy budget, atmospheric circulation, and precipitation. The study area was focused on irrigation in the Great Plains region and the simulations run from 1 May 2001 to 31 July 2001. The land cover scheme was set such that grid cells which contain any fraction of irrigated land are set to contain all irrigated land, and grid cells that are located over the Ogallala Aquifer and are classified as grassland/agriculture mosaic are also set to be irrigated. In the irrigated simulation irrigation was applied at 00 UTC each day (starting on 15 May) by completely saturating the top meter of soil. The authors note that the exaggerated amount of irrigation is made intentionally unrealistic to hopefully accentuate its effects. Their results showed nearly a 50% increase in July precipitation primarily downstream of the irrigated region. They also noted a weaker LLJ due to a local 850 hPa positive height anomaly resulting from surface cooling driven by the irrigation.

## **Summary**

The LLJ has been extensively studied around the world and perhaps in no greater detail than in the Great Plains of the United States. A foundation has been built beginning with Wagner (1939) and leading to the theories of Blackadar (1957) and Holton (1967). Even though numerous case studies have been done and multiple modeling studies executed there remains a debate as to why the GPLLJ has the maximum in frequency where it does. And, it remains in contention as to just how important each mechanism is to its development. Adding to the complexity is an almost equally as large body of work on the influence of anthropogenic forcing due to irrigation. We have come to well understand the effects of irrigation on the surface energy budget and the implications for local precipitation. However, further work is necessary to better

understand regional differences in the response to irrigation, and much uncertainty remains as to the future magnitude and distribution of irrigation especially under a changing climate. This will continue to demand work be done on the regional application.

What this shows is that the pursuit to understand the LLJ shows no signs of slowing, and of course it also shows more work needs to be done. With a greater understanding of the LLJ and by extension the GPLLJ improvements to real-time forecasting and long-term climate modeling can be made through either improved explicit representation or better parameterizations within statistical and dynamic numerical weather and climate models.

## CHAPTER III - THE EFFECTS OF REALISTIC IRRIGATION ON THE GREAT PLAINS LOW-LEVEL JET

### Introduction

The low-level jet (LLJ), a low-level wind maximum, is an atmospheric phenomenon that occurs in many places around the world especially over the Great Plains of the United States (Bonner 1968). Across the Great Plains LLJs significantly impact the regional economy and environment. LLJs provide the primary source of moisture for rain-fed agriculture through development and sustainment of nocturnal convection. Since the region's economy is largely based on agriculture, this rainfall can be pivotal for a good harvest. The forcing provided by LLJs to initiate and sustain convection can also be damaging. When convection comes in the form of severe weather; heavy rains, large hails and tornadoes all have the potential to ruin crops, and are a huge threat to public safety.

Processes such as heat and moisture exchange within the planetary boundary layer (PBL) play an important role in governing LLJ development (Shapiro 2016). Alterations to these fluxes have been shown to be significantly affected by the addition of agricultural irrigation (Harding and Snyder 2012a). Thus, irrigation could directly influence the LLJ. The Great Plains is dominated largely by agriculture, where intensive agricultural practices have given rise to the need for irrigation. Irrigation can lead to changes in soil moisture which have been shown to be important for various meso- to regional- scale circulations (Cook et al. 2014; Harding and Snyder, 2012a and b; Frye and Mote 2010; Basara and Crawford, 2002; Lanicci et al., 1987).

Up until now only a few attempts have been made to identify the effects irrigation has on the LLJ (McCorcle 1988; Huber et al. 2014). Nearly all of these studies have been done as a

sensitivity test using either unrealistic amounts and/or distributions of surface moisture. McCorcle (1988) makes a broad assumption and saturates the surface soil without considering land type. In his case study, he found that the addition of soil moisture resulted in decreased jet velocities. However, McCorcle also noted that the distribution is important and when comparing soil saturation in high (lower) elevations the resulting moisture boundary circulations may increase (decrease) jet speeds with the circulation being in (out of) phase with the nocturnal oscillation. Huber et al. (2014) although taking differing land use types into account, admittedly uses an unrealistic amount of water by saturating the entire top meter of soil daily through the simulation. Huber also found that through the effects of evaporative cooling, regional scale pressure patterns supported decreased LLJ speeds. These studies may not be the most useful when attempting to determine how the atmosphere will actually respond to the effects of irrigation. A study by Zhong and Doran (1997) disputes the usefulness of such sensitivity tests. They show that simplified assumptions on soil moisture amount or distribution often used in idealized numerical simulations tend to result in gross overestimations of the response of the lower atmosphere to underlying heterogeneous surface forcing.

The goal of this research is to take one step further towards answering the question about how changes in soil moisture might affect lower atmosphere circulations. Specifically, the study will examine the effects that a dynamic and realistic irrigation modeling scheme has on the Great Plains low-level jet (GPLLJ).

This study builds upon the past research by attempting to recreate irrigation practices in a much more realistic way. Irrigation in this study is only applied where current land use is characterized as irrigated land, and is only applied when soil conditions call for it based upon current irrigation practices.

## Methods

### *Model Setup*

The Weather Research and Forecasting model (v3.6) is used for this study. A dynamic irrigation scheme was incorporated into this version of WRF as part of the effort to understand the effects of irrigation on the atmosphere (Pei et al. 2016). The model simulations were configured on a single mesh with 30 km grid spacing, and driven by the North American Regional Reanalysis (NARR, Mesinger et al. 2006). The Kain-Fritsch (Kain and Fritsch 1993; Kain 2004) physical parameterization scheme was used for convective rainfall. The WSM6 6-class graupel (Hong and Lim 2006) and the YSU schemes (Hong et al. 2006) were used for microphysics and PBL processes respectively. Shortwave and longwave terrestrial radiation processes were handled with the Dudhia shortwave (Dudhia 1989) and the RRTM longwave radiation (Mlawer et al. 1997) schemes.

To get the subgrid-scale information necessary to aid in the realistic representation of land cover processes the Noah-Mosaic model was embedded within the WRF Noah land surface model. The use of eight dominant subgrid land-use types was determined to be sufficient within each 30 km WRF grid cell to better capture the land use heterogeneity. Within the USGSs' 24 land use categories the 'irrigated cropland and pasture' land use category accounts for all of the irrigated land within the Great Plains (GP).

### *Irrigation Scheme*

The irrigation scheme was calibrated for the GP region of the central United States (Figure 1). The GP region was chosen since it represents an area where the most irrigation is applied in any given year in the contiguous United States. Figure 1 shows the extent of the

simulated irrigation. Irrigation in this area is predominantly applied via sprinkler systems. It is simulated in the WRF model as added precipitation to mimic the sprinkler system. The irrigation trigger depends on the plant available water within the Noah-mosaics second soil layer (10-40 cm below ground), and once triggered water is applied for 2 hours at  $20 \text{ mm hr}^{-1}$  within only the designated fraction of each grid cell. A more detailed description of the irrigation scheme and its validation can be found in Pei et al. (2016).

### *Experimental Setup*

Two simulations were run one with the addition of the irrigation scheme (IRR), and one without (NOIR). The independent variable in this case is the addition of irrigation in the IRR simulation. The two simulations run from June through August (JJA), 2012 with a one-month spin up. The summer of 2012 was chosen for the study due to its relatively hot and dry conditions over the GP region. This will ensure a maximized response of the lower atmosphere to irrigation.

This study utilizes a modified version of Bonner's (1968) original criteria used by Doubler et al. (2015) for identifying LLJs. The criteria for the jet core consist of maximum wind speeds of at least 12 m/s. The jet-top is the height above the core where the wind speed decreases by 6 m/s from the jet core or the 5-km above ground level (AGL), whichever is lower. Similarly, the bottom of the jet is found the same way by locating the height of the next minimum speed below the jet core characterized by a 6 m/s wind speed decrease which must occur above the surface.

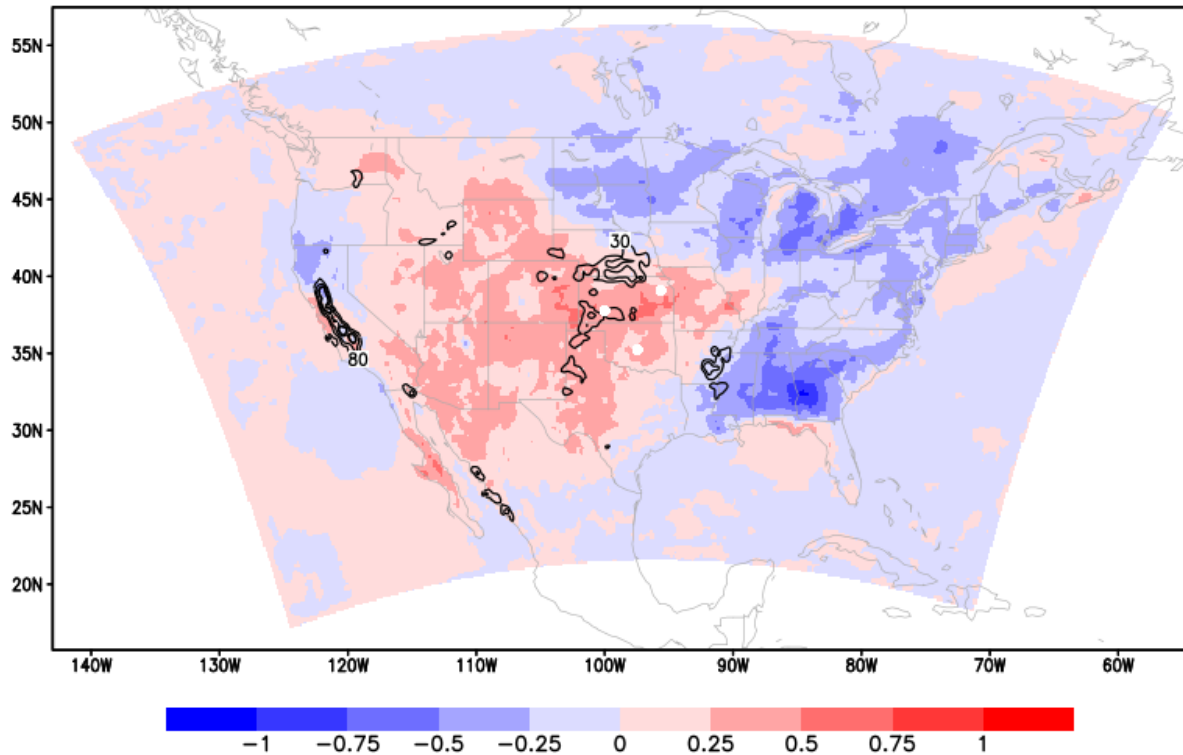


Figure 1. WRF model domain showing the total amount of added irrigation ( $\text{Kg/m}^2$ ) as black contours. The 3-month mean difference (IRR-NOIR) in surface temperature (color shading) between the simulations (celsius). Station locations used for verification (white dots).

### *Data & Analysis*

When modeling the LLJ, it is logical to begin with an overview of the LLJ climatology within the region of interest. Next, the analysis moves to a summary of the 2012 summer season and LLJ by means of the NARR which has been shown to adequately represent the atmospheric conditions as well as LLJ characteristics (Doubler et al. 2015), and has been shown to be an adequate dataset for climatological analysis (Walters et al., 2014). Next, the NARR data will be compared against both the IRR and NOIR simulations. It's worth noting here that although the non-irrigated simulation is considered the control between the set of simulations it would be expected that the addition of irrigation should be closer to reality and potentially better match the

NARR data. Although the NARR contains no explicit irrigation, it does contain observations which would contain the influence of irrigation. The evaluation begins at the surface examining relevant variables, and progresses upwards examining the vertical structure against multiple observed soundings throughout the region of highest jet frequency.

## **Results**

### *Simulations vs. NARR*

Before assessing the impact of irrigation, the two simulations were first evaluated using NARR data.

Reanalysis datasets such as the NARR offer the potential to examine LLJs on considerably finer spatial and temporal scales compared to observations. The resulting dataset although finer in scale isn't an exact representation of reality and care should be taken with their use. Walters et al. (2014) examined the pros and cons of using NARR data in place of rawinsonde observations for use in climatological studies. Reduced LLJ frequency derived from NARR was the most notable difference when compared to observations. Their results indicated that the NARR is a viable replacement doing a decent job of representing low-level wind maxima.

Doubler et al. (2015) examined the climatology of multiple LLJ regions grouped by their geographical location, relative direction, and seasonality throughout North America. Using the NARR dataset they found that southerly-LLJs dominate in frequency across the Great Plains during the summer months. Specifically, in June, July and August the highest frequencies move from south Texas to southern Nebraska respectively. The strongest LLJ speeds for the Great Plains annually are focused over Kansas and Missouri. For the JJA period June has on average

the fastest speeds across the Great Plains averaging about 18-20  $\text{ms}^{-1}$ . July and August show similar distributions, however, the magnitudes are decreased to about 14-16  $\text{ms}^{-1}$ .

Over the GP the jet speeds of the two WRF simulations compare reasonably well to the NARR. Both the IRR and NOIR simulations overestimate jet speeds with maximum wind speeds just over 20 m/s compared to the maximum speeds between 16 and 17 m/s in NARR. When comparing the distribution of speeds both simulations show a broad and large area of intense jet speeds stretching from the northern panhandle of Texas past the US-Canadian border. The NARR shows a similar pattern, however, its maximum speeds in the region are confined between northeast Nebraska and southern Minnesota.

The jet core heights (Figure 2), which are similar between the two WRF simulations, are on average about 300 m lower than the jet core height in NARR. Due to the similarities of the two WRF simulations relative to the NARR only the IRR simulation is presented here. The IRR and NOIR simulations are homogenous throughout the Great Plains with mean jet core height varying between 300 and 500 m AGL, unlike those of the NARR which are predominantly over 600m.

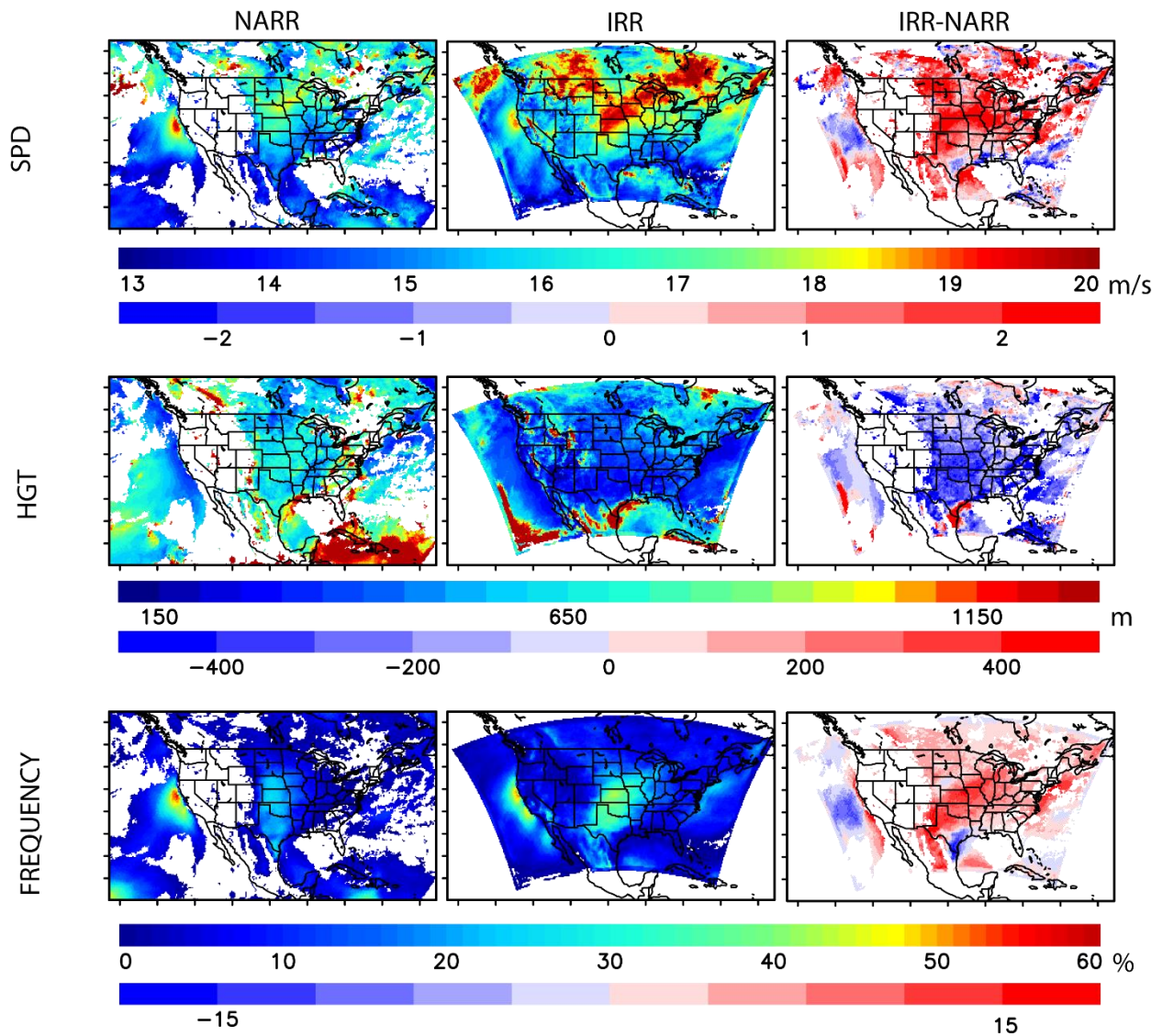


Figure 2. JJA 2012 LLJ features between the IRR simulation and the NARR.

The frequency of occurrence or counts (Figure 2) represented as a percentage shows that the simulations have a larger number of jet occurrences with the area of maximum coverage tilted slightly southwest to northeast from west-central Texas to Iowa. On average the percentage is 10 to 20% higher in the IRR and NOIR simulations than that of NARR.

Overall, the simulations agree relatively well with the NARR derived LLJs despite the simulated jets being somewhat faster, slightly lower, and slightly more frequent than the NARR.

### *GPLLJ Model Validation*

#### *Vertical Profiles*

The model's ability in capturing the observed vertical jets structure is examined at select locations (Topeka and Dodge City, KS, and Norman, OK). These sites were chosen for their location within the area of maximum LLJ occurrence as well as the need for locations with local radiosonde sites.

The LLJ events in question are on 19 June, 4 July, and 25 July 2012. The vertical profiles for each of the simulations are in close agreement with the observations across all times (Figure 3). The temperature profiles in the simulations are generally warmer than what was observed and neither simulation is as moist as the sounding in the lower levels. The simulations struggle to capture the strength of the inversions observed below 700 hPa. The vertical profiles of wind speed show that both simulations place the LLJ too low.

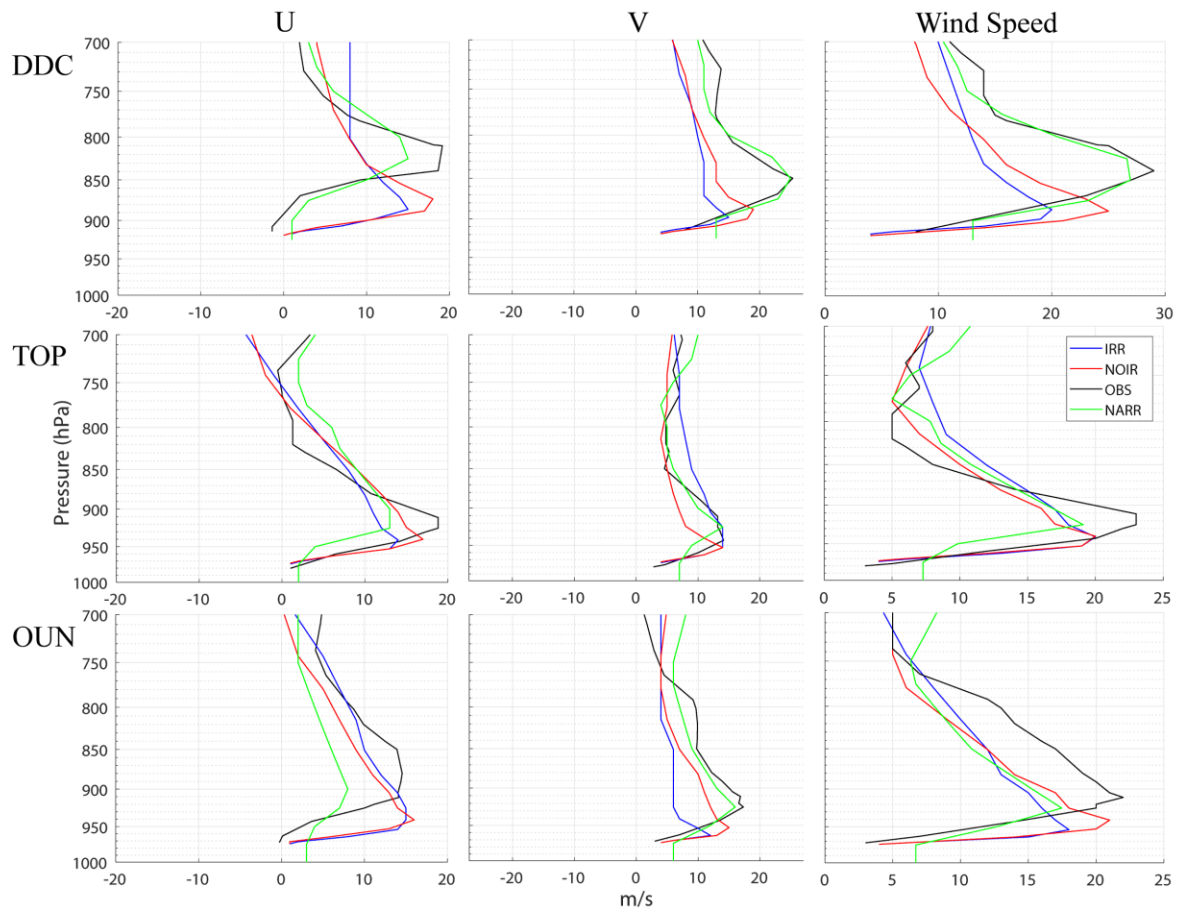


Figure 3. U, v and wind speed (12 UTC) profiles for the three verification sites and times. Dodge City, KS (DDC) on 19 June 2012, Topeka, KS (TOP) on 4 July 2012, and Norman, OK (OUN) on 25 July 2012.

### *IRR & NOIR Comparison*

All variables that characterize the LLJ, such as peak jet core speed, jet core height, and occurrence show at least some degree of difference between the IRR and NOIR simulations with certain variables being affected more than others.

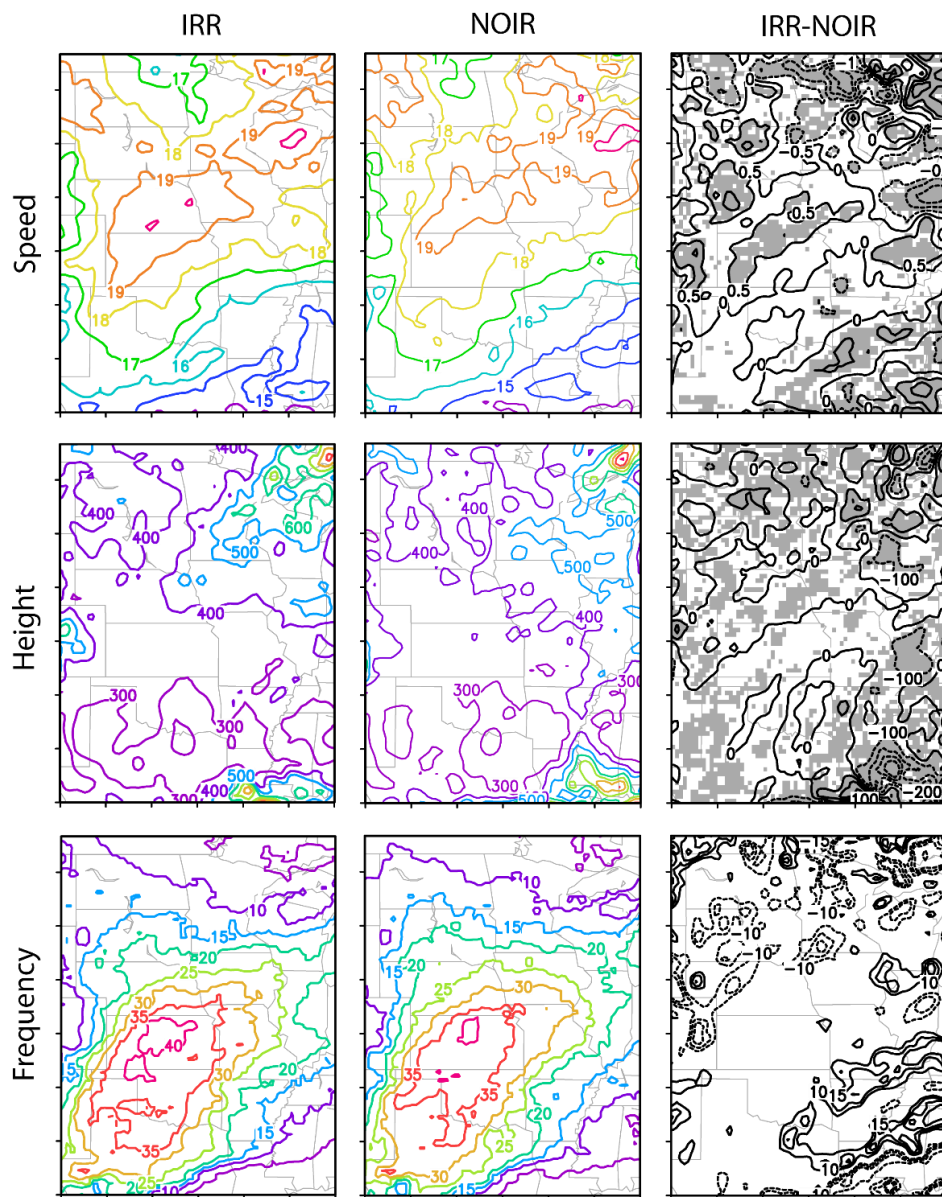


Figure 4. JJA mean and difference of GPLLJ core speed (m/s), height (m), and frequency (%) for the IRR and NOIR simulations. Shaded areas for the speed and height represent grid cells where the difference is statistically significant.

Figure 4 shows the differences in the JJA (seasonal) mean jet speed between the IRR and NOIR simulations (IRR-NOIR). There are small statistically significant increases in jet core speed of just under 1 m/s over portions of Kansas and Nebraska where the majority of irrigation is applied for these simulations (Figure 1). Areas to the south and east as well as areas to the north and east of the increase in speeds are areas of predominantly decreased GPLLJ core speeds with magnitudes similar to that of the increased speeds of just under 1 m/s. When visually comparing between the IRR and NOIR simulations it also appears that the area of more intense jet speeds has expanded so that not only are we seeing faster speeds at a particular grid cell but also an increase in the area of more intense jets.

The occurrences of LLJs (Figure 4) here is defined as the number of times in a particular grid cell that the criteria for LLJs are met. Over the months of June, July, and August the total number of time-steps is 368 based on 6-hourly model output. This means that LLJs are occurring about 40% of the time in the simulation in the peak areas with an increase of about 10% between the IRR and NOIR simulations around Kansas, Oklahoma, and north Texas. The occurrences exhibit similar patterns to the jet speed in that a general increase in occurrence is shown over most of Kansas, along with a general expansion of the area LLJs occur especially south east of the main axis along a line from Texas northeast into Missouri. However, this increase in occurrence corresponds with a decrease in the jet speed. The changes in the height of the jet core maximum wind speed show little variation and in most cases, vary by less than 10% or under 30 m.

There are two possible reasons for the changes to LLJ speed due to irrigation: changes to the pressure gradient force (PGF), and changes in the thermal structure of the boundary layer. Both mechanisms allude to the basic theories of LLJ development reaching back to Blackadar

(1957) and Holton (1967). Cook et al. (2008) examined the GPLLJ with future climate projections. It was concluded that an expansion of the Bermuda High increased the gradient geopotential heights enough to account for increases in GPLLJ speeds of about 1 m/s. Huber et al. (2014) concluded that the cooling due to irrigation led to corresponding height rises and an ageostrophic circulation resulting in weaker jet speeds. The average layer temperature and corresponding height rises over the central US in this study would not add up to an enhancement of the PGF (Figure 5). However, if each layer is examined individually the height falls over Nebraska may coincide with a local enhancement of the PGF leading to increased wind speeds.

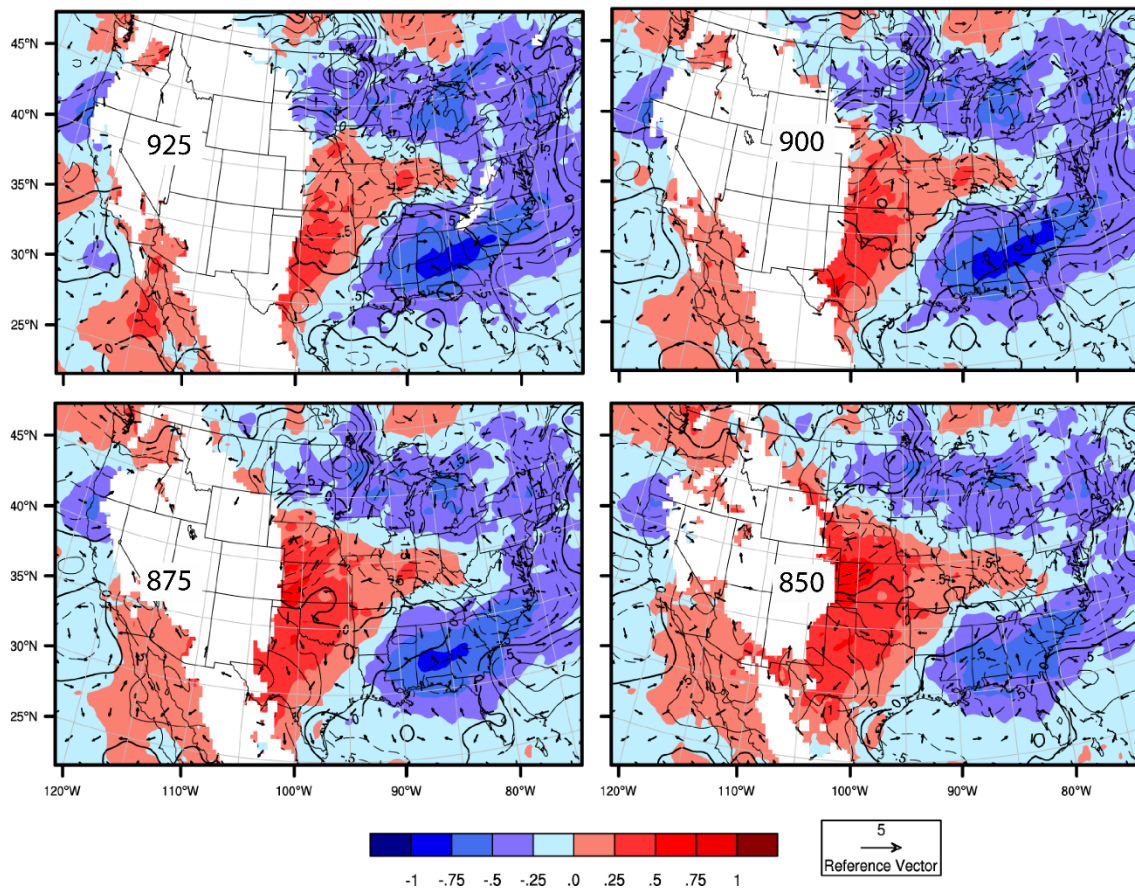


Figure 5. JJA mean 12 UTC temperature (Celsius) difference and vector wind (m/s) difference (IRR -NOIR). Increases in geopotential height (solid black lines) and decreases in geopotential height (dashed black lines) are plotted for each layer (m).

## Discussion

In agreement with other studies (Pei et al. 2016; Cook et al. 2008) the increase in low level moisture provided by a realistic amount of irrigation is enough to change synoptic-scale circulation patterns, specifically by decreasing precipitation over the irrigated regions while increasing precipitation downstream as more moisture is advected downstream (Pei et al. 2016). It is possible that the increase to the Bermuda High circulation and central US high pressure pattern may at least partially responsible for changes to the LLJs. Alterations to these synoptic patterns also resulted in suppressed precipitation throughout the central US which is believed to be the responsible climatic feedback leading to uncharacteristic warming throughout the irrigated region. Figure 2 shows about a 1 degree Celsius warming in irrigated areas of the Great Plains and cooling downstream.

The results of this study highlight the interesting relationships between the GPLLJ and a realistic amount of simulated irrigation. Contrary to other studies (e.g., Huber et al. 2014) the addition of a dynamic and realistic irrigation scheme has resulted in an average increase in jet velocity over the irrigated region, a slight increase in the occurrence of jets and small changes to jet height. It appears that the enhanced gradient in geopotential height as result of height falls over the irrigated region is contributing to the increase in jet speeds. McCorcle (1988) investigated the difference heterogeneous and homogeneous distributions of changing soil moisture. His findings pointed to the importance of analyzing varying spatial distribution of soil moisture. This study acknowledges and elaborates upon this point through the addition of the dynamic irrigation scheme. By including the Noah-Mosaic land surface model and differentiating sub grid-scale land-use types this model is able to more appropriately handle a realistic and heterogeneous distribution of soil moisture.

Another important aspect of this study is that it is run over a particularly hot and dry year. This was rationalized to maximize the effect that a realistic irrigation scheme may produce. To expand on this study and the potential feedbacks which could arise due to differing climatological conditions, future work could involve a similar approach including climatologically normal and pluvial years. It may be the case that the feedbacks on adding irrigation in this fashion could end with different results based upon the background conditions. With respect to this simulation it is also worth noting that although the focus of this study is on the Great Plains the model domain covers the entire US, and also the amounts of irrigation in other regions was admittedly less comparable to the observations. The changes caused by the additional irrigation outside of the focus area may be compounding through larger scale circulations ultimately having a potential effect over the GP.

Understanding real world impacts to the LLJ will be critical in the formation of the next generation of atmospheric models. These models will attempt to combine interactions between the physical environment and anthropogenic factors in realistic ways. To solve tomorrow's problems a more complete representation of reality will be necessary. This research is just one step towards bridging the gap between models and reality. This research shows, that even though small, the changes brought about by only the addition of a modest amount of water near the surface can have compounding effects on the LLJ. This may be worth considering when developing parameterizations for operational forecast models and when making projection on future climate.

## **Conclusion**

The results of this study show that the addition of a realistic irrigation scheme creates enough of a change originating from the surface to alter the GPLLJ. At the surface, the IRR

simulation shows changes in temperature and precipitation. Aloft, warming continues through the lower atmosphere over the central US. Higher heights over the central US and lower heights to the east correspond to the general changes in precipitation as noted by Pei et al. (2016). The changes in this study are similar in magnitude to those found in a study done by Huber et al. (2014). This is especially so when considering the realistic nature of the irrigation in the present study compared to the amount added in the aforementioned sensitivity study. As expected, a comparison between a realistic amount of irrigation and a sensitivity test results in suppressed effects of similar magnitudes over the irrigated areas when compared to simulations with no irrigation. At the 850 hPa level Huber et al. (2014) found height changes on the order of 6 m, this study found differences on the order of 1 m. In the realistic irrigation simulation and the sensitivity study temperatures changed by about 1 and 4.7°C respectively. In this case the sign of the temperature difference is opposite, and most likely due to the already warm and dry background conditions across the GP in 2012. Downstream, both studies noted increases to precipitation. Also, the magnitude of these changes are on par with other studies which have looked at changes to the LLJ from a climatological perspective with forcings of similar magnitudes.

The focus of this study is on the differences in the LLJ. The most notable change is a nearly 1 m/s statistically significant increase in mean LLJ core speeds over the irrigated region. Huber et al. (2014) found changes to the LLJ of between 20-30% between the irrigated and control simulation, or about 2-3 m/s. Other changes found in this study include largely statistically insignificant increases in mean jet core heights on the order of less than 100 m, and a slight increase in jet frequency of less than 10%.

## CHAPTER IV - SUPPLEMENTARY RESULTS

The domain of the WRF simulations includes the entire contiguous US (CONUS), therefore, it is worth analyzing how the simulations behaved across the rest of the domain. This chapter contains a further examination of other noteworthy LLJ locations as well as further analysis into the simulated differences between the NOIR and IRR WRF simulations.

There are two other notable regions in addition the Great Plains where irrigation was applied in the IRR simulation in relatively large amounts. The first is the Central Valley in California (CCV) where the most irrigation was applied with respect to overall magnitude. The second region is the Lower Mississippi Valley (LMV). These two areas are shown in Figure 1. The effects of these regions may be small, but could have an influence on the behavior of the atmosphere downstream over the Great Plains and so they are important to at least mention in this investigation.

This chapter contains a brief summarization of the North American LLJ including its multiple locations of highest frequency, seasonality among other features. Highlighting the LLJs which occur near the other irrigated regions mentioned above. Next, the CCV and LMV regions will be compared against the NARR for the summer of 2012 complementing the comparison from the previous chapter. Finally, further analysis and statistics will be presented on the simulated differences of the IRR and NOIR simulations.

## NA LLJ Climatology

Doubler et al. (2015) noted multiple regions where LLJs are common across North America (NA). Because the simulations for the present study are for the summer months of June, July and August (JJA) this summary will focus on other common areas of summer time jets.

Doubler et al. (2015) analyzed the following regions and the NARR's ability to properly represent them. The first most familiar region of LLJ development is across the Great Plains. LLJs which form just off the west coast of the US is another notable area for LLJ development. In the summertime, these coastal jets are predominantly northerly with peak speeds of about 17 m/s. the elevation of these jets tends to be under 400 m above ground level (AGL) until you reach their southern extent where they tend to form above 400 m. These two regions, the Great Plains and the west coast represent the two dominant regions where LLJs are found near the US for the summer months.

The Gulf of California is another area where LLJs are found in the summer. These jets tend to be southerly with peak wind speeds occurring over the north end of the Gulf of California stretching to northwestern Arizona. Doubler et al (2015) found that in the NARR their elevation tended to be between 200 m and 400m AGL with peak wind speeds of around 20 m/s. Two other regions discussed by Doubler et al. (2015) are Atlantic LLJs and LLJs that form over the Gulf of Mexico. Remember though, that Doubler et al. (2015) found these jets to occur only between 2-5% of time.

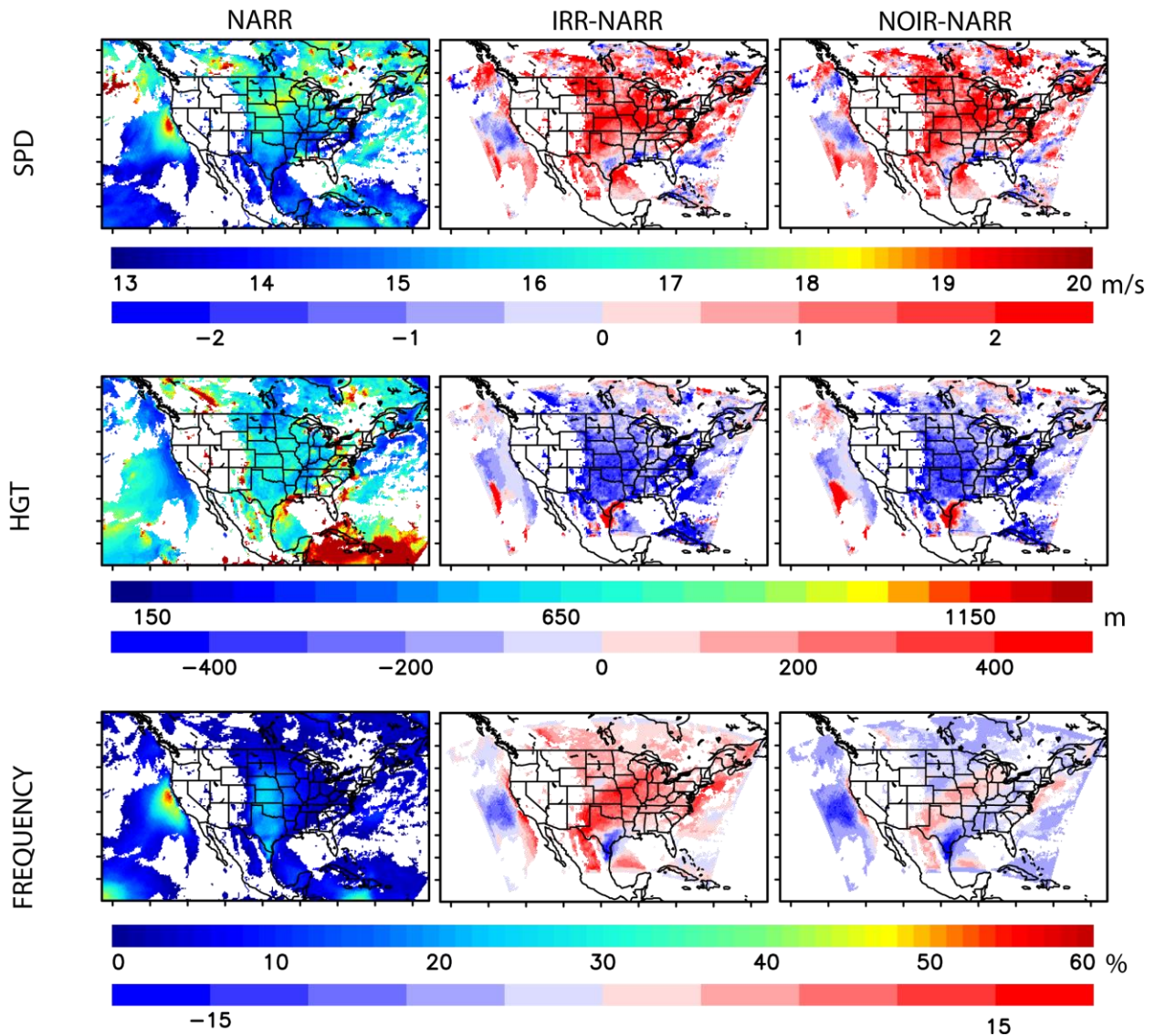


Figure 6. Comparison of LLJ speed, height, and frequency between the NARR, IRR and NOIR simulations for the Contiguous United States.

Figure 6 shows the comparison between the NARR and the two WRF simulations. Of the two major regions where LLJs are found during the summer months, both the Great Plains and the west coast compare well against the NARR for both jet speed and height. The east coast Atlantic LLJ is not as homogenous, however, it still shows up for this summer season. The Gulf of California is the most underrepresented LLJ region in the 2012 NARR data where nearly no LLJs are recorded.

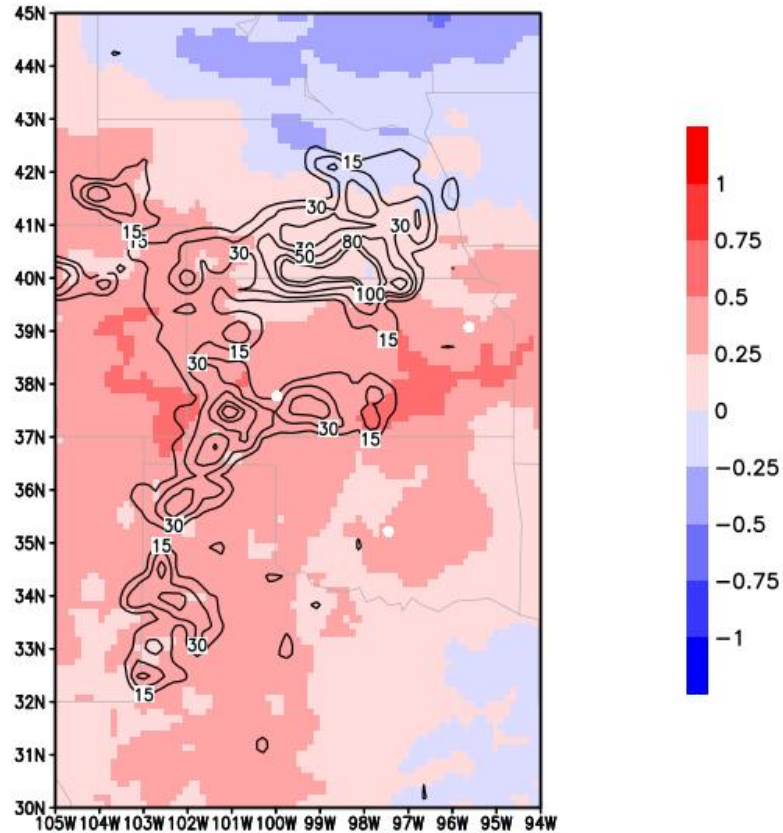


Figure 7. Accumulated irrigation throughout the entire irrigated simulation (JJA) for the Great Plains. Black contours show irrigation in  $\text{kg/m}^2$ . Color shading shows the JJA mean surface temperature difference (Celsius).

### **Irrigation vs. No Irrigation**

#### *Great Plains, California Central Valley & Lower Mississippi Valley*

The region of interest for this study is the central United States and the surrounding region. This region was chosen for two main reasons. First, the Great Plains Low Level Jet (GPLLJ) is one of the most often studied region with respect to LLJ development. Second, this is the region the WRF irrigation scheme was calibrated for. There are also other regions where irrigation was applied in an appreciable amount. The Lower Mississippi Valley, where irrigation amounts are both lower in magnitude and spatial distribution as compared to the irrigation applied in the GP. The second region is California's Central Valley. Although the area irrigation

is applied here is relatively small, the amount that was applied in the IRR simulation is more than double the magnitude as what was applied over the GP. With the addition of irrigation in these other regions it possible that any effects to the local-regional circulation may influence the atmospheric circulations elsewhere within the domain. In general, the effects of irrigation in California at the surface are what you would expect. Figure 1 and Figures 7-9 show the extent to which irrigation was applied by the end of the simulated period. Over  $180 \text{ kg/m}^2$  of irrigation water was added in CCV while both the GP and LMV have just over  $120 \text{ kg/m}^2$ . Figures 8 and 9 show some degree of cooling especially over the LMV. This is the expected behavior as temperatures generally cool due to the evaporation of the added irrigation. The warming shown in Figure 7 across the GP has been attributed to a climate feedback of an irrigation induced lack of precipitation over the irrigated region. This lack of precipitation comes along with an increase and expansion of central US anticyclonic circulation (Pei et al. 2016).

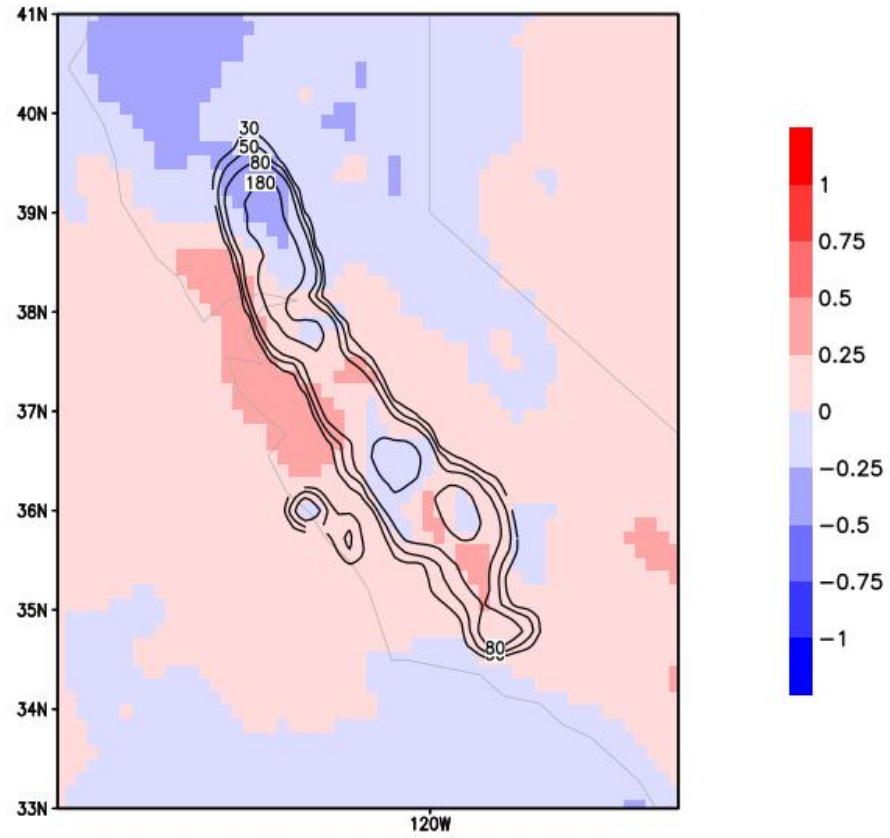


Figure 8. As in Figure 7, but over California's Central Valley.

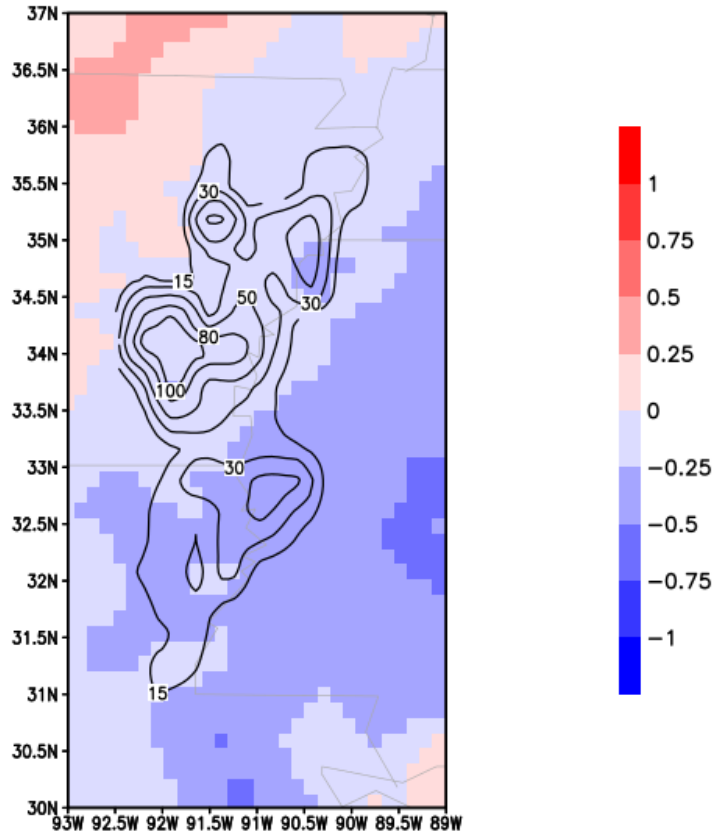


Figure 9. As in Figure 7, but over the Lower Mississippi River Valley.

### *Surface Moisture and Energy Budget*

Irrigation is the only addition between the two simulations, and the effects are expected to begin at surface and propagate upwards. To follow, the summary of the differences between the simulations will start from the ground and work upwards.

Beginning on the ground Figures 10-13 show the difference in soil moisture at the first soil level (0-10 cm) between the IRR and NOIR simulations. Across the GP there are both increases and decreases in the soil moisture. The decreases are possibly linked to the decreases in the precipitation patterns. Across the CCV and LMV expected increases in soil moisture on the

order of about  $0.1 \text{ m}^3/\text{m}^3$ . With the addition of irrigation, the magnitude of evaporational cooling is also expected to increase with the additional water that is added. During the day, the additional water is expected to decrease surface temperature, and at night temperatures are expected stay slightly higher as condensation prevents additional cooling.

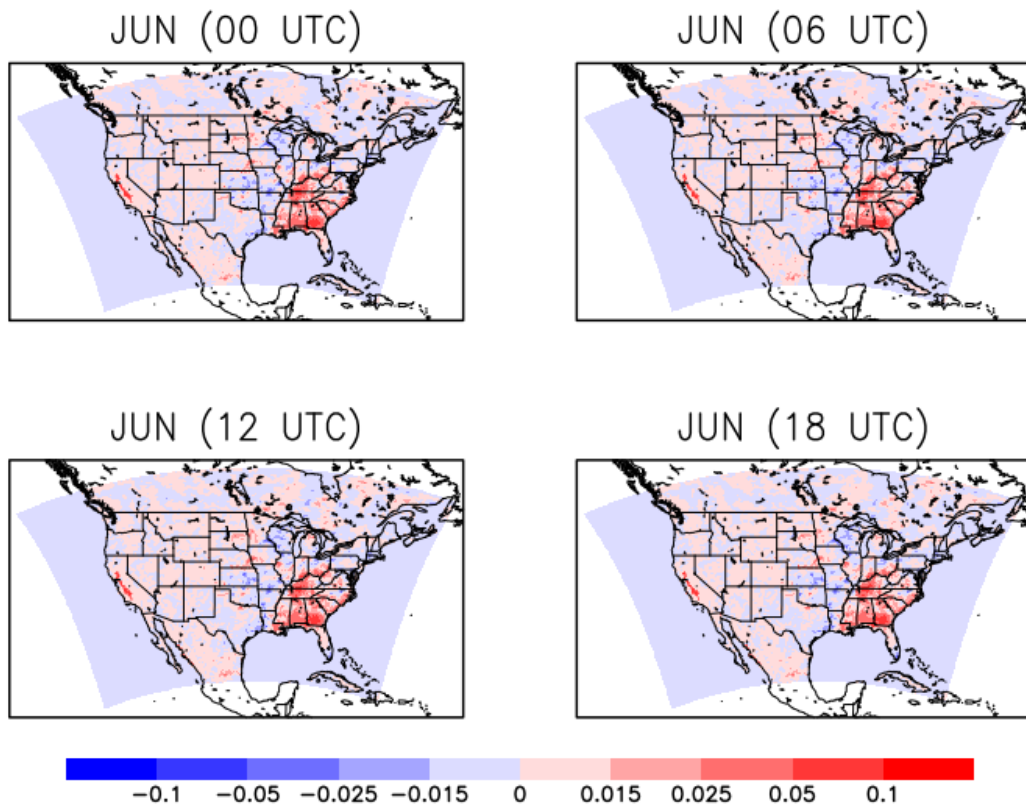


Figure 10. Mean diurnal distribution of June surface (0-10 cm) soil moisture ( $\text{m}^3/\text{m}^3$ ) differences (IRR-NOIR).

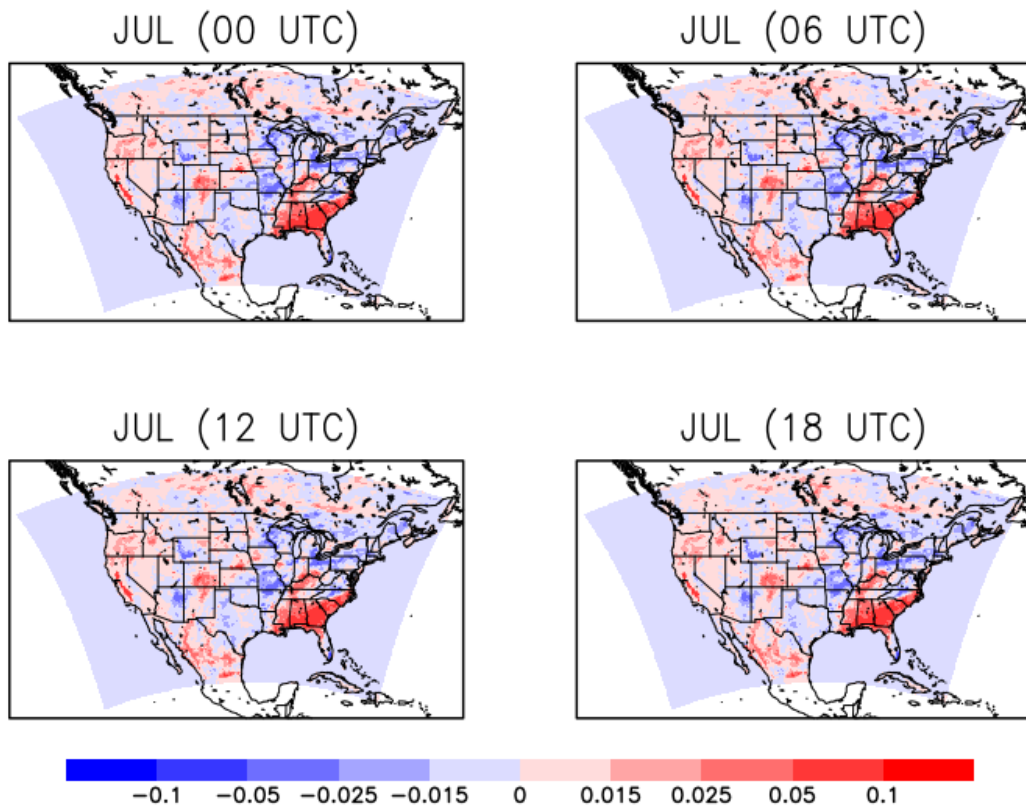


Figure 11. Mean diurnal distribution of July surface (0-10 cm) soil moisture ( $\text{m}^3/\text{m}^3$ ) differences (IRR-NOIR).

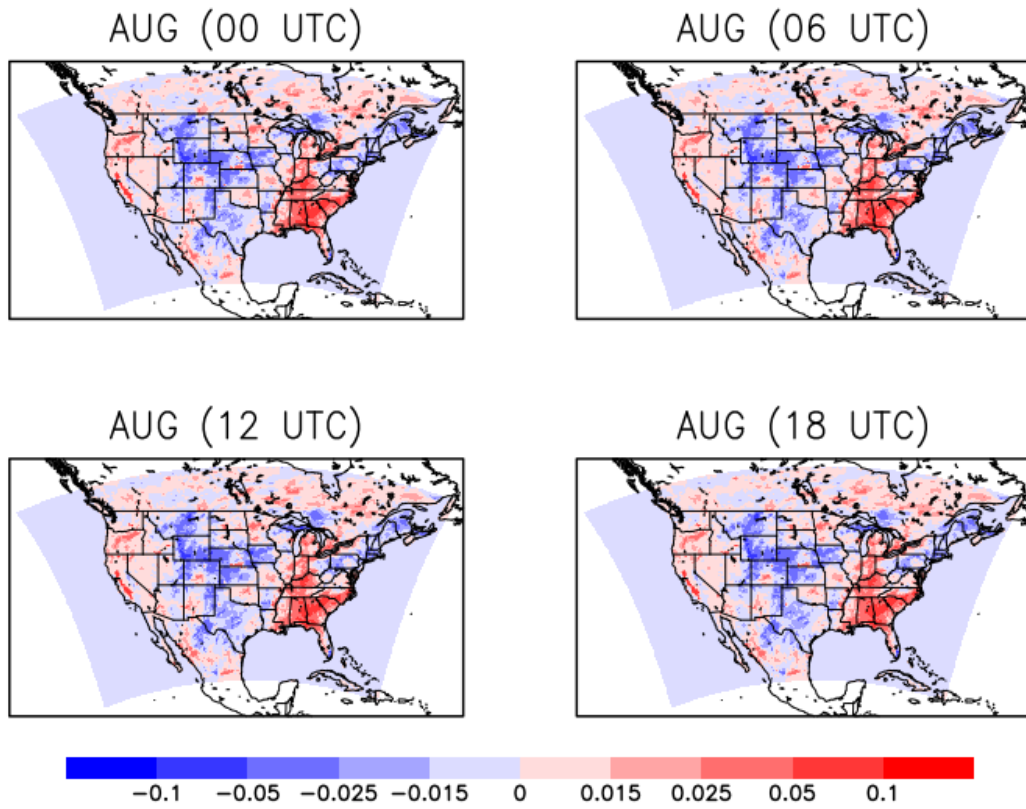


Figure 12. Mean diurnal distribution of August surface (0-10 cm) soil moisture ( $m^3/m^3$ ) differences (IRR-NOIR).

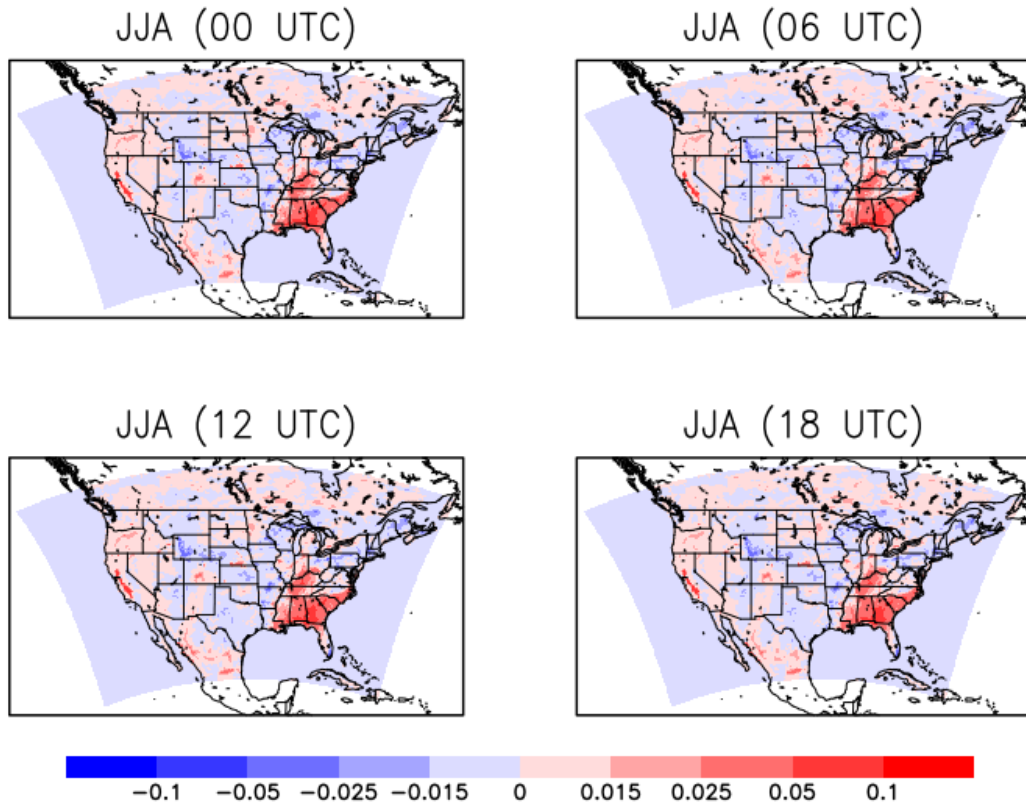


Figure 13. June, July, and August mean diurnal distribution of surface (0-10 cm) soil moisture ( $\text{m}^3/\text{m}^3$ ) differences (IRR-NOIR).

The expected changes in temperature are connected to expected changes in the surface energy flux. With higher rates of evaporation at the surface the latent heat flux is expected to rise alongside a decrease in sensible heat exchange. Figures 14-21 show the changes in surface latent (Figures 18-21) and sensible heat flux (Figures 14-17). What stands out are the expected diurnal differences between 00-18 UTC and 06-12 UTC in the CCV and the LMV and some unexpected differences throughout the GP. Where irrigation is most intense we see decreases in sensible heat flux and increases in latent heat flux in all three regions across all months, most notably in August. However, across the GP in areas of Kansas where the irrigation amounts aren't quite as large some increases in sensible and corresponding decreases in latent heat are shown.

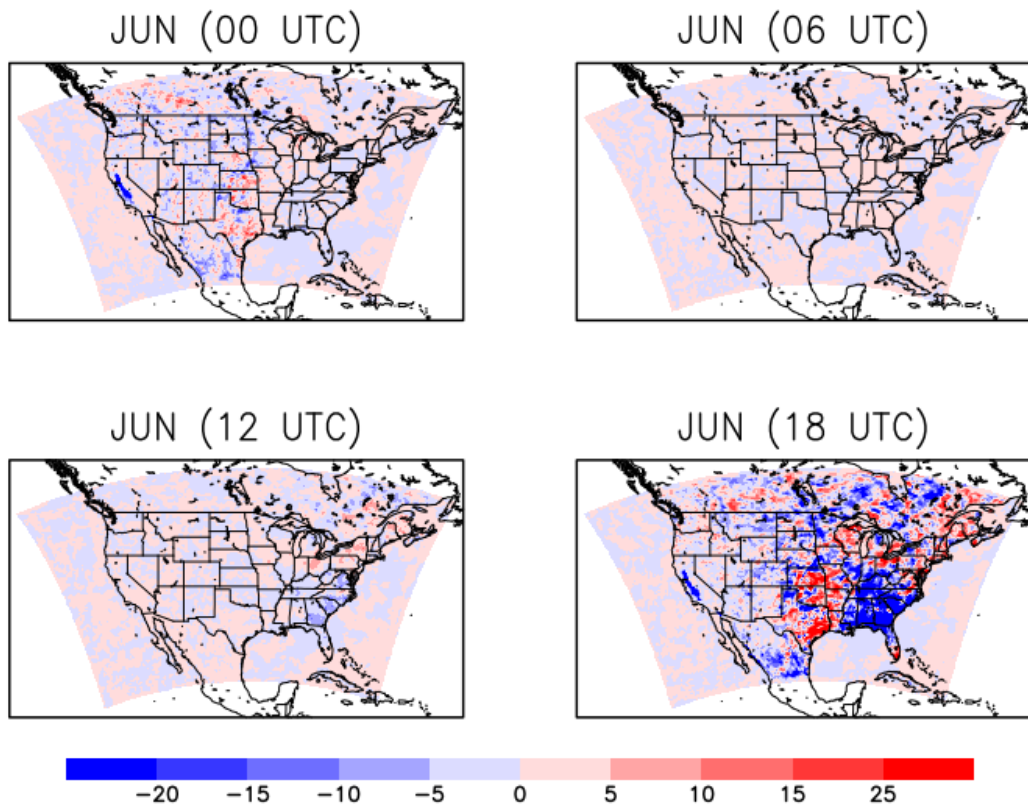


Figure 14. Mean differences (IRR-NOIR) of June diurnal surface sensible heat flux ( $\text{W/m}^2$ ).

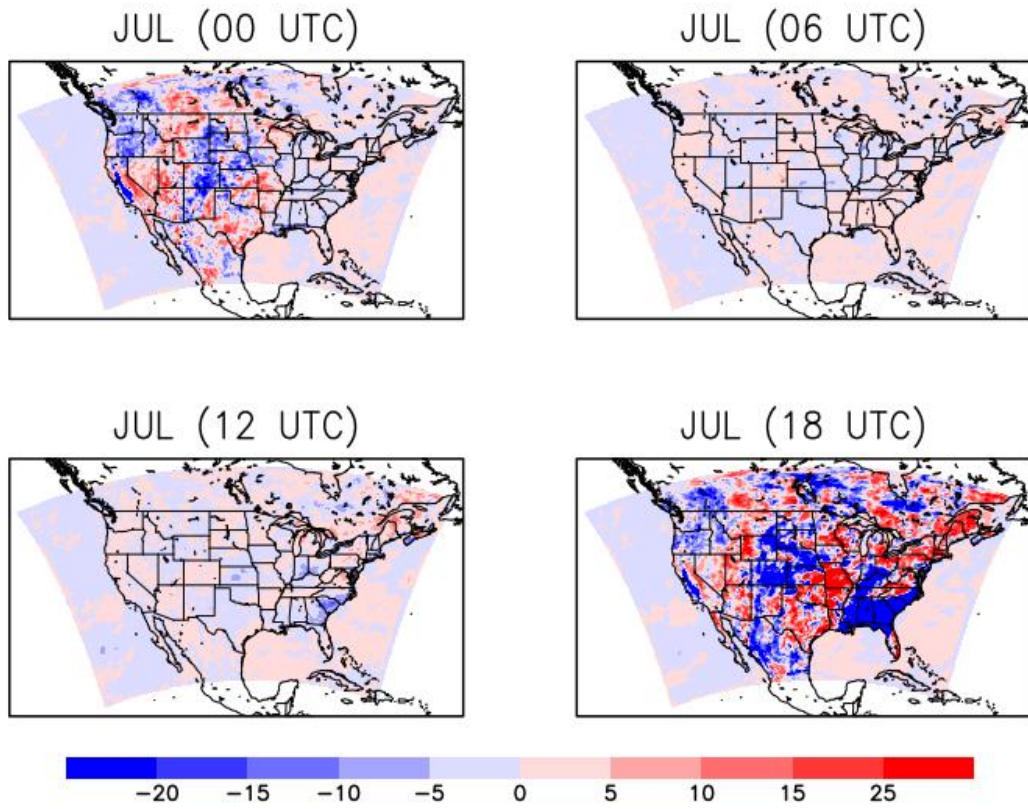


Figure 15. Mean differences (IRR-NOIR) of July diurnal surface sensible heat flux ( $\text{W/m}^2$ ).

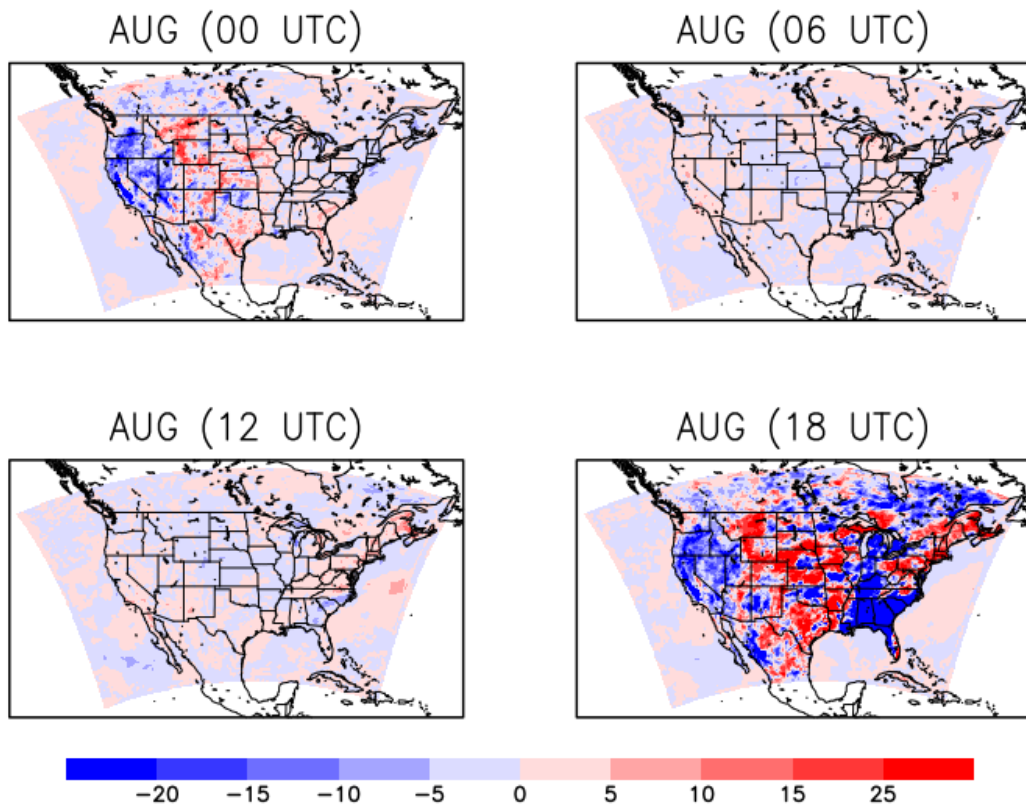


Figure 16. Mean differences (IRR-NOIR) of August diurnal surface sensible heat flux ( $\text{W/m}^2$ )

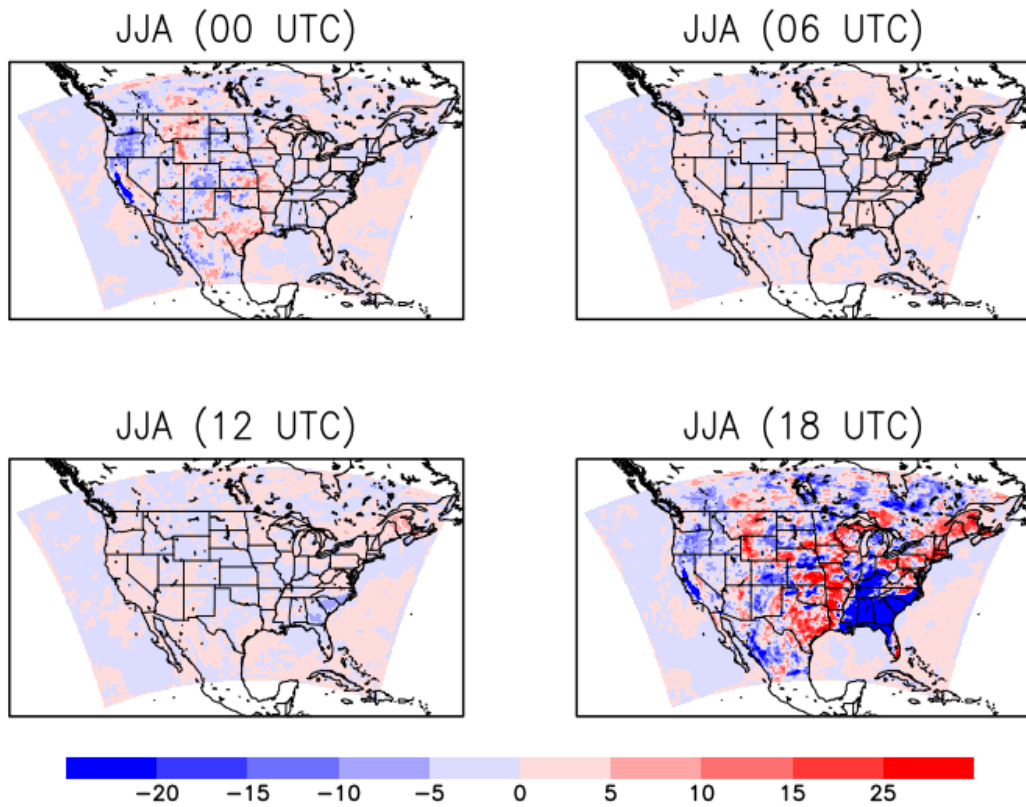


Figure 17. June, July, and August mean differences (IRR-NOIR) of diurnal surface sensible heat flux ( $W/m^2$ ).

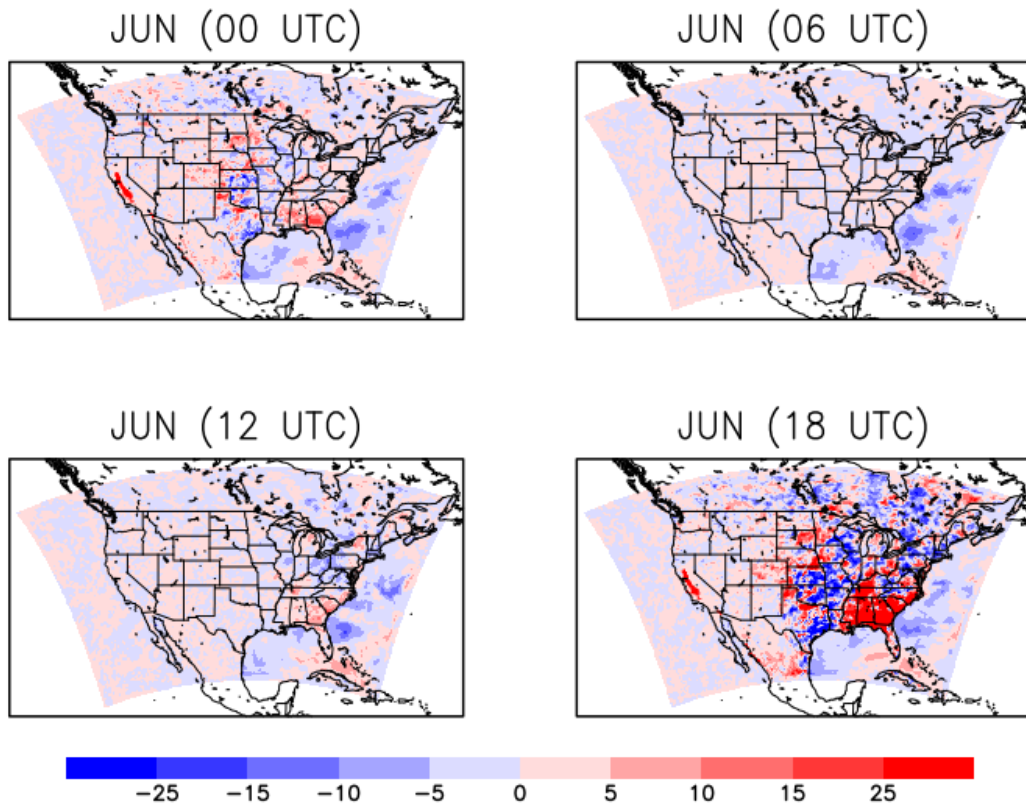


Figure 18. Mean June diurnal surface latent heat flux ( $\text{W/m}^2$ ) differences (IRR-NOIR).

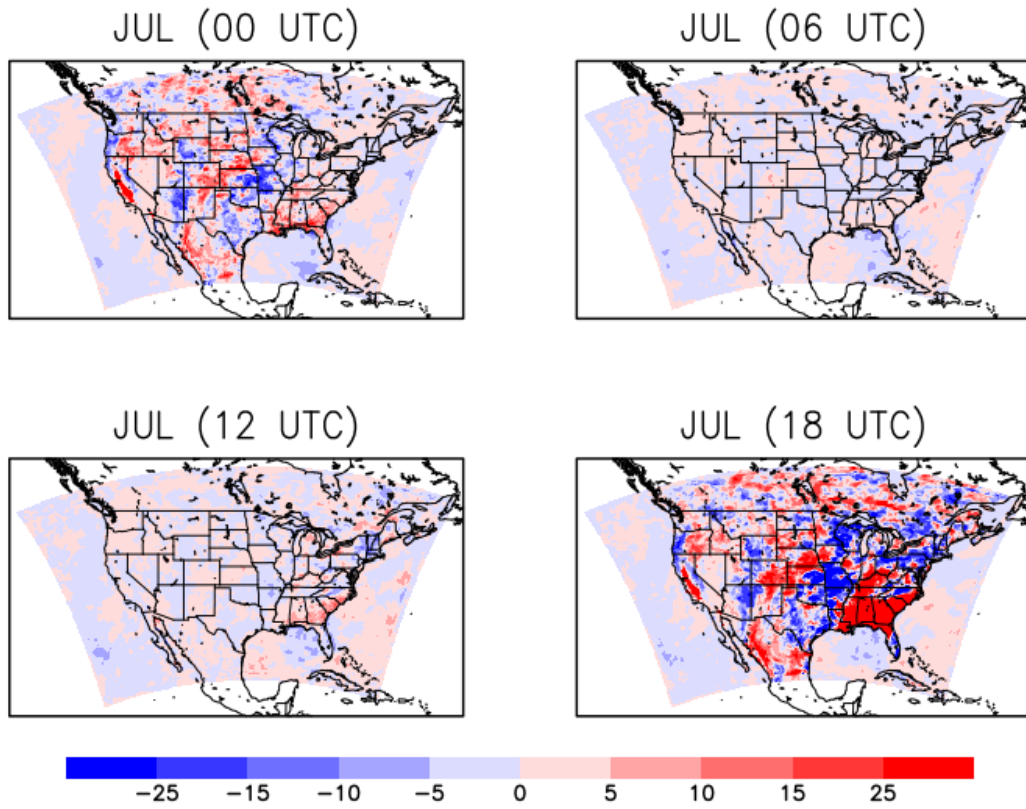


Figure 19. Mean July diurnal surface latent heat flux ( $\text{W/m}^2$ ) differences (IRR-NOIR).

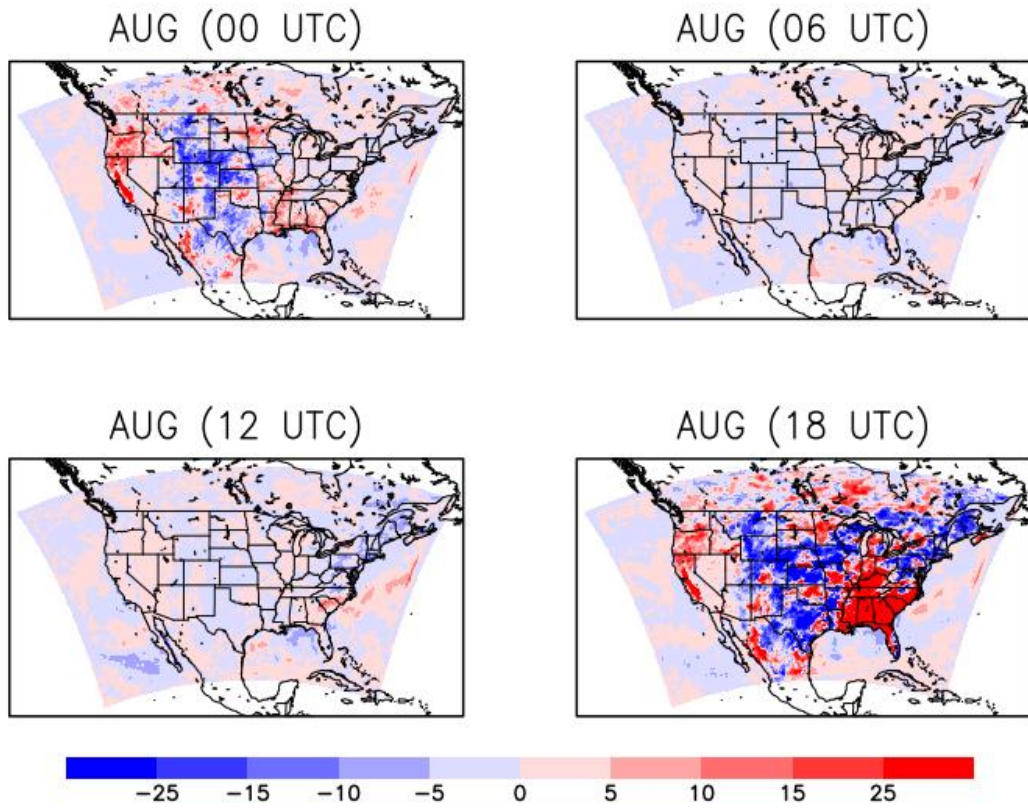


Figure 20. Mean August diurnal surface latent heat flux ( $W/m^2$ ) differences (IRR-NOIR).

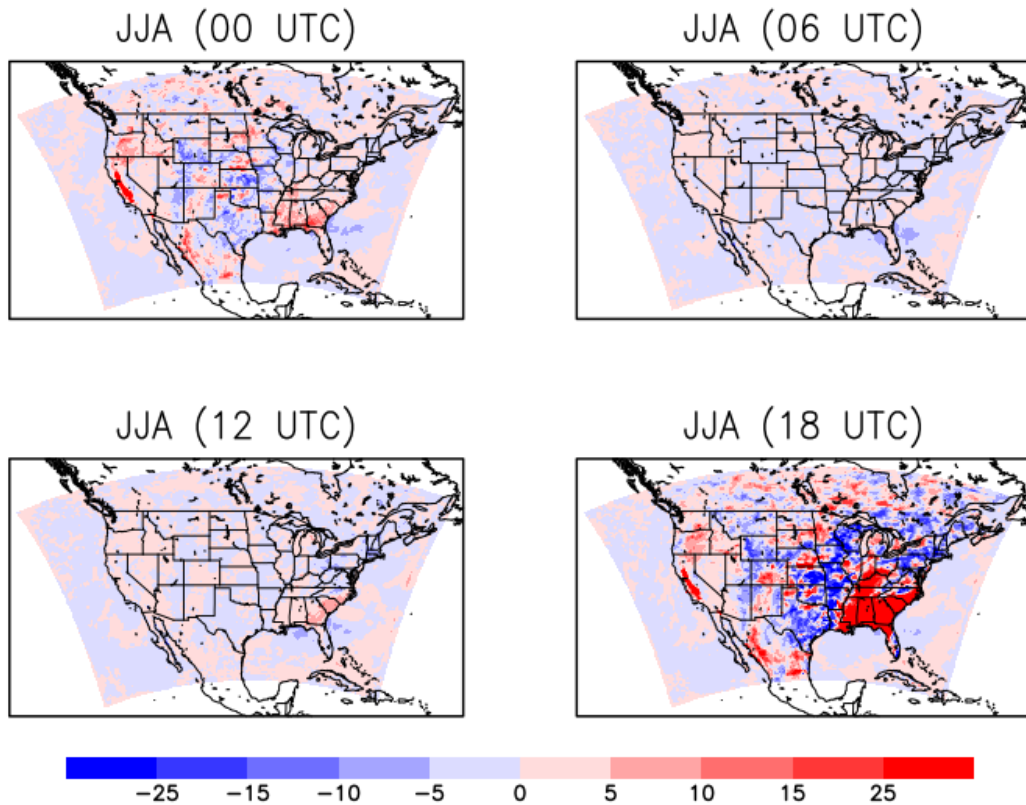


Figure 21. June, July, and August mean diurnal surface latent heat flux ( $\text{W/m}^2$ ) differences (IRR-NOIR).

With the changes to the surface energy partitioning come corresponding changes in surface and skin temperature (Figures 22-25). As has been mentioned before the changes to the precipitation patterns in the irrigated simulation result in unconventional changes to the temperature with respect irrigation. These changes are reflected in both the skin and surface temperatures. The diurnal pattern across the CCV shows the typical warming during the overnight hours and cooling during the afternoon hours that is expected with the addition of irrigation. During June the first month of the simulation, the cooling is already prominent throughout the CCV and the LMV over the afternoon hours. There is cooling across the GP as well, however, there is also warming in portions of southern Kansas and Oklahoma where

irrigation is less prominent. These diurnal trends continue for the CCV and LMV throughout the entire simulation. For the GP by July and especially through August the cooling that was occurring becomes overwhelmingly a warming trend for nearly all hours. In some areas of central Kansas warming is as much as 2 degrees celsius for 00 UTC & 18 UTC in August and slightly less when averaged over all three months.

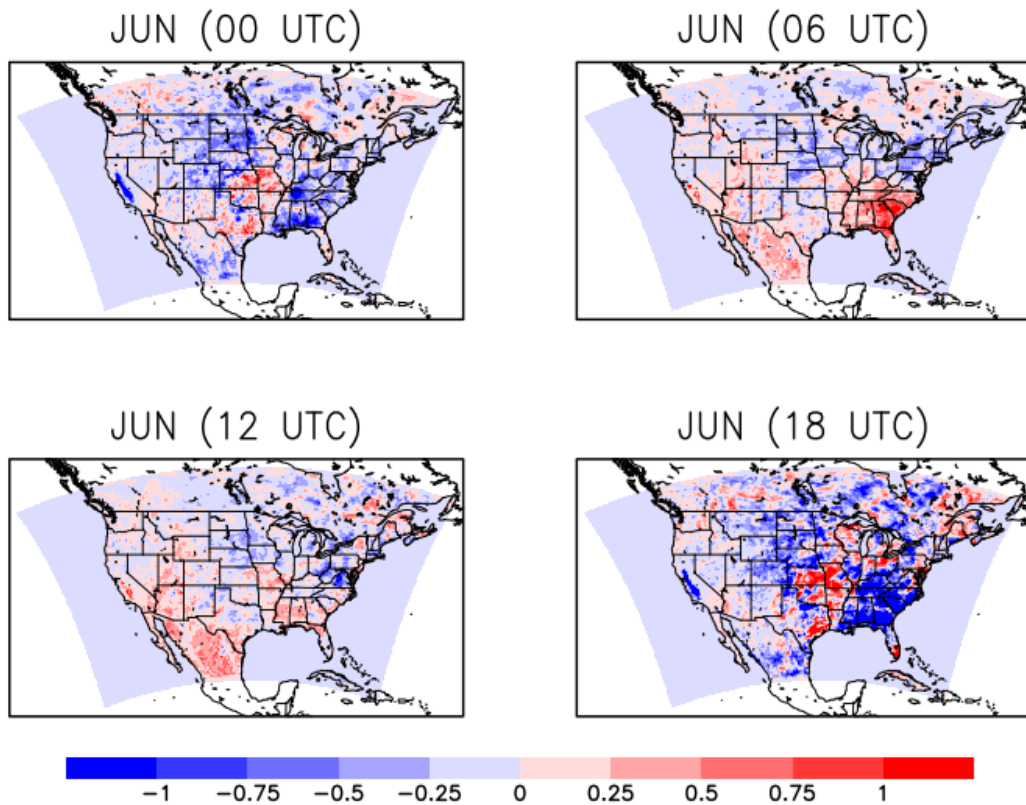


Figure 22. Mean diurnal June surface skin temperature (Celsius) differences (IRR-NOIR).

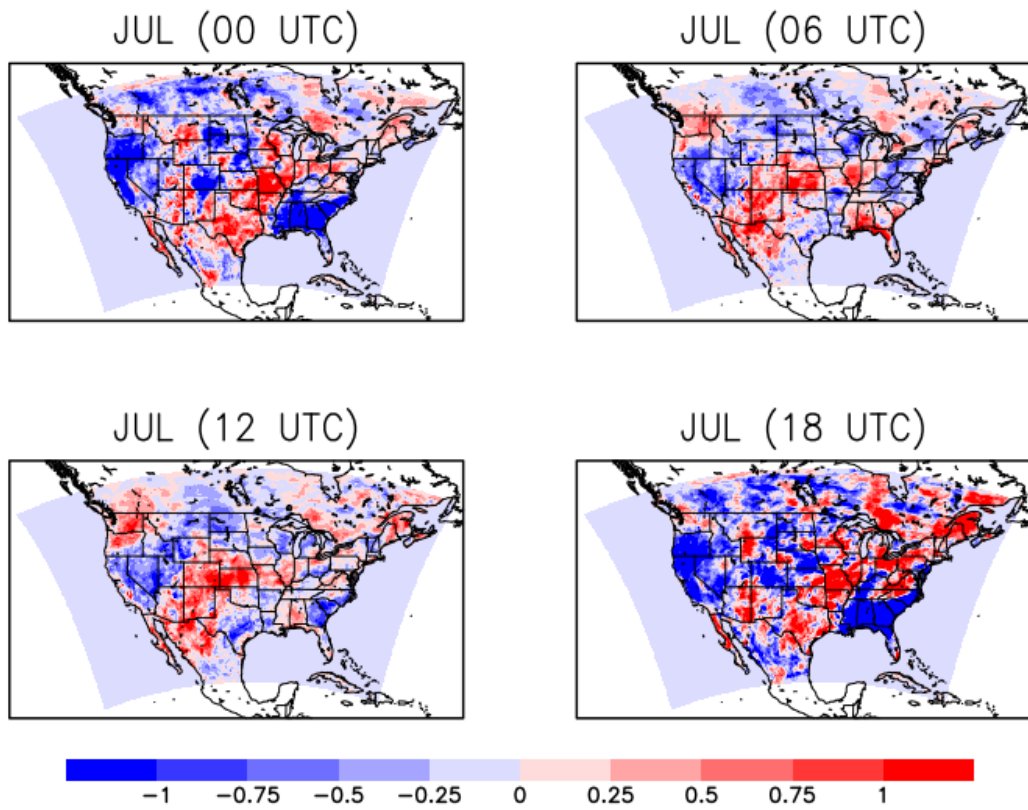


Figure 23. Mean diurnal July surface skin temperature (Celsius) differences (IRR-NOIR).

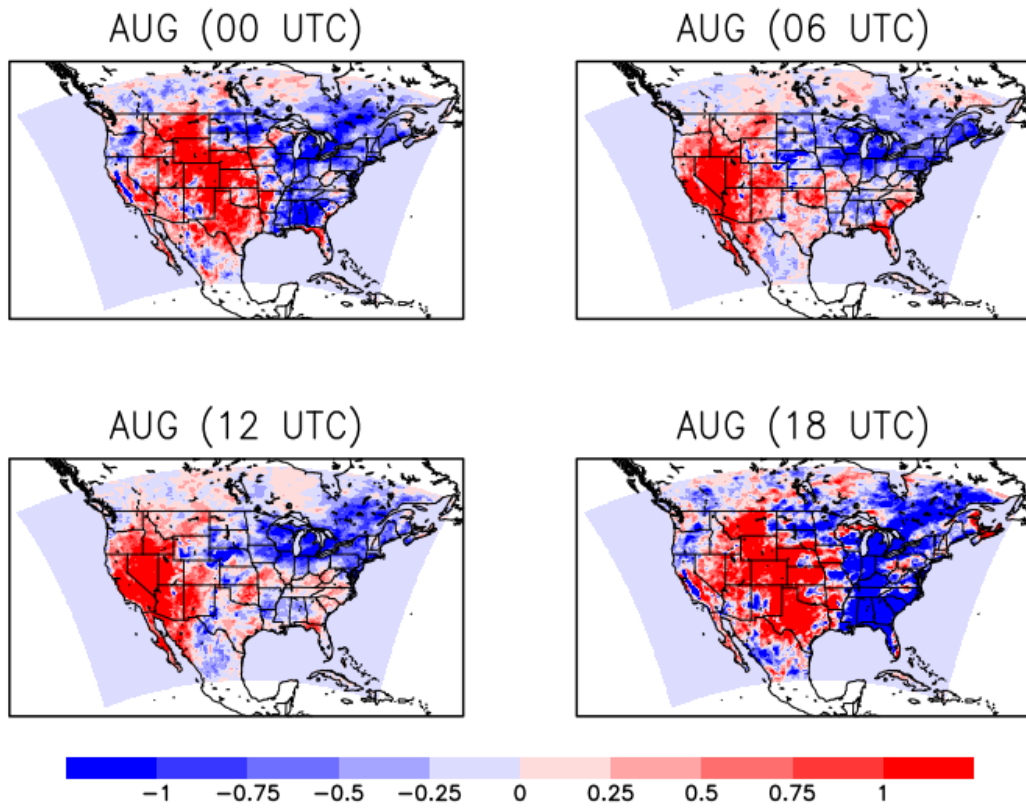


Figure 24. Mean diurnal August surface skin temperature (Celsius) differences (IRR-NOIR).

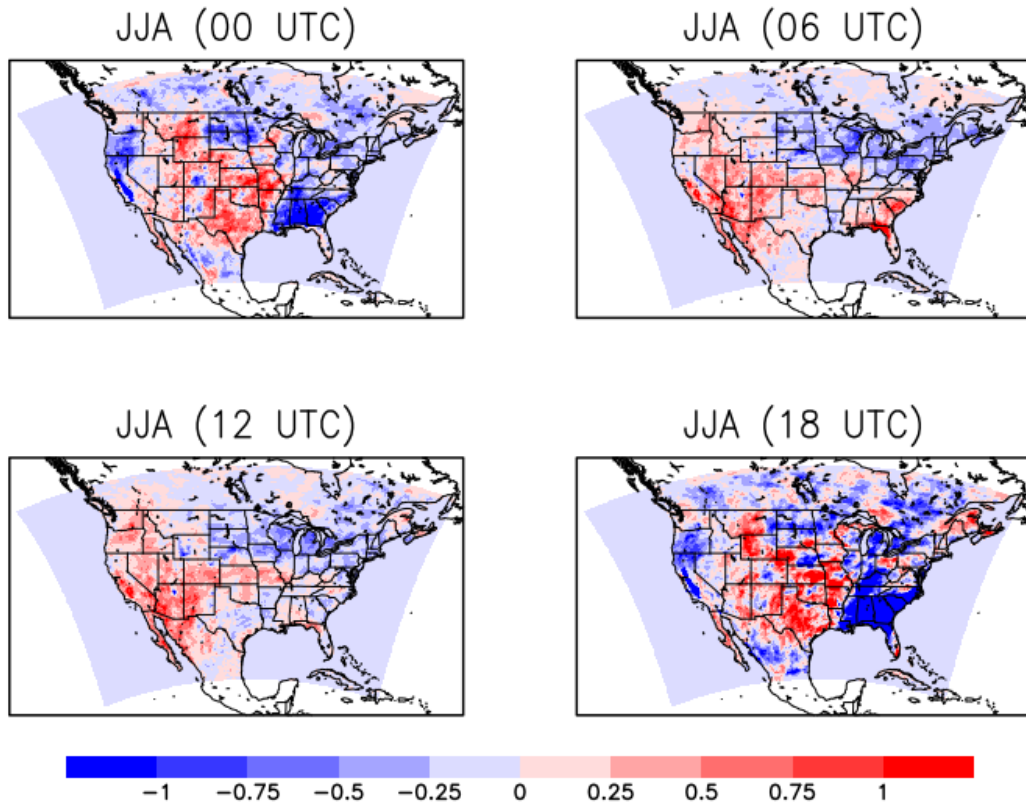


Figure 25. June, July, and August mean diurnal surface skin temperature (Celsius) differences (IRR-NOIR).

### *Great Plains Circulation*

Across the GP the planetary boundary layer (PBL) also increases and decreases in relation to the location of most intense irrigation as the temperature and heat flux does (Figures 26-29). Pei et al. (2016) notes this may be due to both the addition of irrigation as well as the changes in the precipitation pattern. Differences between the simulations range between 20-300 m. The large variability is due to the diurnal pattern of LLJ. LLJs during the afternoon are typically much higher than jets that occur over night (Bonner 1968; Doubler et al. 2015). July shows some of the largest differences between the IRR and NOIR simulations. Daytime PBL heights over parts of the north central GP are over 300 m lower, and in the south-eastern GP over

300 m higher in the IRR simulation compared to the NOIR simulation. August shows a different distribution than July where PBL heights to the east become predominantly lower in the IRR simulation and higher to the west over the Rocky Mountains. When averaged over the entire three-month simulation Figure 29 shows the decrease in PBL heights over the heavily irrigated regions during the afternoon hours and small increases to PBL heights overnight.

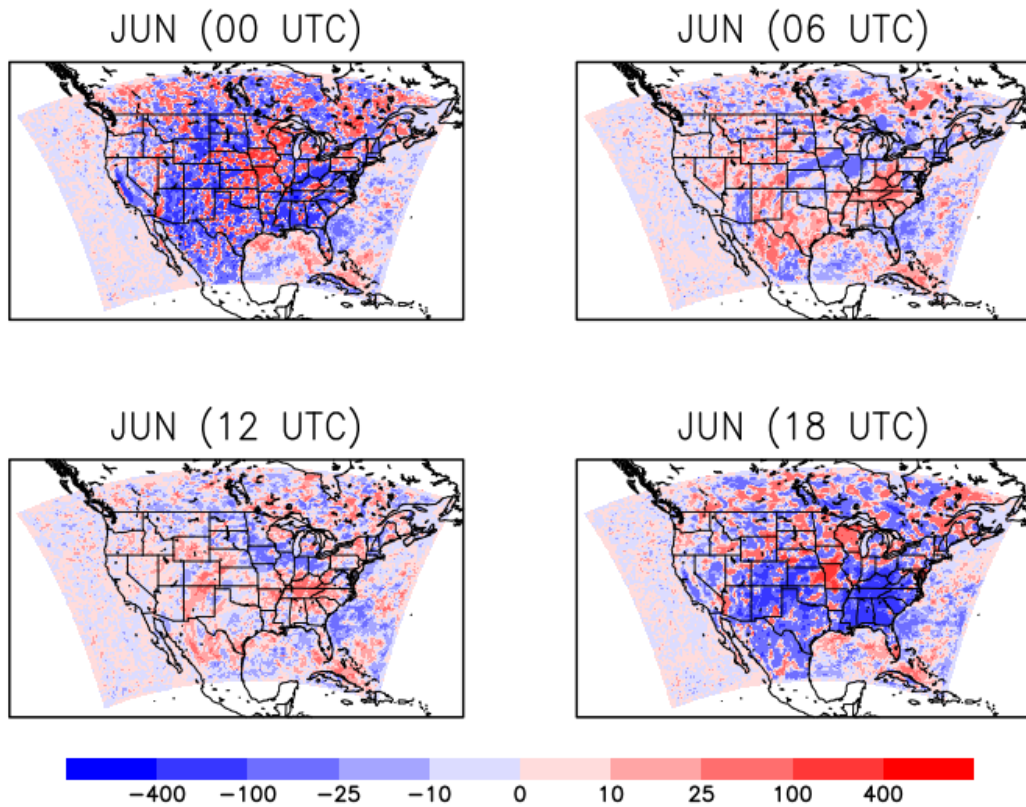


Figure 26. Mean diurnal planetary boundary layer height (PBLH) differences (IRR-NOIR) for June (meters).

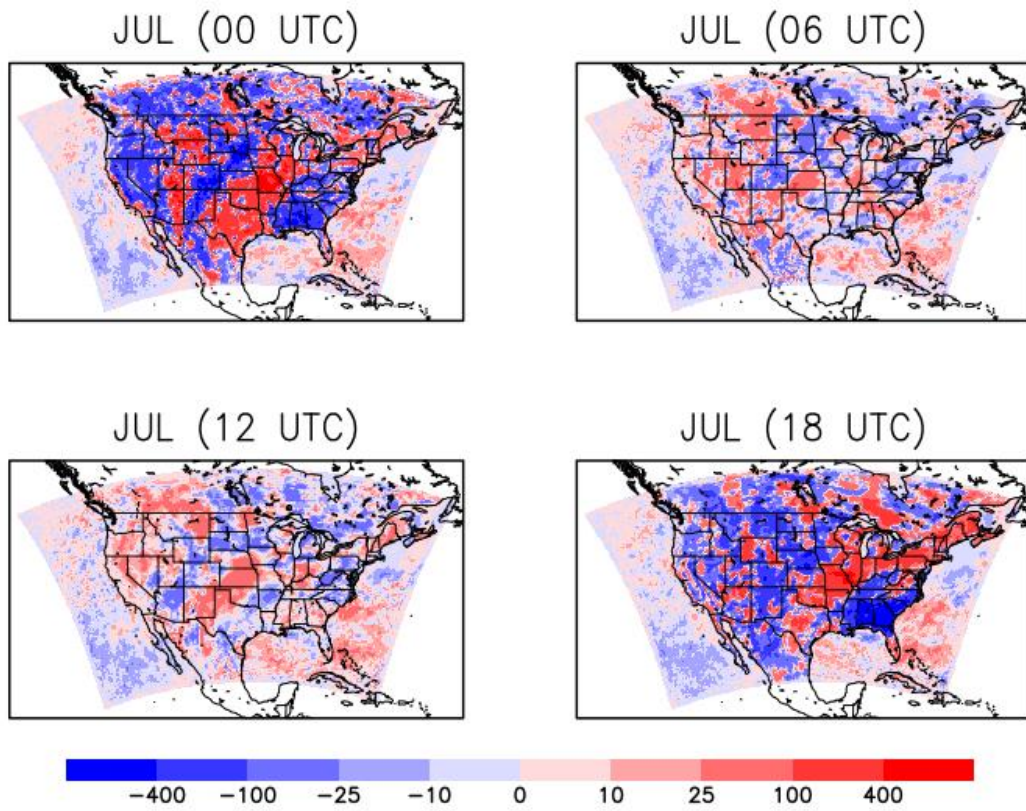


Figure 27. Mean diurnal planetary boundary layer height (PBLH) differences (IRR-NOIR) for July (meters).

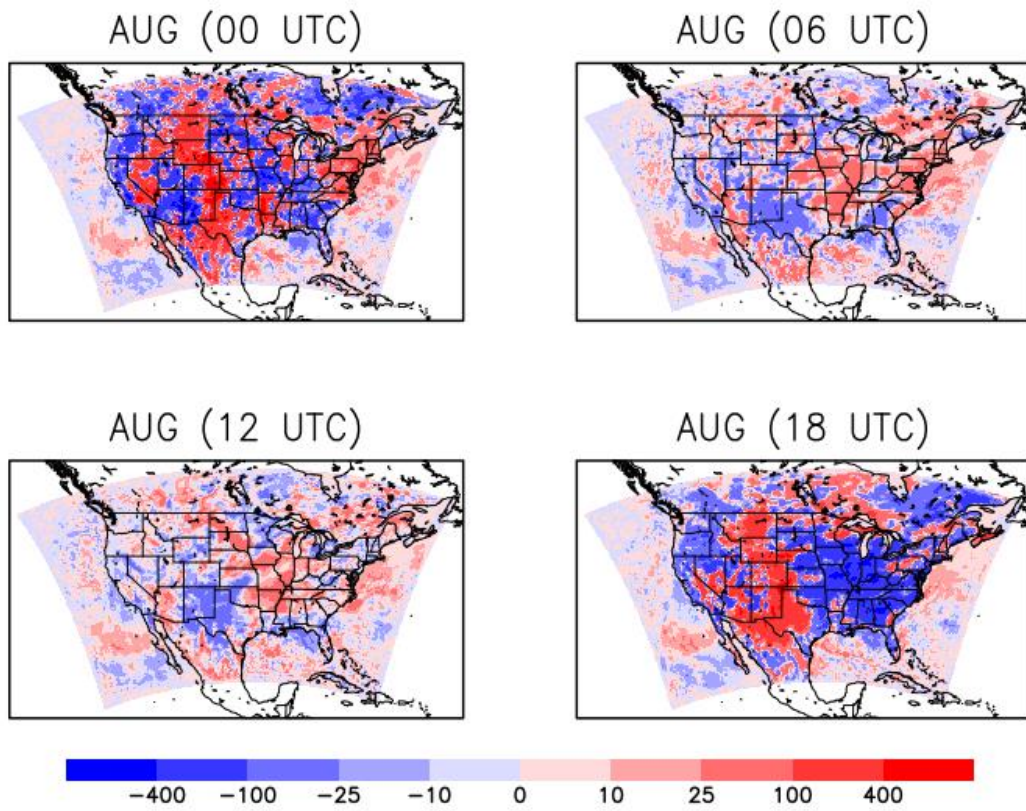


Figure 28. Mean diurnal planetary boundary layer height (PBLH) differences (IRR-NOIR) for August (meters).

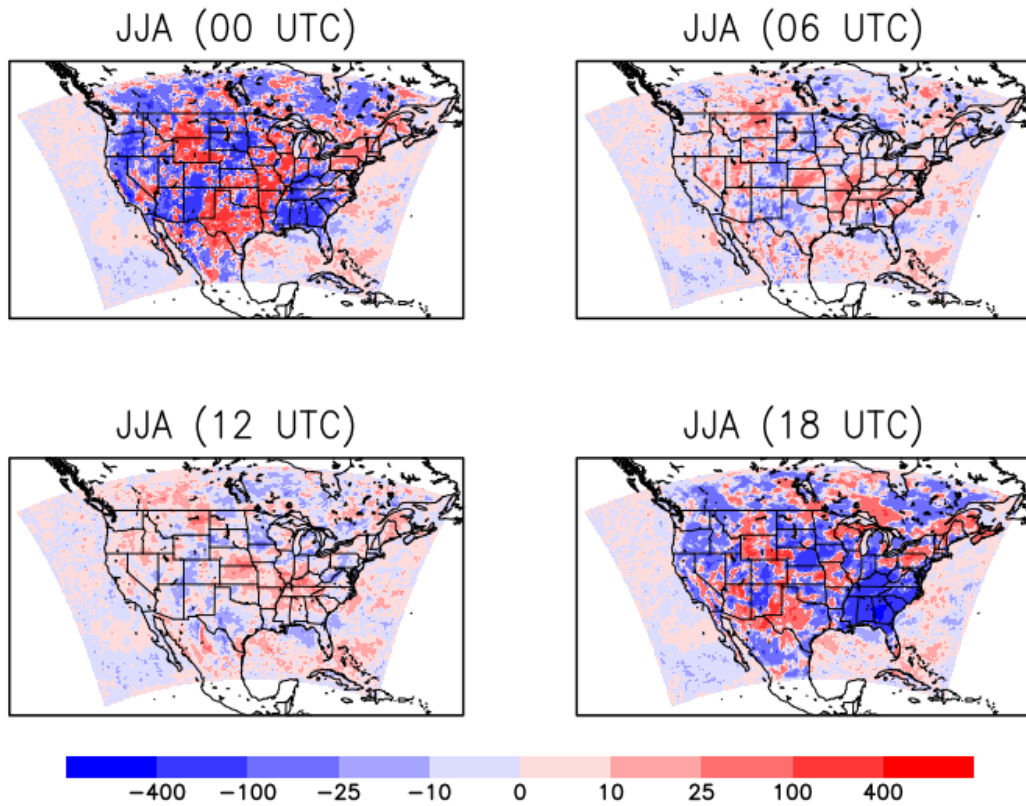


Figure 29. Mean diurnal planetary boundary layer height (PBLH) differences (IRR-NOIR) for June, July, and August (meters).

Figures 30-33 show the three-month mean difference in geopotential height for four significant levels. Nearest to the surface at 925 hPa there are lower heights towards the northeast US and heights are slightly decreased over the north central US as well. In fact, across all level the decreased heights along the north east are consistent. Along with these height decreases, are height increases throughout the central US. These height differences with lower heights to the east and higher heights throughout the central US generally agree with the overall total grid precipitation differences in Figure 34. The major changes to the precipitation pattern are the increase toward the east coast and southeast lower midwestern states along with noticeable decreases throughout much of the central US where much of the irrigation is added.

Geopotential Height Difference 925 JJA

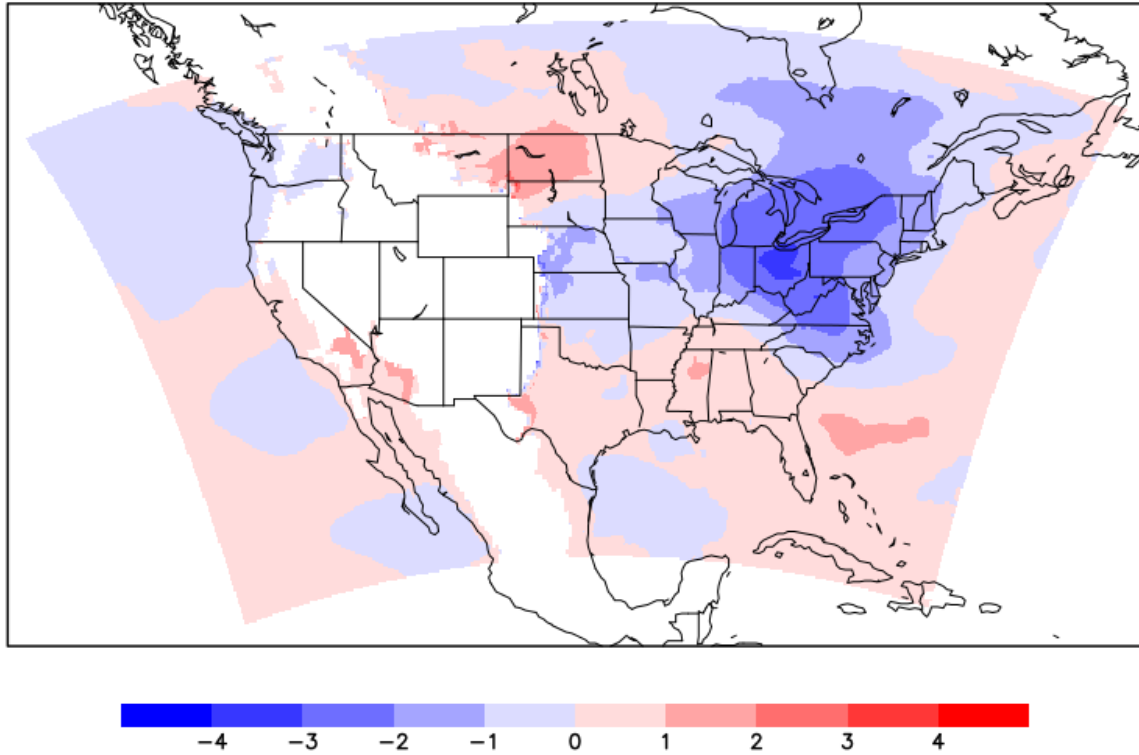


Figure 30. June, July, and August mean geopotential height difference in meters (IRR-NOIR) at 925 hPa.

Geopotential Height Difference 850 JJA

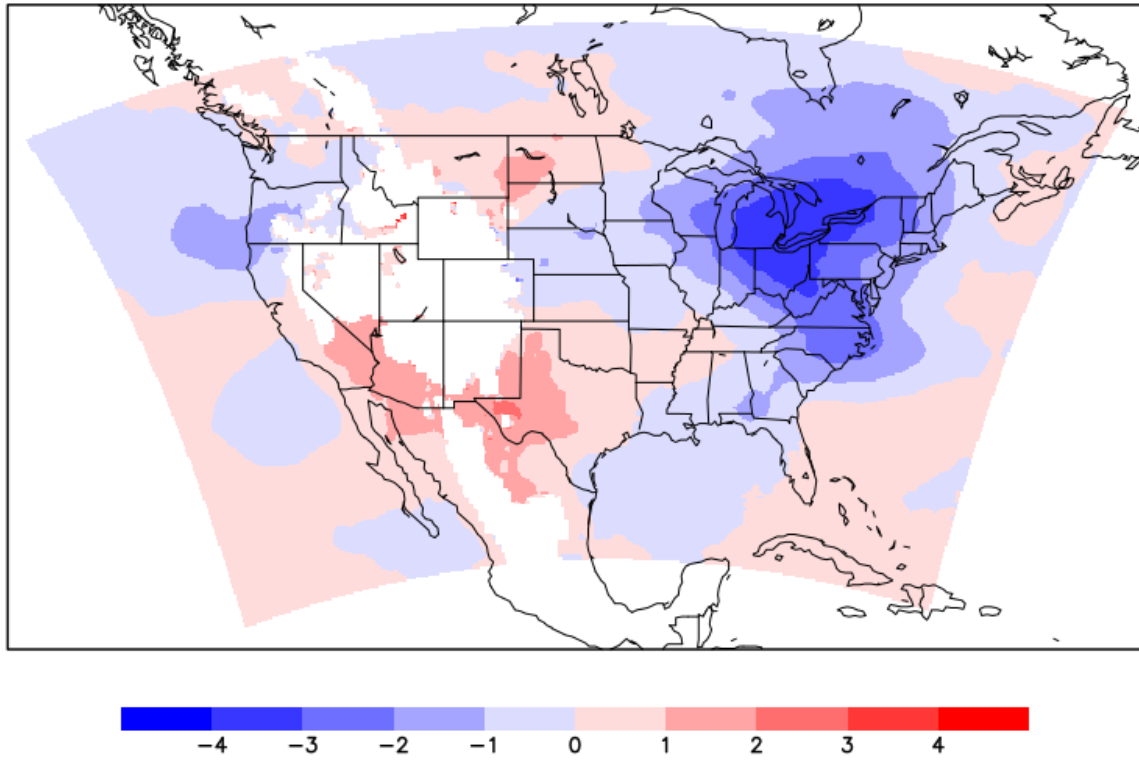


Figure 31. June, July, and August mean geopotential height difference in meters (IRR-NOIR) at 850 hPa.

Geopotential Height Difference 700 JJA

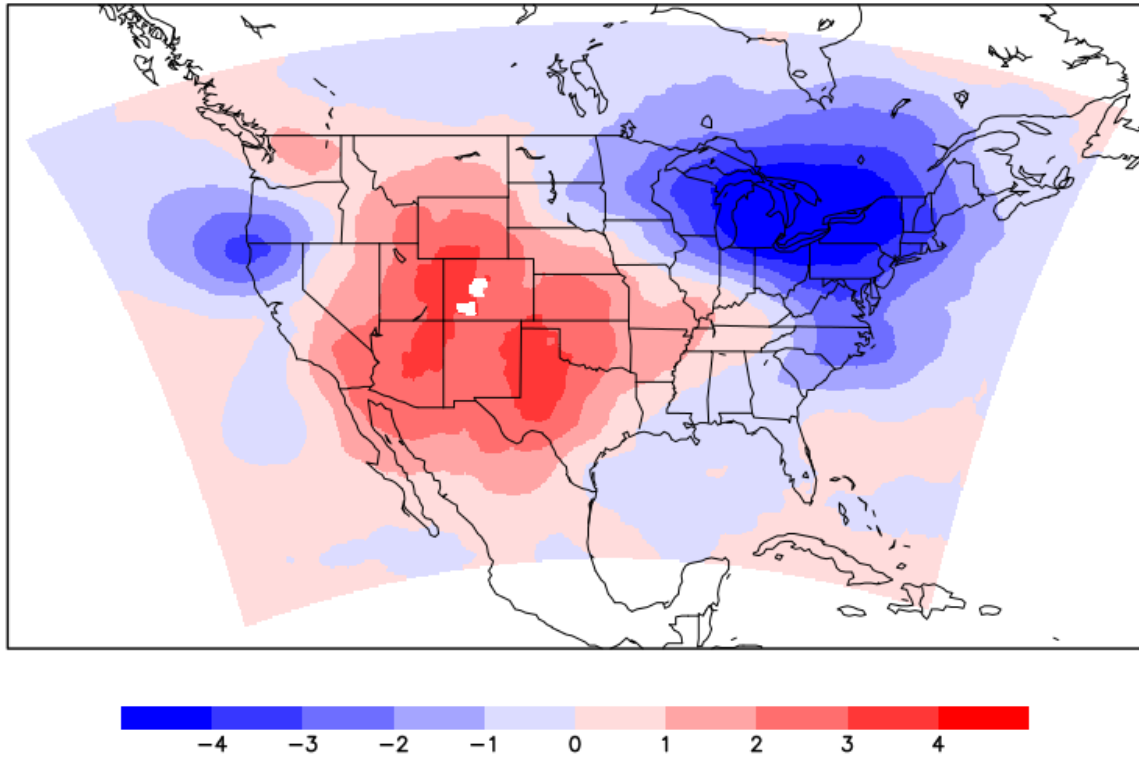


Figure 32. June, July, and August mean geopotential height difference in meters (IRR-NOIR) at 700 hPa.

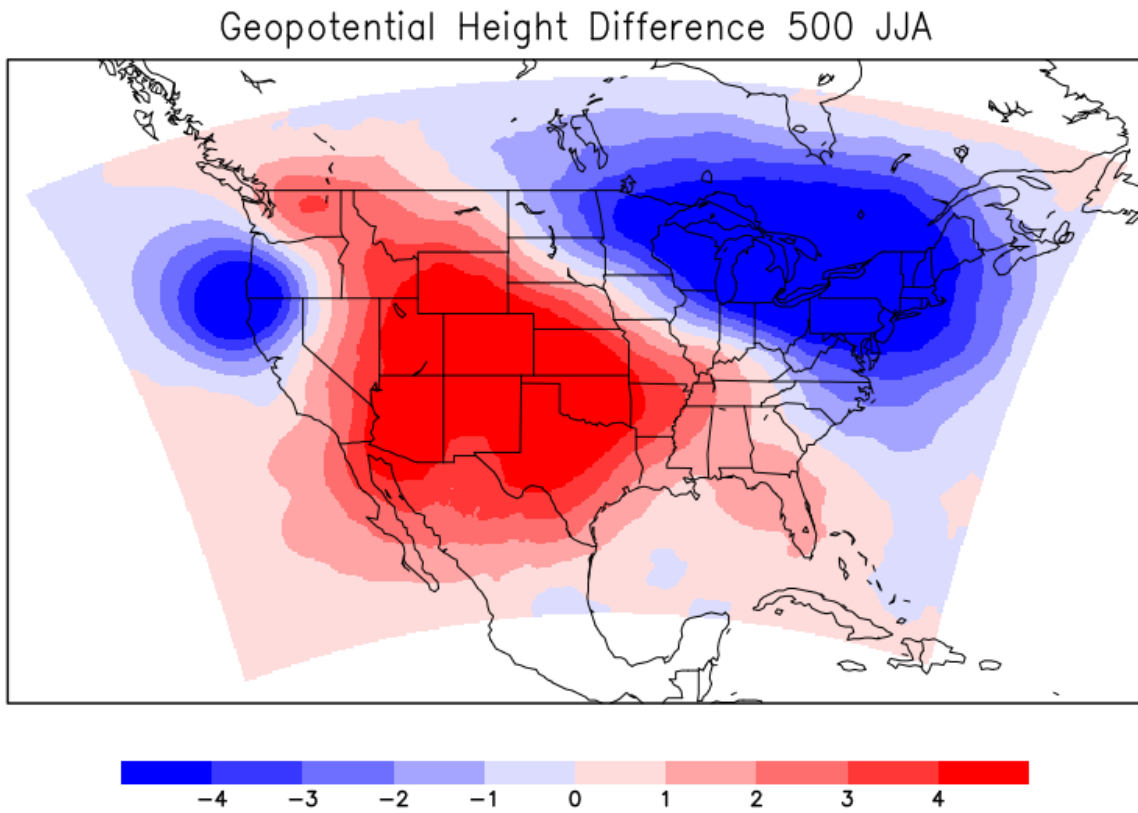


Figure 33. June, July, and August mean geopotential height difference in meters (IRR-NOIR) at 500 hPa.

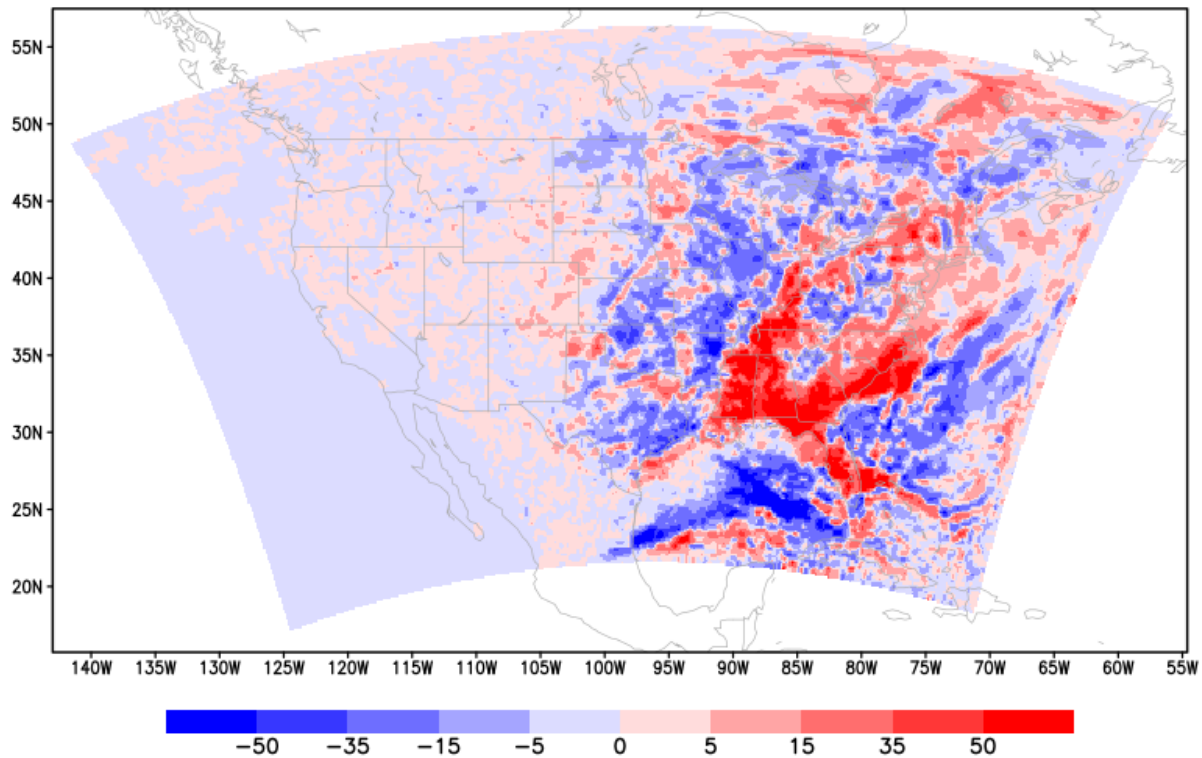


Figure 34. June, July, and August total precipitation difference in mm (IRR-NOIR).

GP cross-sections of mean wind speed differences (IRR-NOIR) are shown in figures 35-38. Starting in June the low-level winds have predominantly decreased during all hours of the simulation in some areas by as much as 2 m/s. Upper level wind speeds, however, have mostly increased on the order of 1 m/s. In July this pattern switches and the majority of upper level winds have decreased while winds beneath 700 hPa have dramatically increased by as much as 2 m/s. August shows wind speed differences more similar to June except for overnight, specifically for 06 UTC. For the entire three month simulation upper-level winds have primarily increased while low-level winds decrease more as you move eastward. There is also an area of increased

low to mid-level winds along the gently upward sloping terrain moving towards the Rocky Mountains.

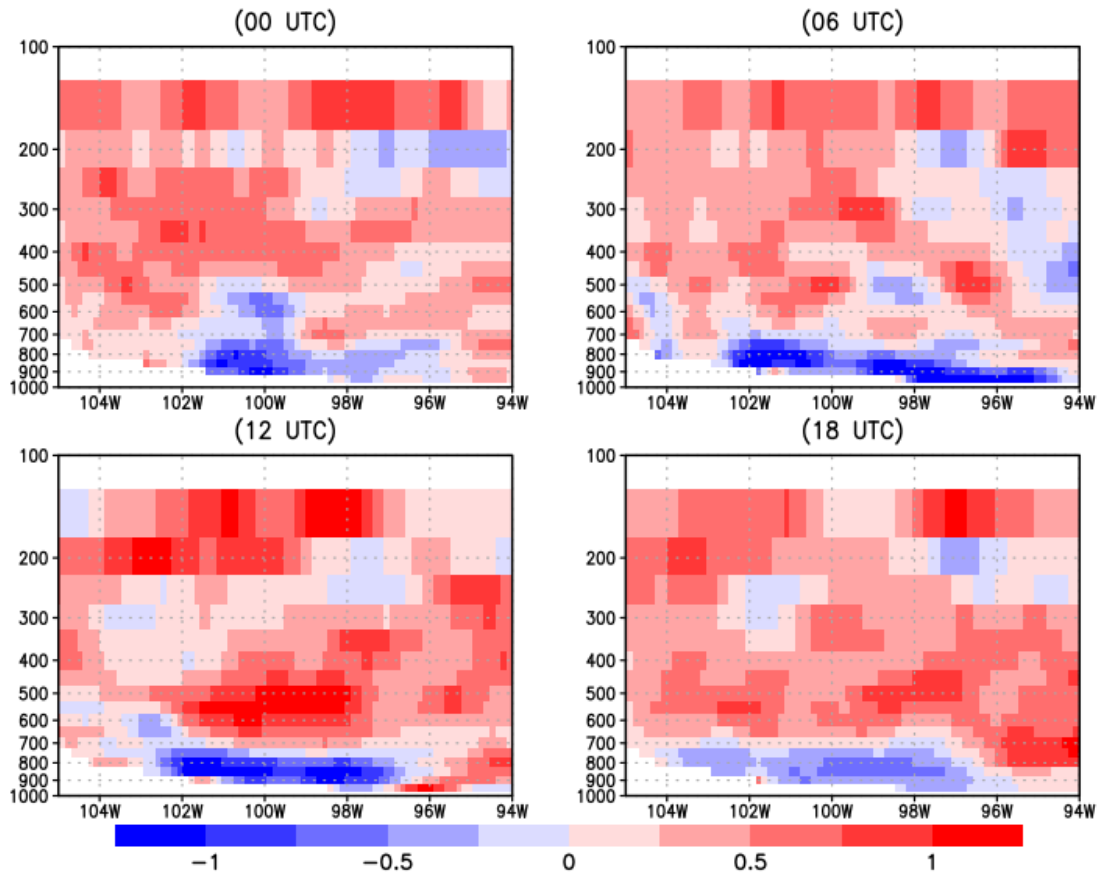


Figure 35. June mean vertical wind speed (m/s) cross-section differences (IRR-NOIR). Cross-section centered on latitude 37.5°N spanning longitudes 105°W-94°W.

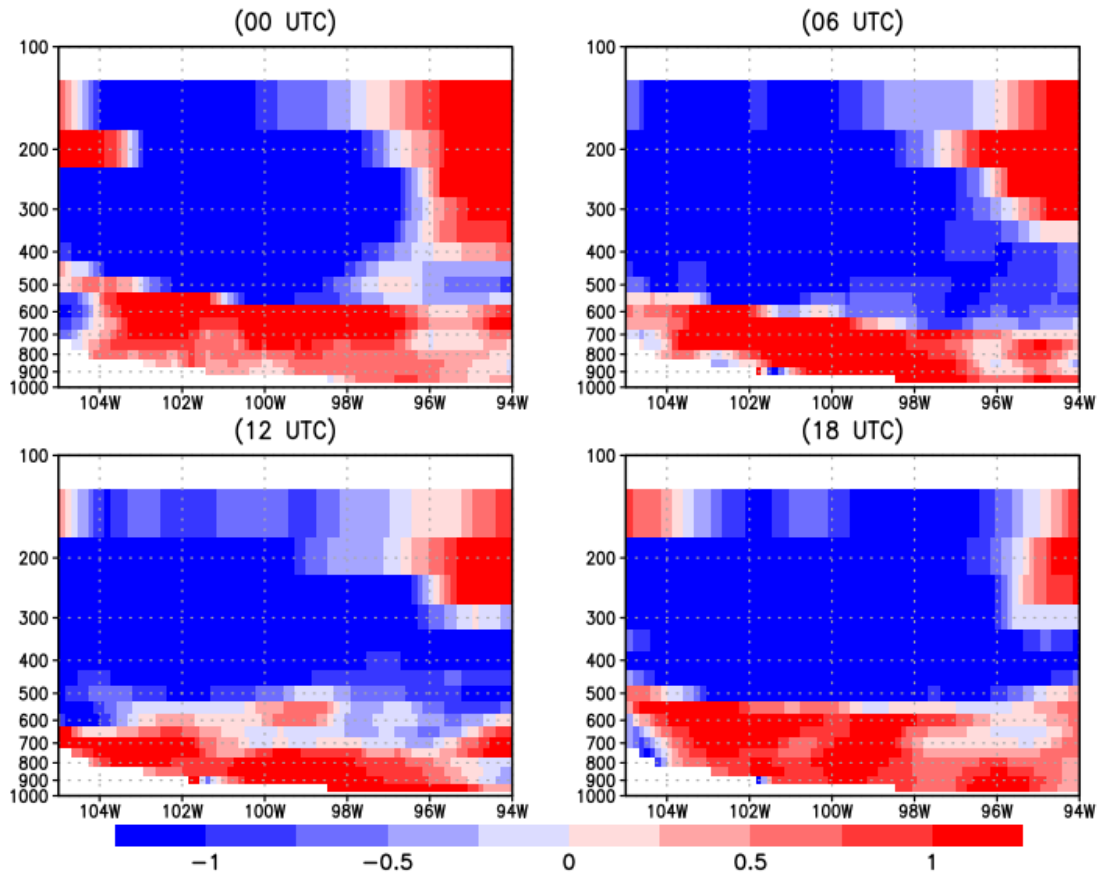


Figure 36. July mean vertical wind speed (m/s) cross-section differences (IRR-NOIR). Cross-section centered on latitude 37.5°N spanning longitudes 105°W-94°W.

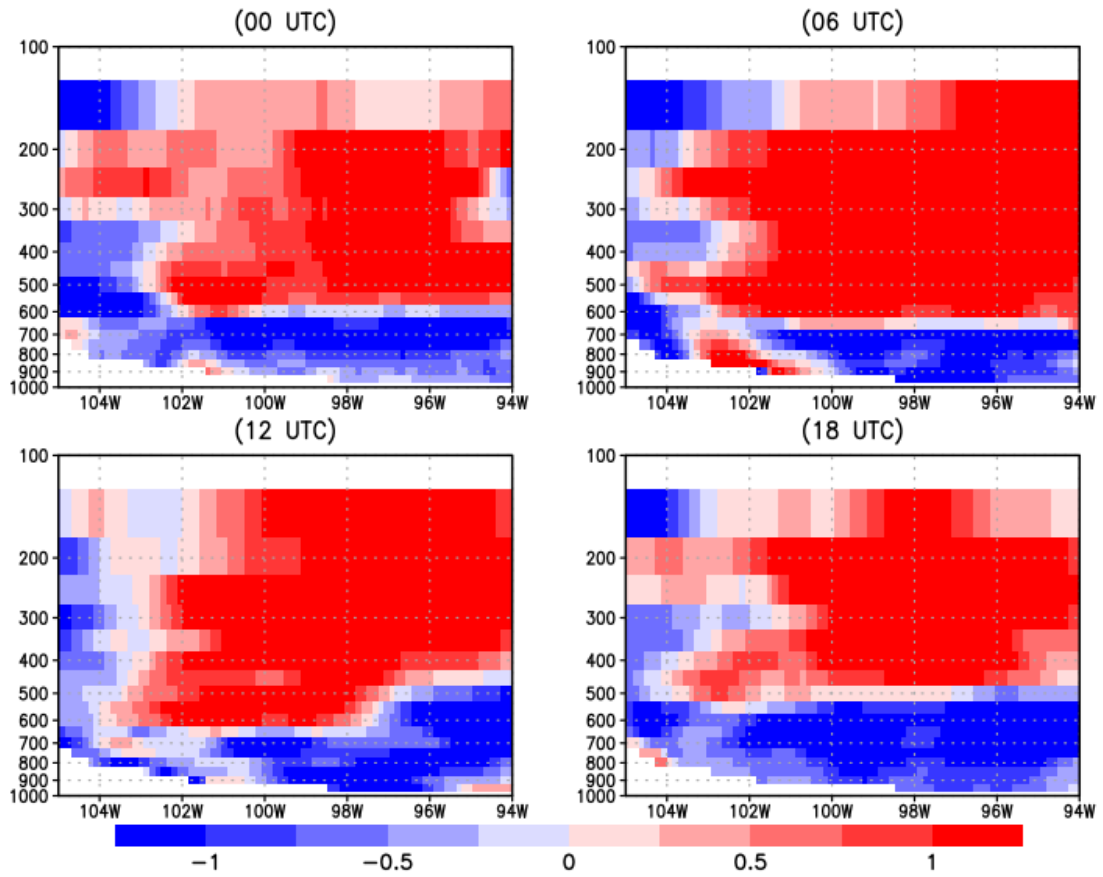


Figure 37. August mean vertical wind speed (m/s) cross-section differences (IRR-NOIR). Cross-section centered on latitude 37.5°N spanning longitudes 105°W-94°W.

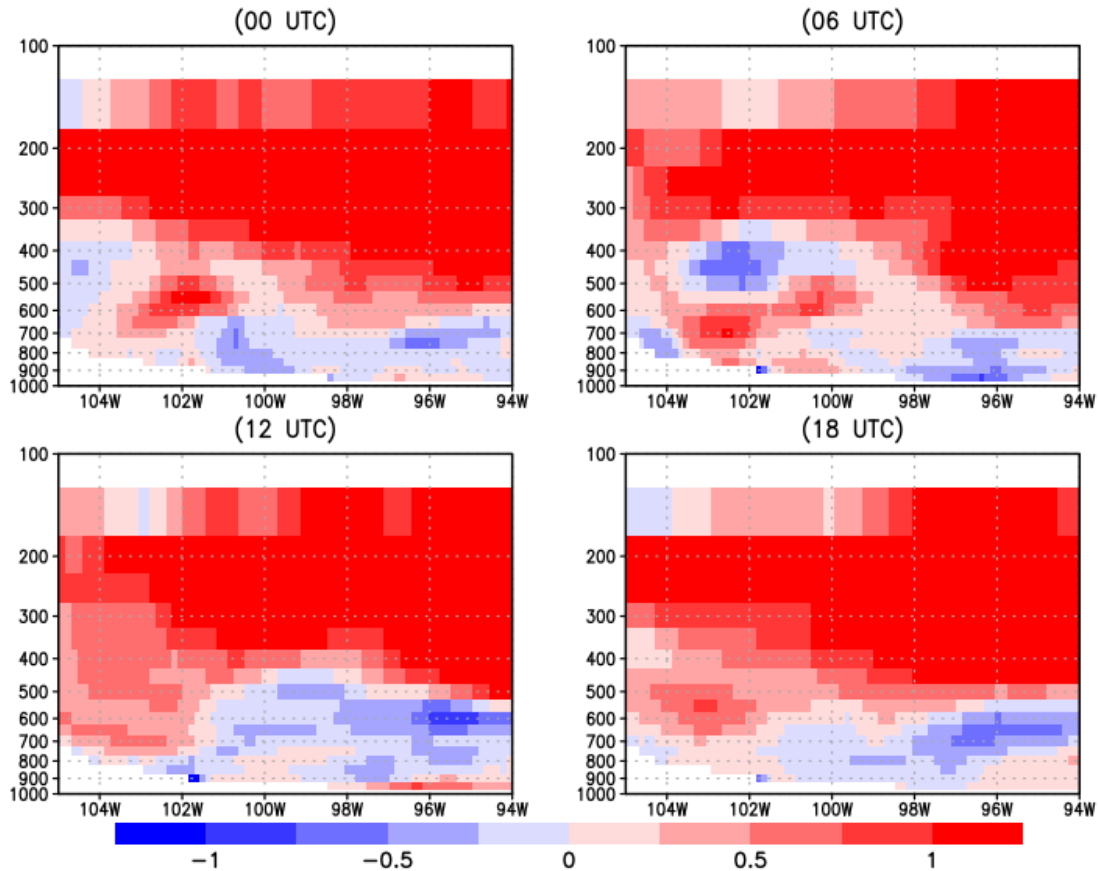


Figure 38. June, July, and August mean vertical wind speed (m/s) cross-section differences (IRR-NOIR). Cross-section centered on latitude 37.5°N spanning longitudes 105°W-94°W.

Separating the wind into its U (Figures 39-42) and V (Figures 43-46) components where differences in June for U and V are relatively small to the changes in July and August. In July, the U component is larger nearly the entire width of the cross-section. In August, the western portion decreases possibly due in part to the strengthened central high pressure mentioned above. The V component increases greatly in July where the southerly component of the wind is larger across the all low-level winds corresponding with the increased GPLLJ speeds. July seems to dominate the three-month mean as August V-component speeds are mostly smaller except for the eastern edge of the GP as the terrain begins to rise. The W-component (Figures 47-50) of the wind does not show strong spatial nor diurnal patterns.

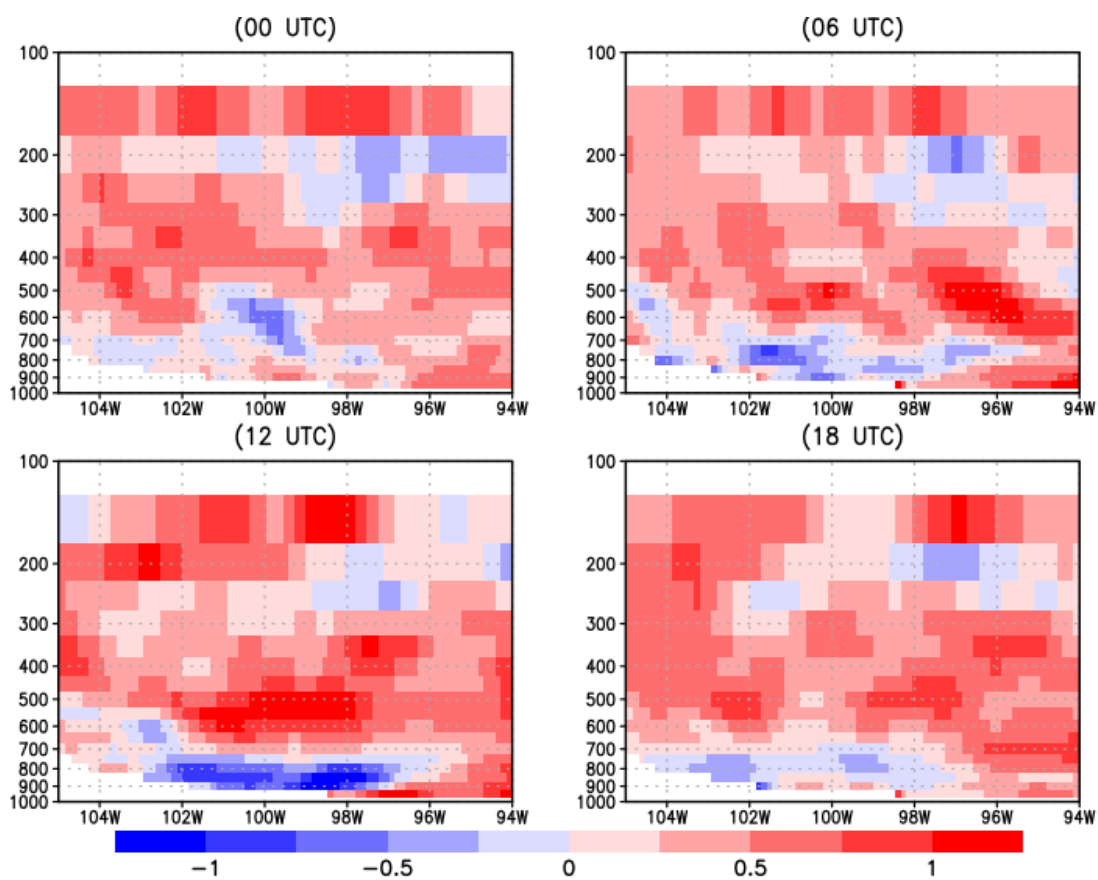


Figure 39. June mean u-wind component (m/s) vertical cross-section difference (IRR-NOIR). Cross-section centered on latitude 37.5°N spanning longitudes 105°W-94°W.

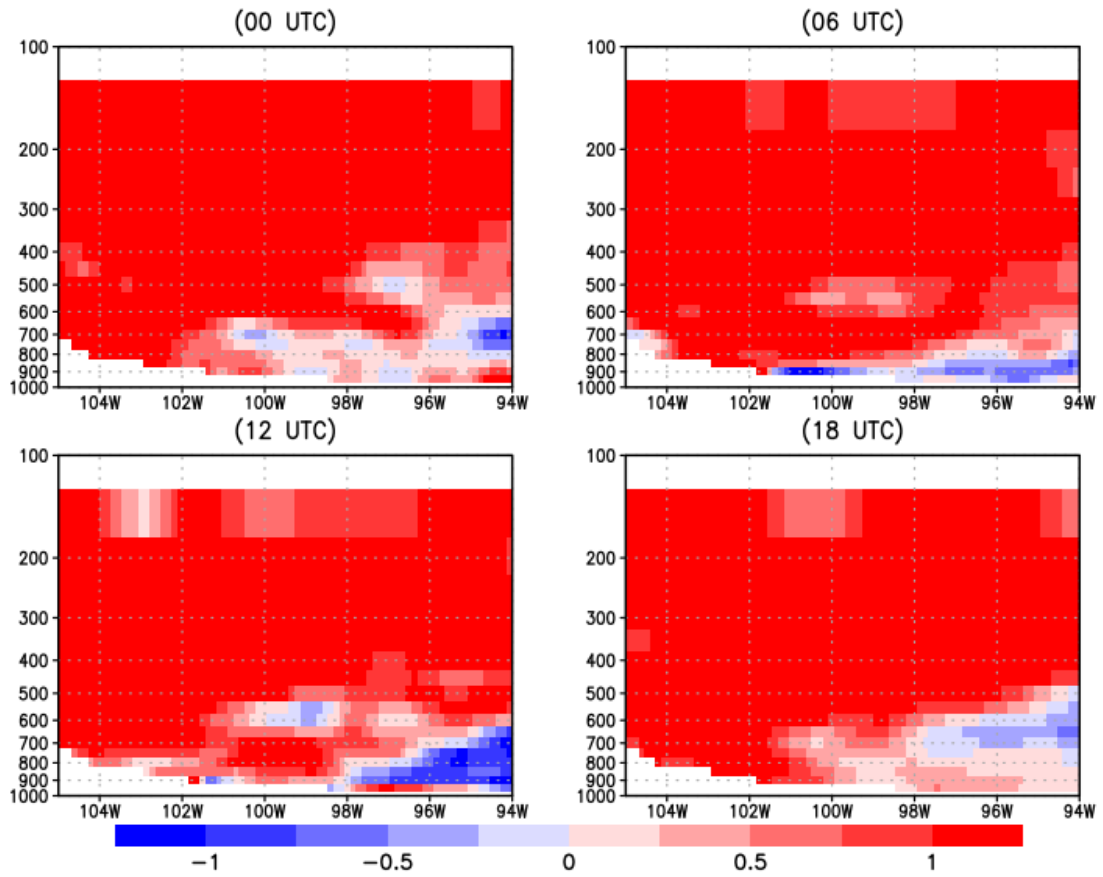


Figure 40. July mean u-wind component (m/s) vertical cross-section difference (IRR-NOIR). Cross-section centered on latitude  $37.5^{\circ}\text{N}$  spanning longitudes  $105^{\circ}\text{W}$ - $94^{\circ}\text{W}$ .

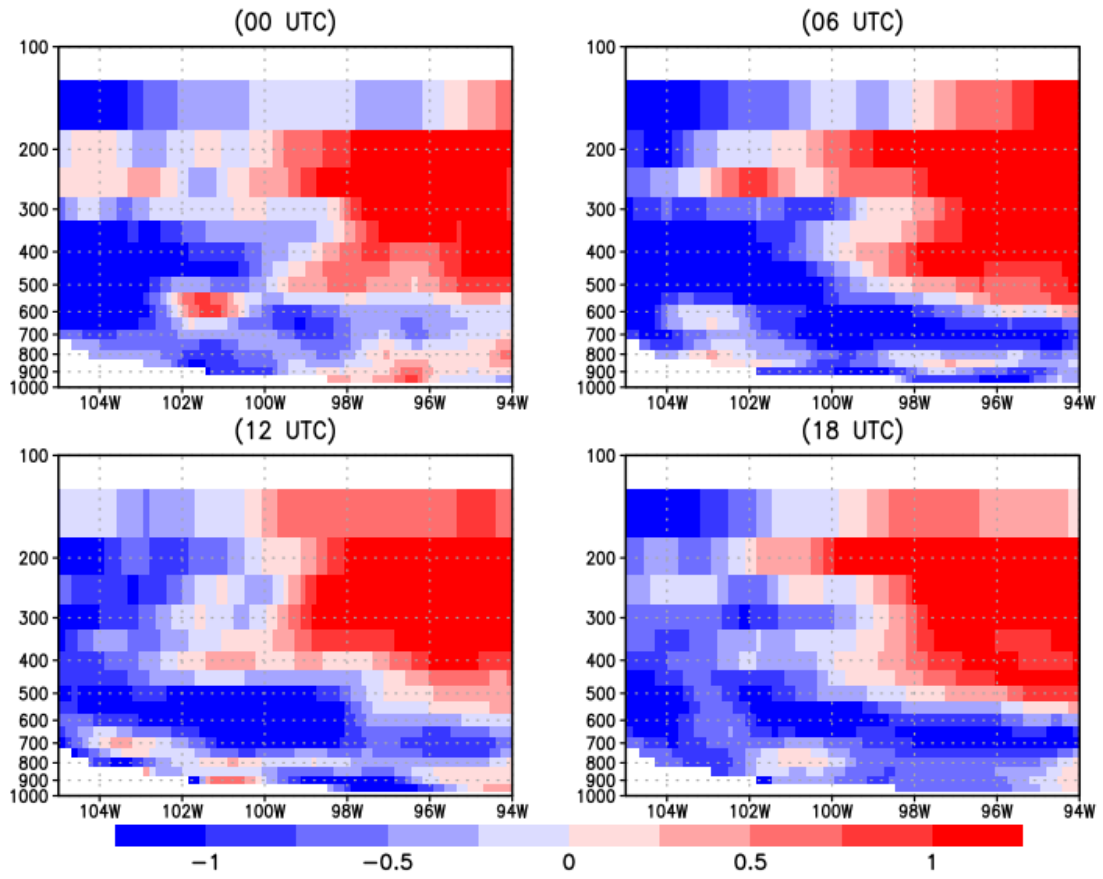


Figure 41. August mean u-wind component (m/s) vertical cross-section difference (IRR-NOIR). Cross-section centered on latitude 37.5°N spanning longitudes 105°W-94°W.

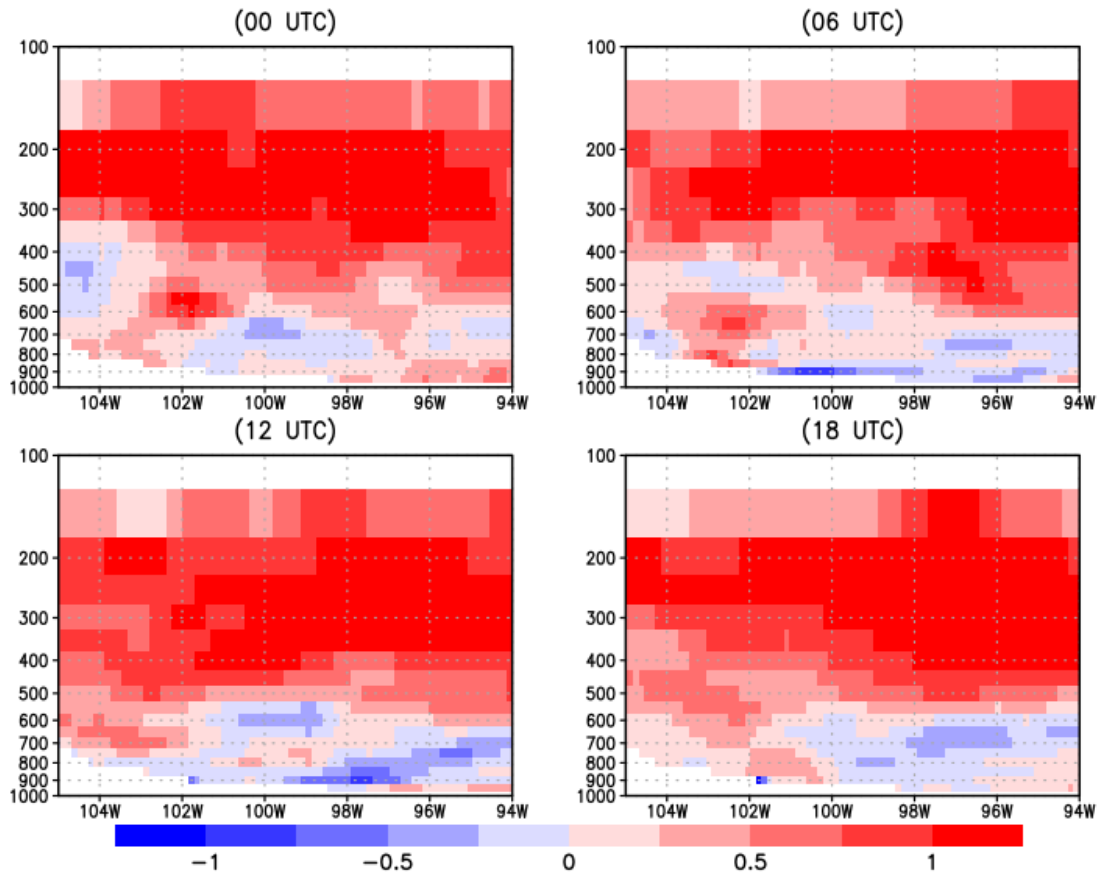


Figure 42. June, July, and August mean u-wind component (m/s) vertical cross-section difference (IRR-NOIR). Cross-section centered on latitude  $37.5^{\circ}\text{N}$  spanning longitudes  $105^{\circ}\text{W}$ - $94^{\circ}\text{W}$ .

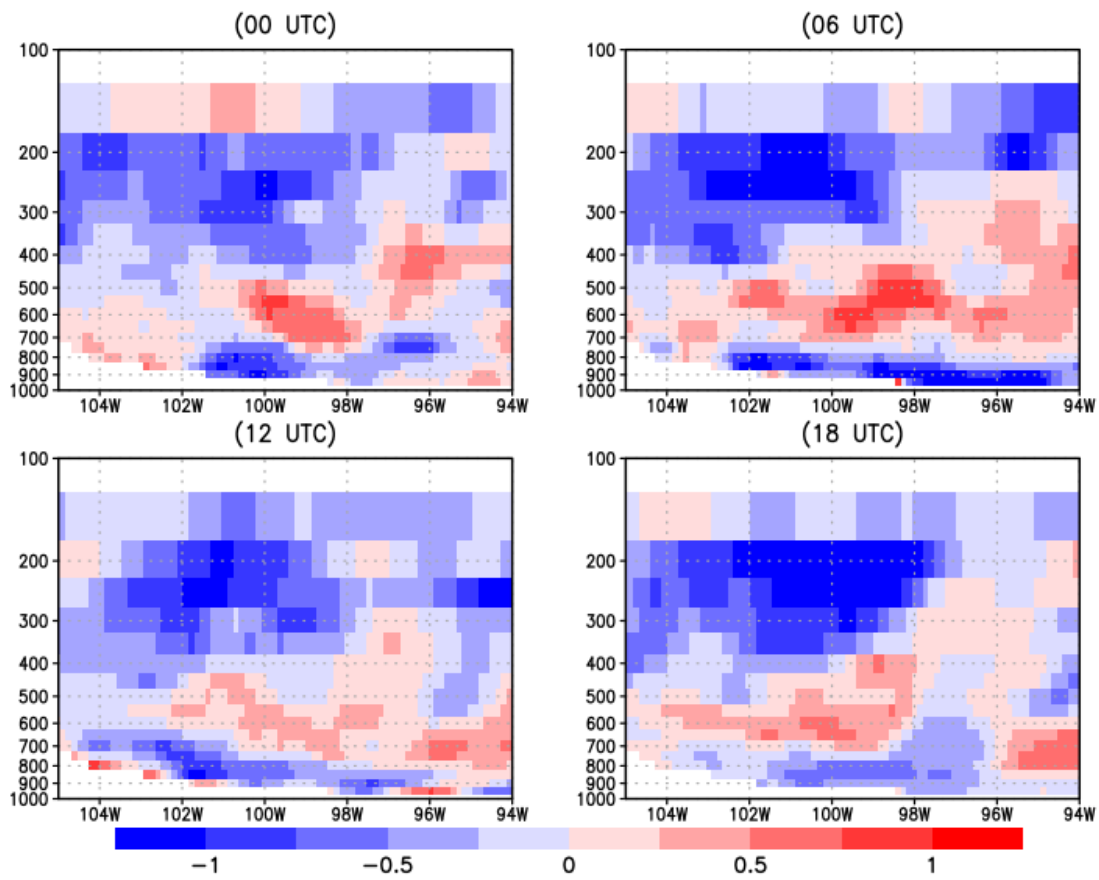


Figure 43. June mean v-wind component (m/s) vertical cross-section difference (IRR-NOIR). Cross-section centered on latitude 37.5°N spanning longitudes 105°W-94°W.

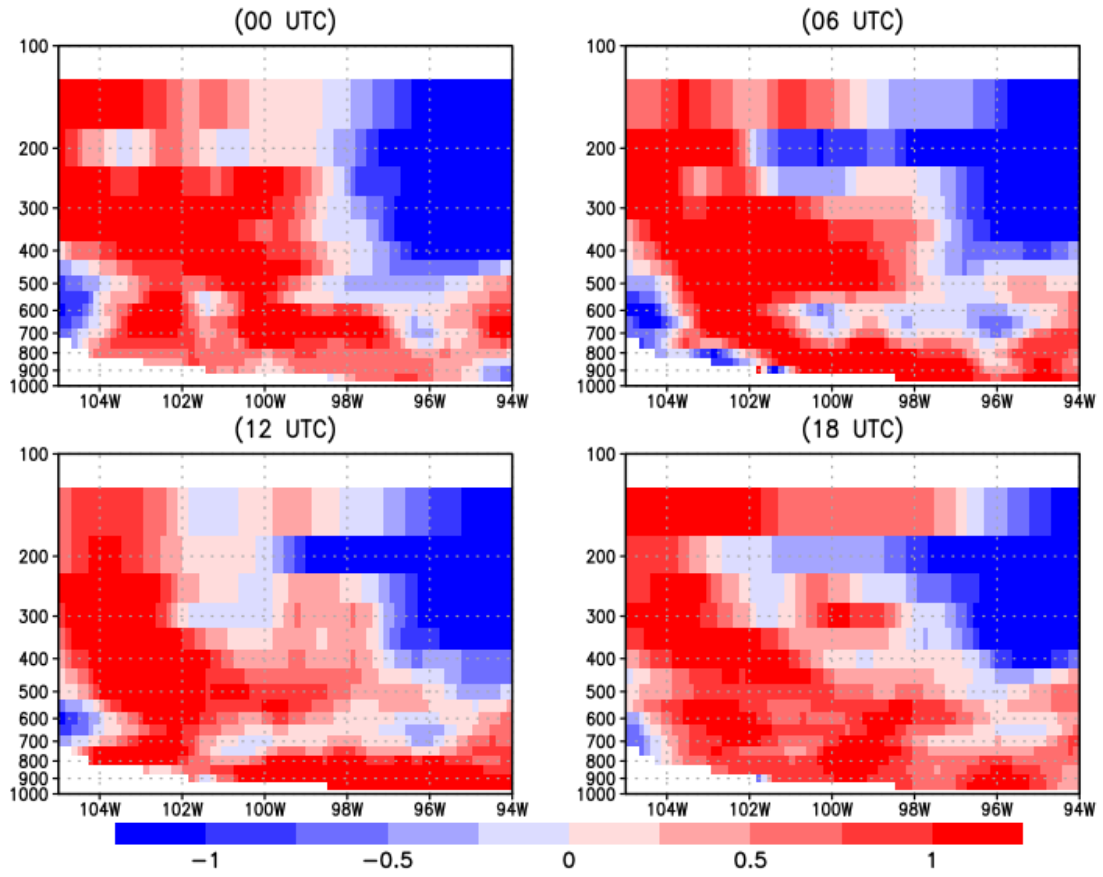


Figure 44. July mean v-wind component (m/s) vertical cross-section difference (IRR-NOIR). Cross-section centered on latitude 37.5°N spanning longitudes 105°W-94°W.

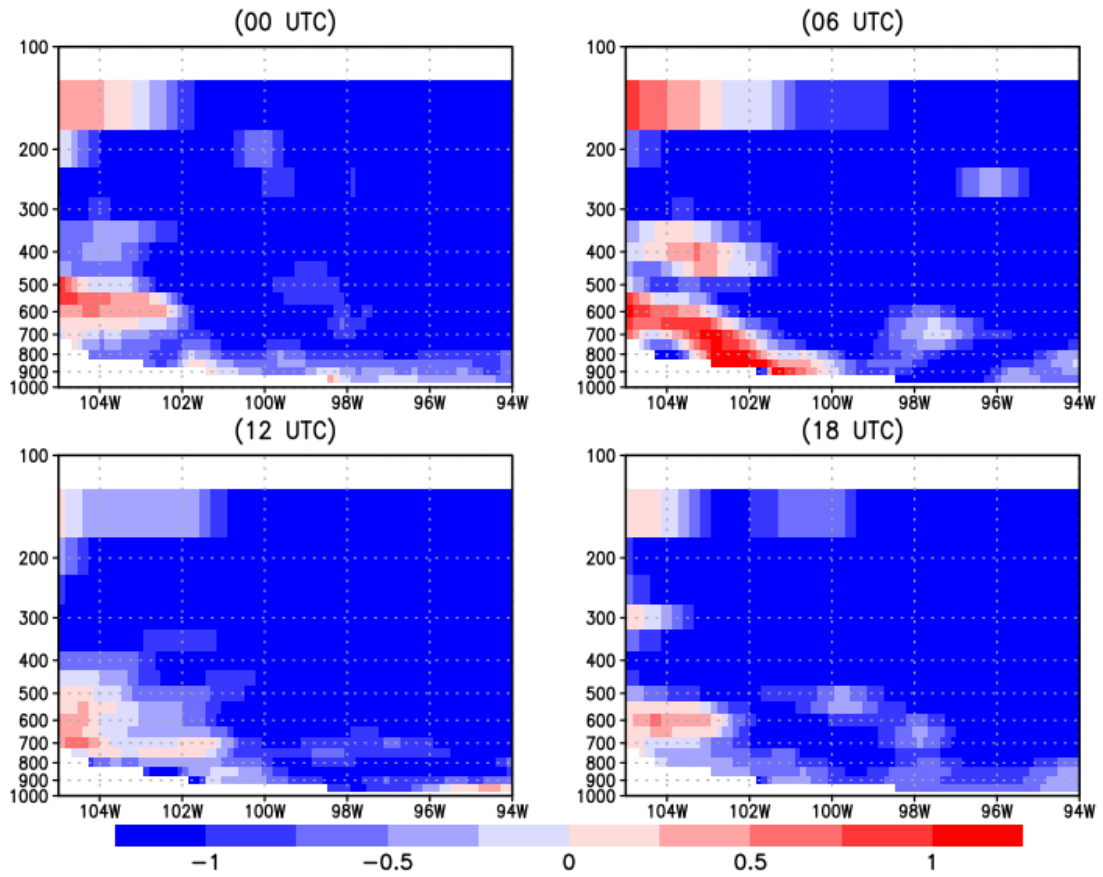


Figure 45. August mean v-wind component (m/s) vertical cross-section difference (IRR-NOIR). Cross-section centered on latitude 37.5°N spanning longitudes 105°W-94°W.

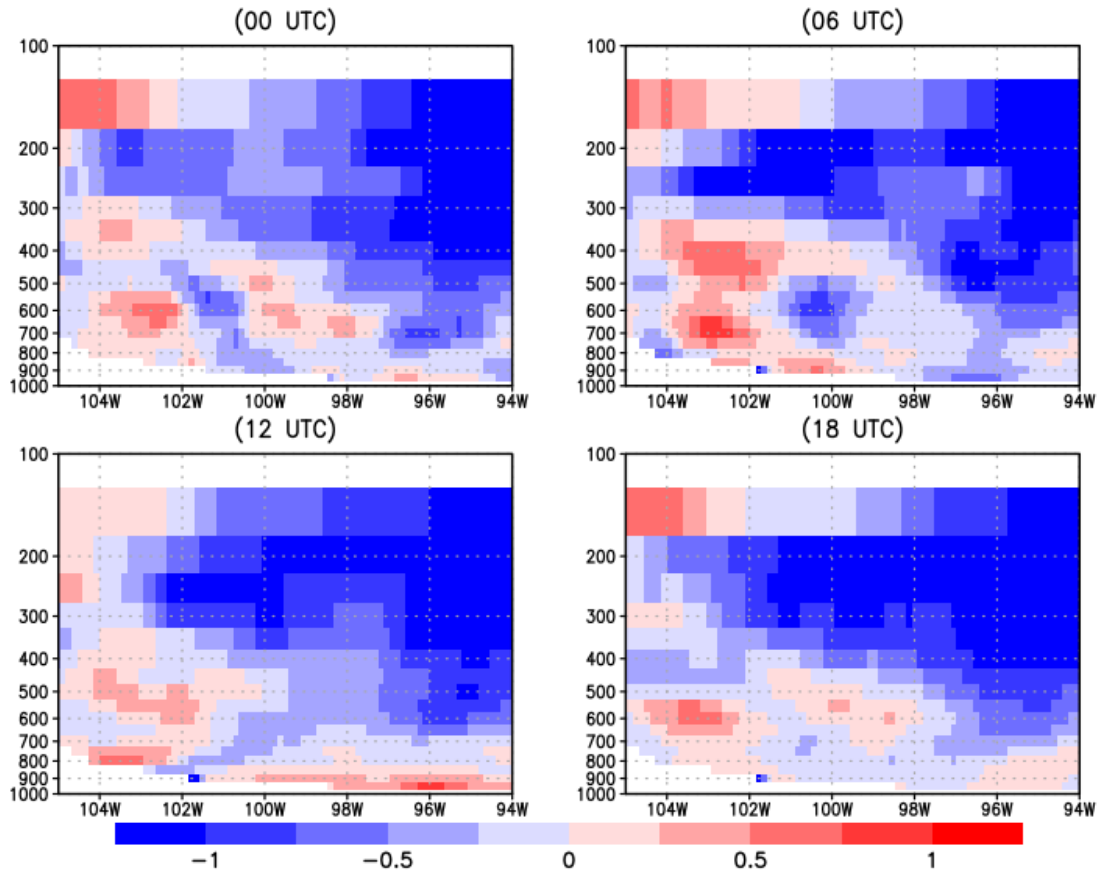


Figure 46. June, July, and August mean v-wind component (m/s) vertical cross-section difference (IRR-NOIR). Cross-section centered on latitude 37.5°N spanning longitudes 105°W-94°W.

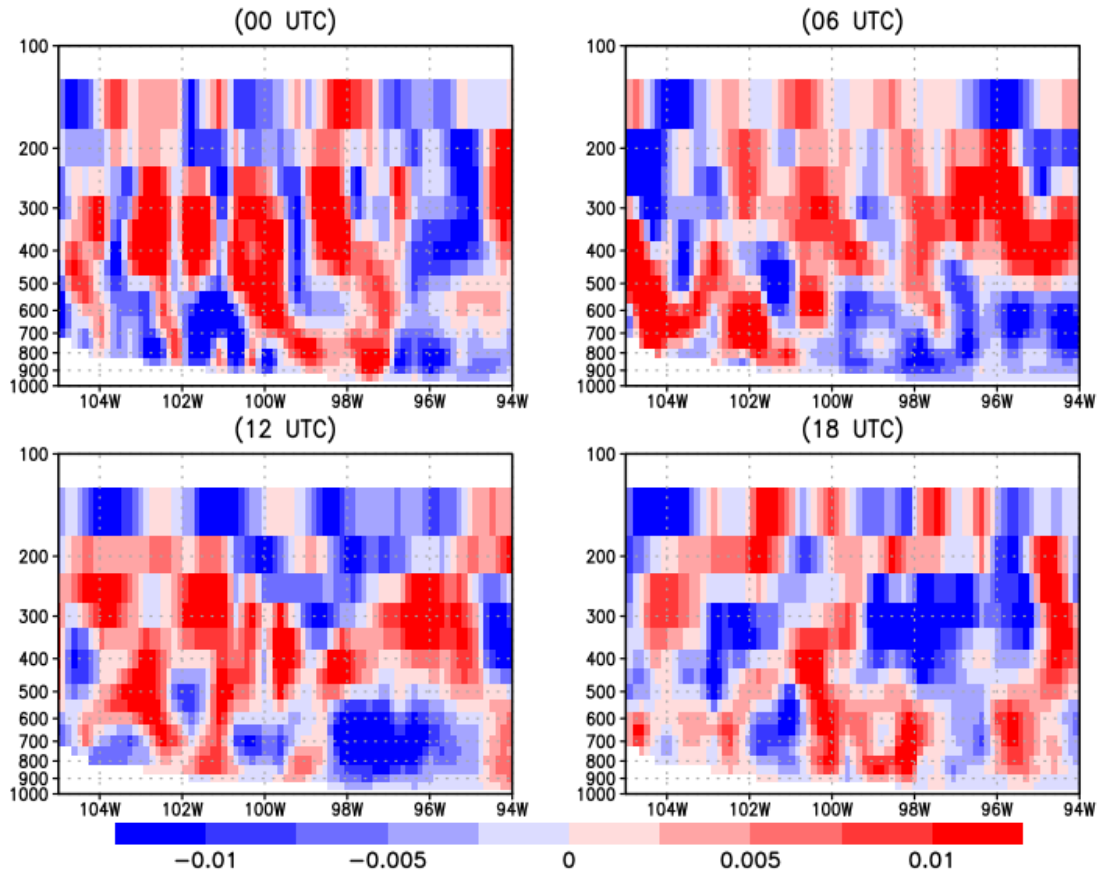


Figure 47. June mean w-wind component (m/s) vertical cross-section difference (IRR-NOIR). Cross-section centered on latitude 37.5°N spanning longitudes 105°W-94°W.

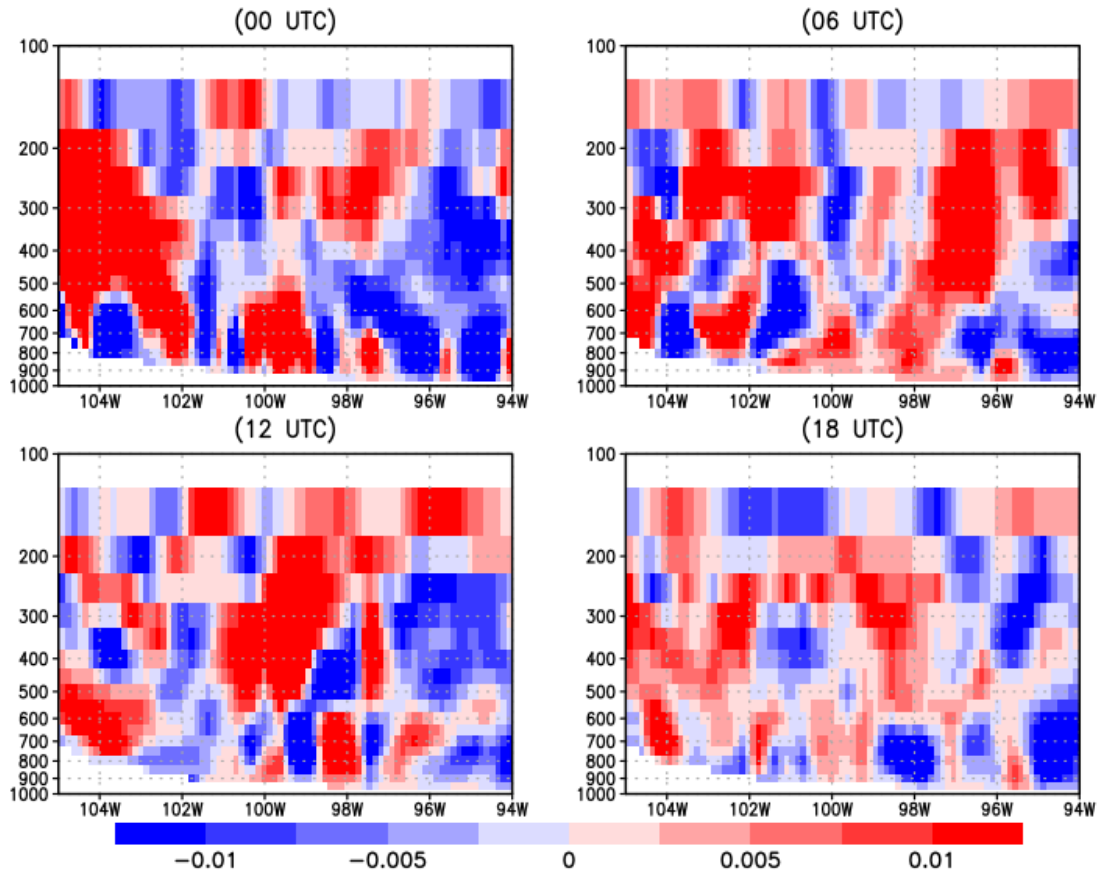


Figure 48. July mean w-wind component (m/s) vertical cross-section difference (IRR-NOIR). Cross-section centered on latitude 37.5°N spanning longitudes 105°W-94°W.

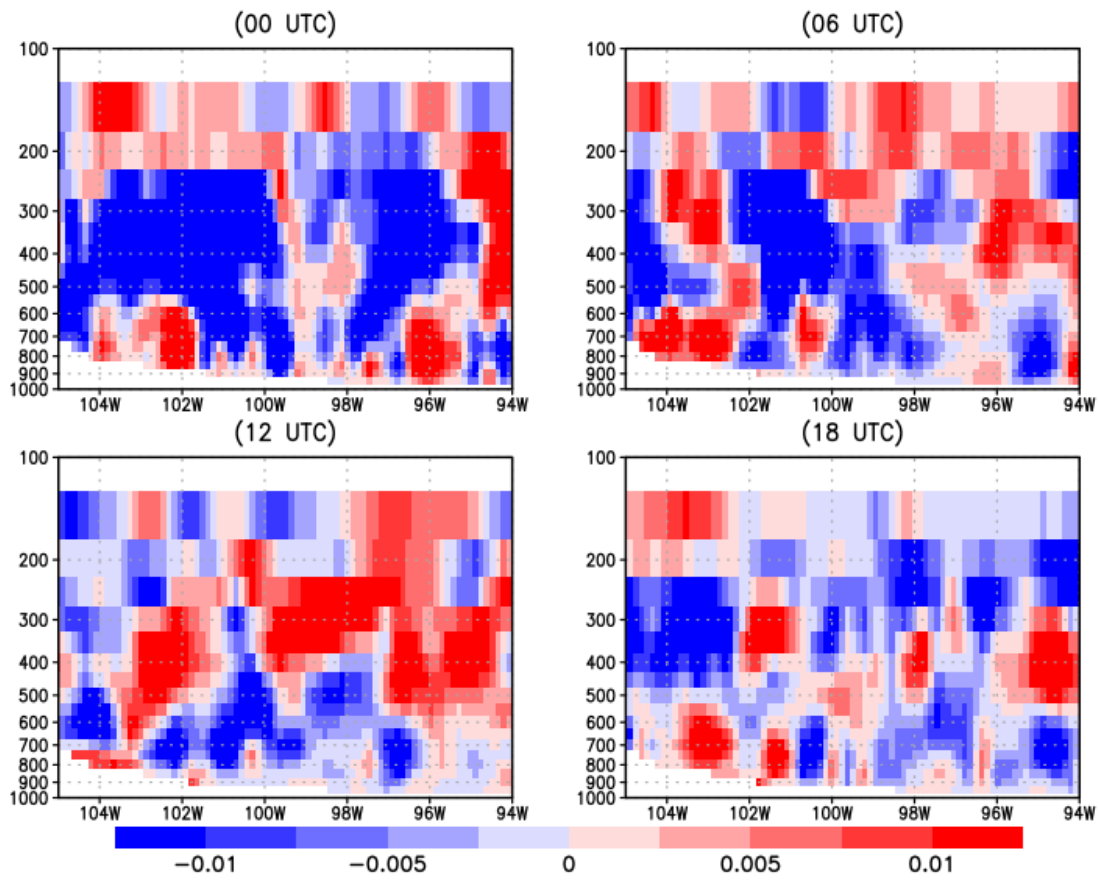


Figure 49. August mean w-wind component (m/s) vertical cross-section difference (IRR-NOIR). Cross-section centered on latitude 37.5°N spanning longitudes 105°W-94°W.

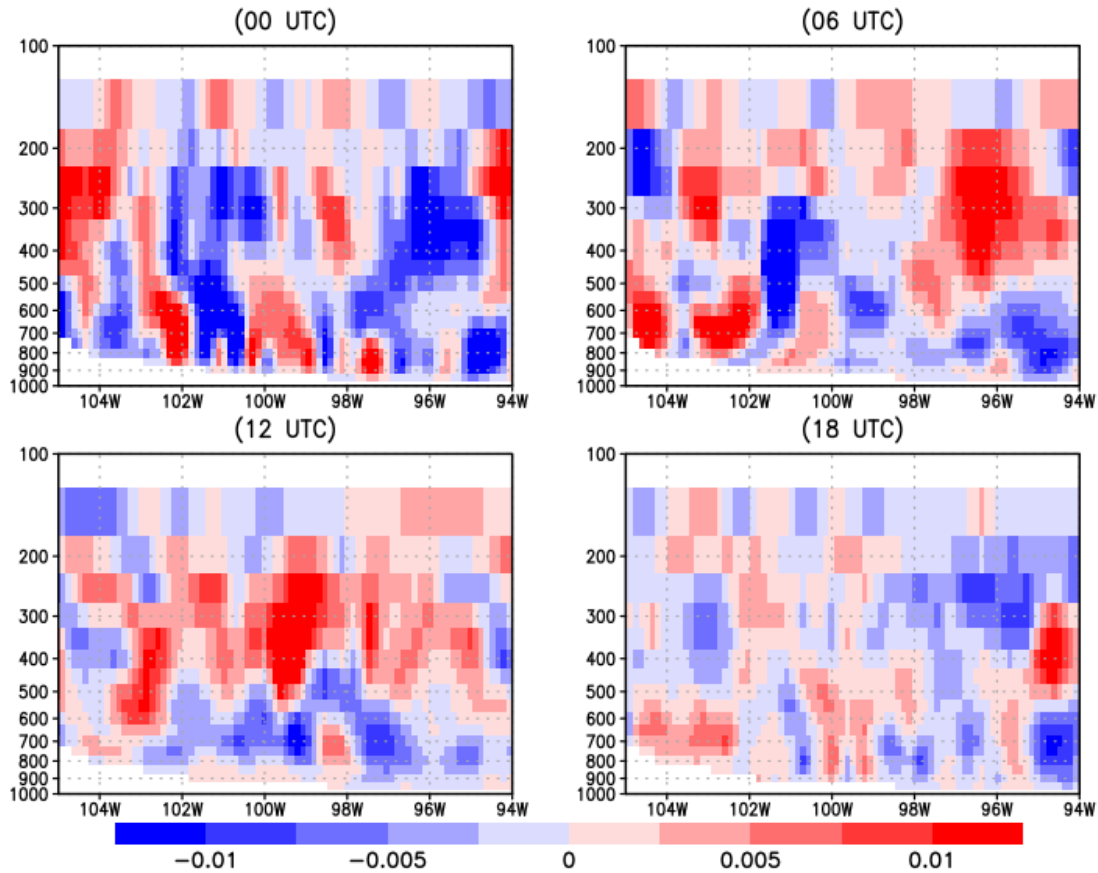


Figure 50. June, July, and August mean w-wind component (m/s) vertical cross-section difference (IRR-NOIR). Cross-section centered on latitude  $37.5^{\circ}\text{N}$  spanning longitudes  $105^{\circ}\text{W}$ - $94^{\circ}\text{W}$ .

Figures 51-54 show the mean difference in vertical water vapor mixing ratio. In June before much irrigation has been applied there is little difference between the two simulations. In July the mixing ratios through 500 hPa show at least some degree of increased water vapor with similar increases at all times of the day. By August the extent to which irrigation has suppressed precipitation and dried out what was already an exceptionally dry year is obvious as the lowest levels of the atmosphere have decreased mixing ratios. The trend towards decreasing mixing ratios comes through more strongly when averaged across all three months where most of the figure shows decreased mixing ratios.

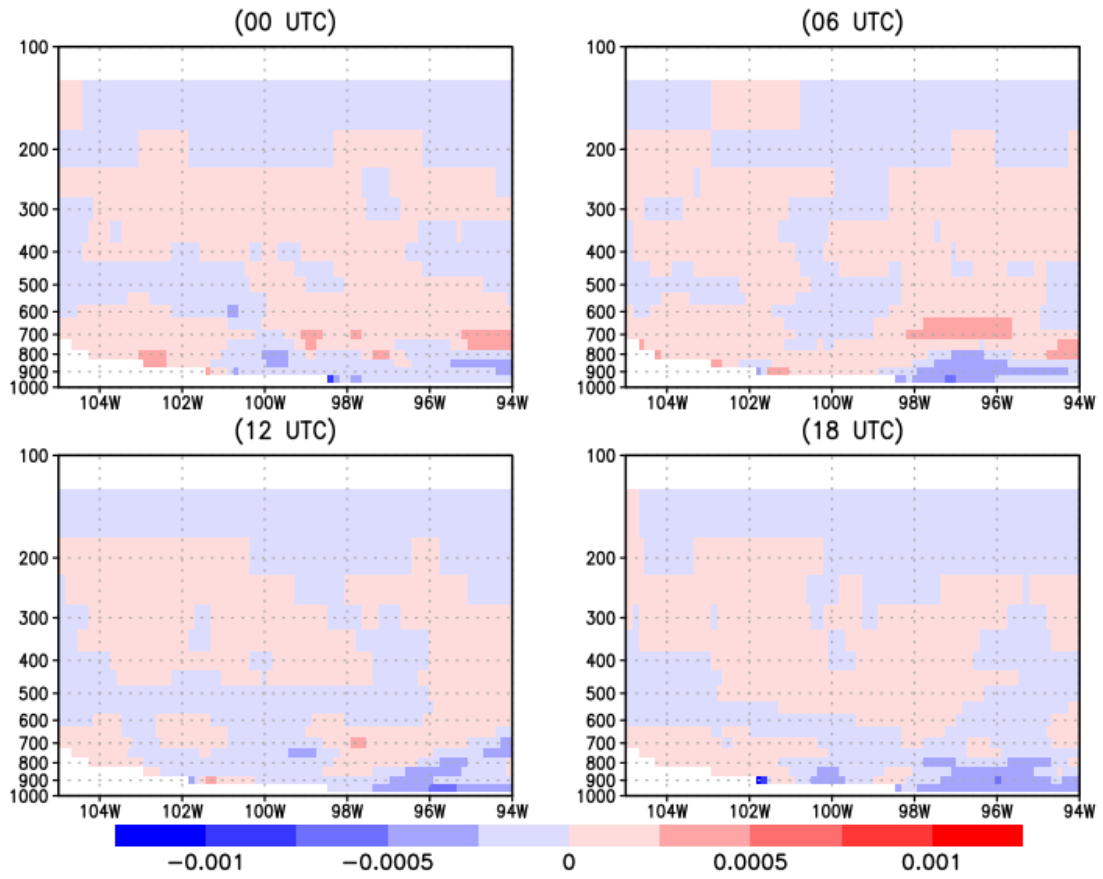


Figure 51. June mean water vapor mixing ratio (kg/kg) vertical cross-section difference (IRR-NOIR). Cross-section centered on latitude 37.5°N spanning longitudes 105°W-94°W

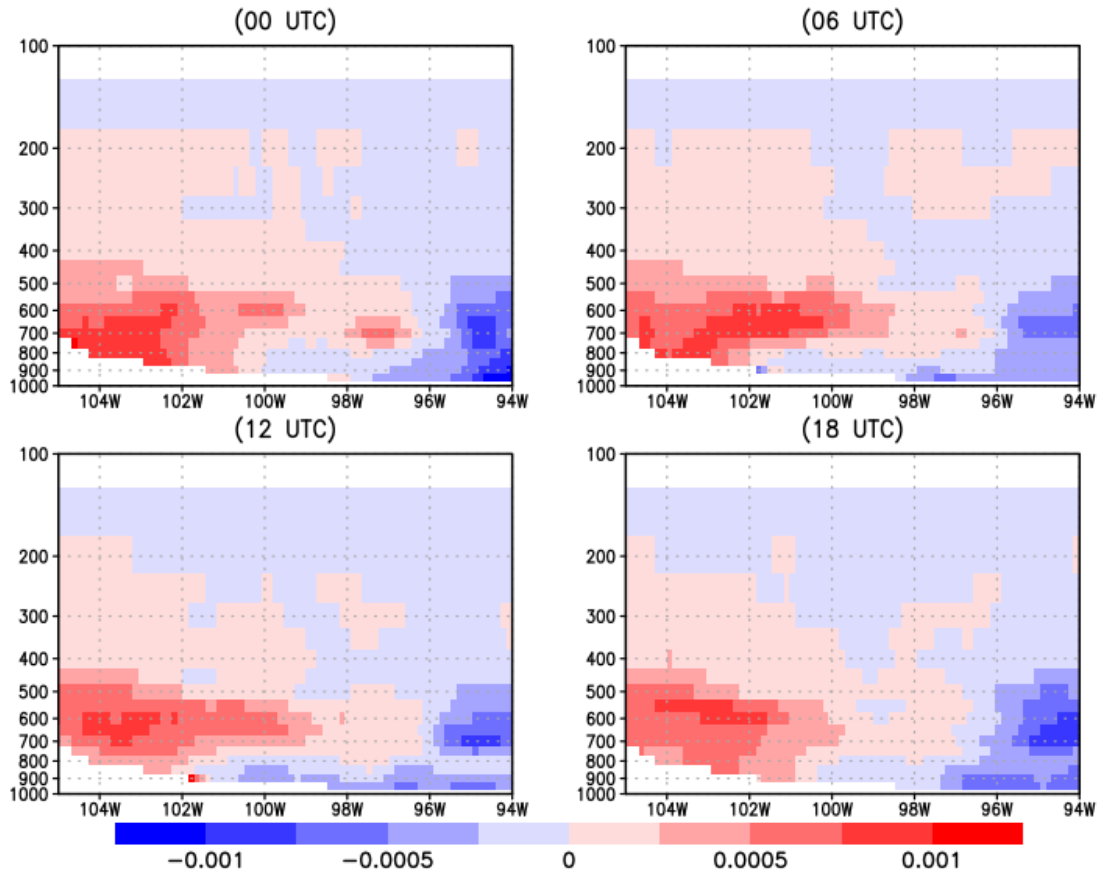


Figure 52. July mean water vapor mixing ratio (kg/kg) vertical cross-section difference (IRR-NOIR). Cross-section centered on latitude 37.5°N spanning longitudes 105°W-94°W.

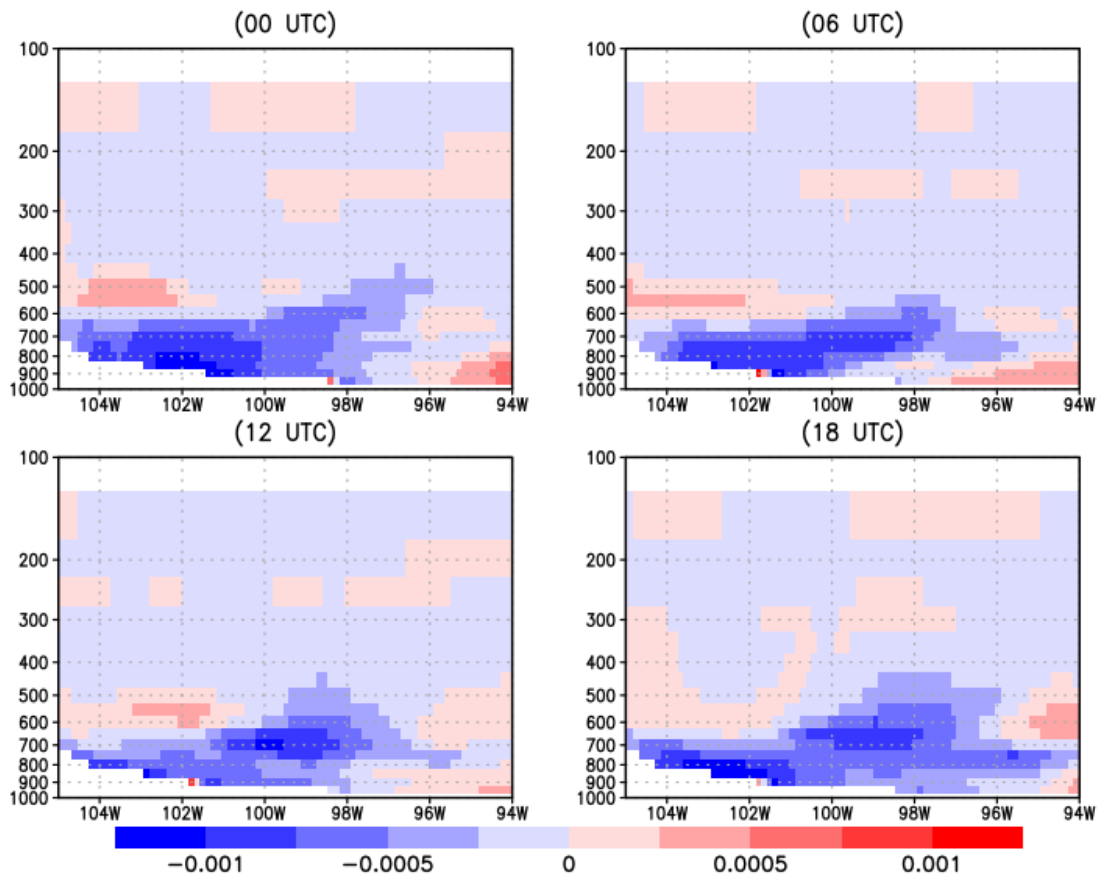


Figure 53. August mean water vapor mixing ratio (kg/kg) vertical cross-section difference (IRR-NOIR). Cross-section centered on latitude 37.5°N spanning longitudes 105°W-94°W.

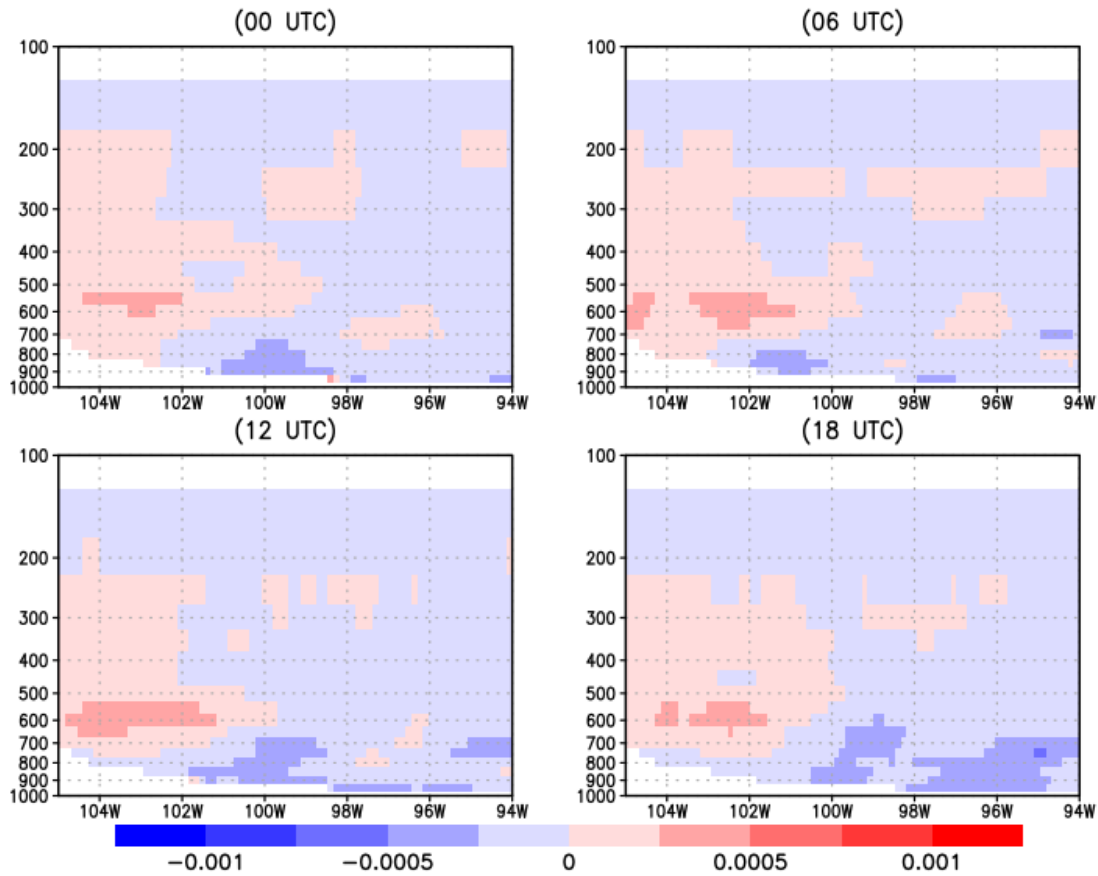


Figure 54. June, July, and August mean water vapor mixing ratio (kg/kg) vertical cross-section difference (IRR-NOIR). Cross-section centered on latitude 37.5°N spanning longitudes 105°W-94°W.

The vertical U, V, W, and total wind speed wind profiles shown in Figures 55 – 58 show vertical mean differences across the GP between 105°W 94°W and 30°N and 45°N. Figure 55 shows the vertical profiles for the U component of the wind for four different times throughout the day and across all three months of the simulation. In June, the differences are very small across all hours, but are consistently larger throughout the depth of the atmosphere. In July, the two times stand out, 06 UTC and 12 UTC. Below around 800 hPa the 06 UTC profile is slower in the IRR simulation than the NOIR, and for 12 UTC the IRR simulation is about the same magnitude stronger. Otherwise, as in June the upper level U-component is consistently larger. In

August, the magnitude of the differences is similar on either of the zero line. The interesting difference is that below 800 hPa all times of the day the differences are negative. For the JJA average the slightly strengthened westerlies show up as well as a slight decrease in the lower levels most strongly at 06 UTC. With respect to the GPLLJ it the V or north-south component that is most important, and compared the U-component Figure 56 shows much larger differences. For June, the lower levels show negative differences, between 750 hPa and 500 hPa positive differences, and above 500 hPa small negative differences. July is the month with the largest differences in the lower half of the atmosphere, with values approaching 0.75 m/s. This would suggest that the southerly component of wind is increased and potentially stronger LLJs. Also note, that the largest differences with stronger southerly V-components are for 06 UTC and 12 UTC the times where the GPLLJs are most common and the strongest. The differences in the W-component (Figure 57) of the wind after the month of June show predominantly larger than zero values, especially for the lower half of the atmosphere. Suggesting reduced vertical motion, supporting the relative lack of precipitation and stronger high pressure throughout the central US.

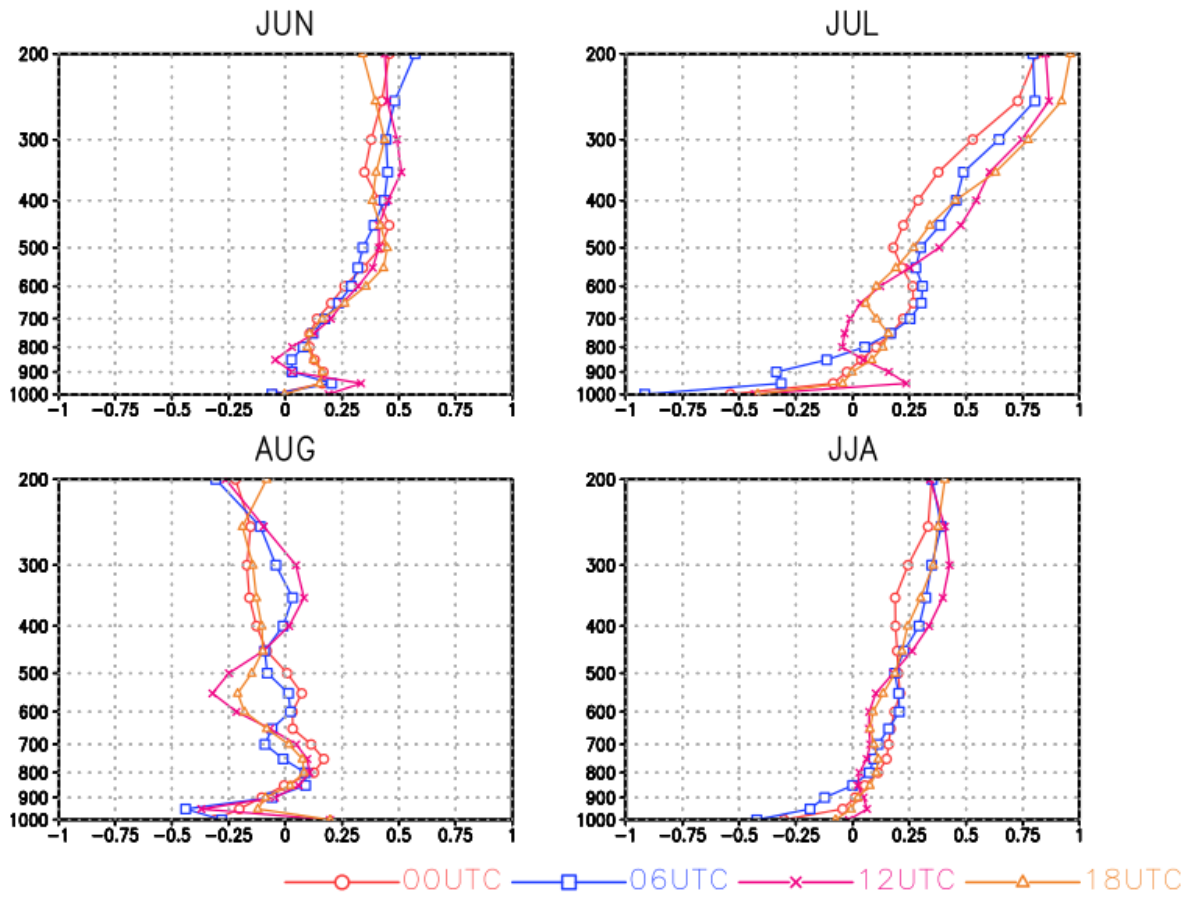


Figure 55. Mean vertical diurnal profiles of the u-wind component (m/s) difference (IRR-NOIR) over the Great Plains. Averaged for a box bounded between 105°W–94°W and 30°N–45°N.

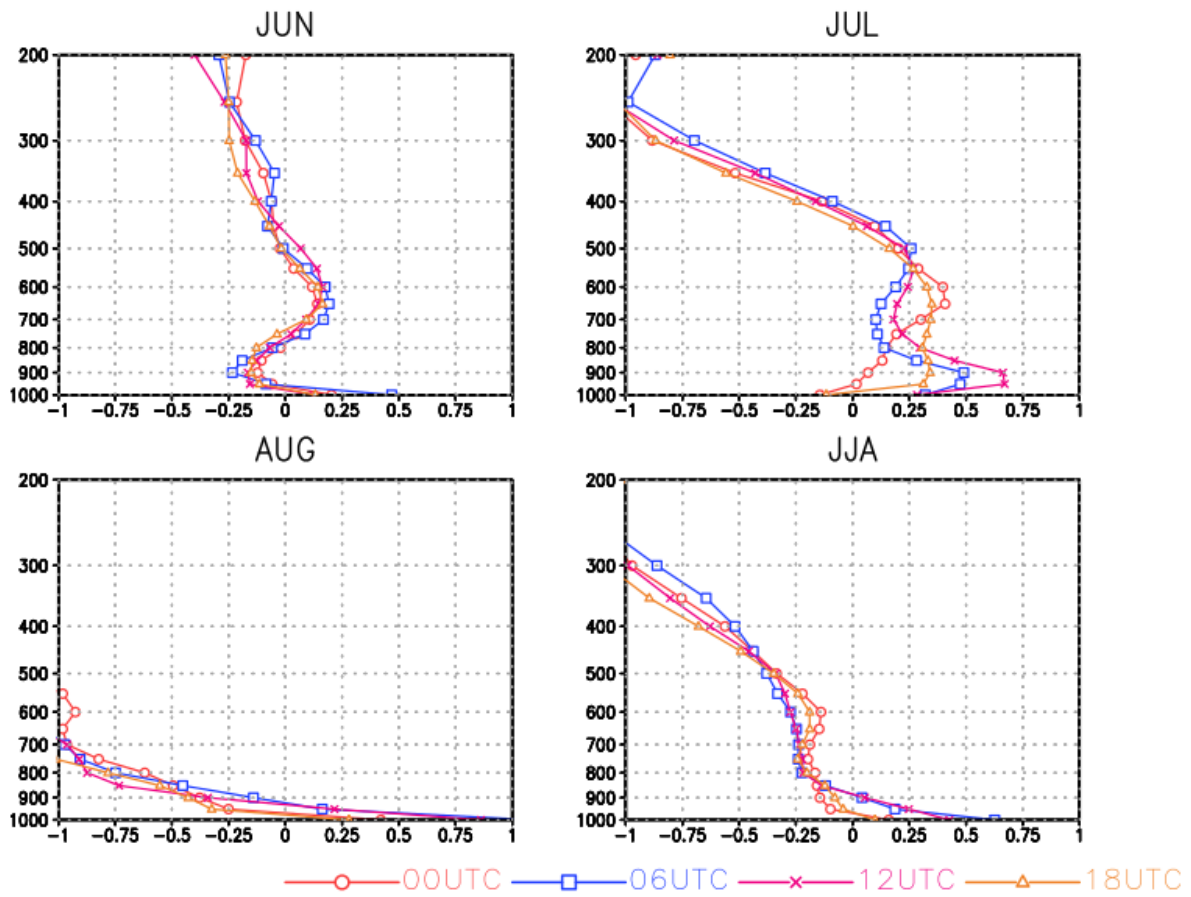


Figure 56. Mean vertical diurnal profiles of the v-wind component (m/s) difference (IRR-NOIR) over the Great Plains. Averaged for a box bounded between 105°W–94°W and 30°N–45°N.

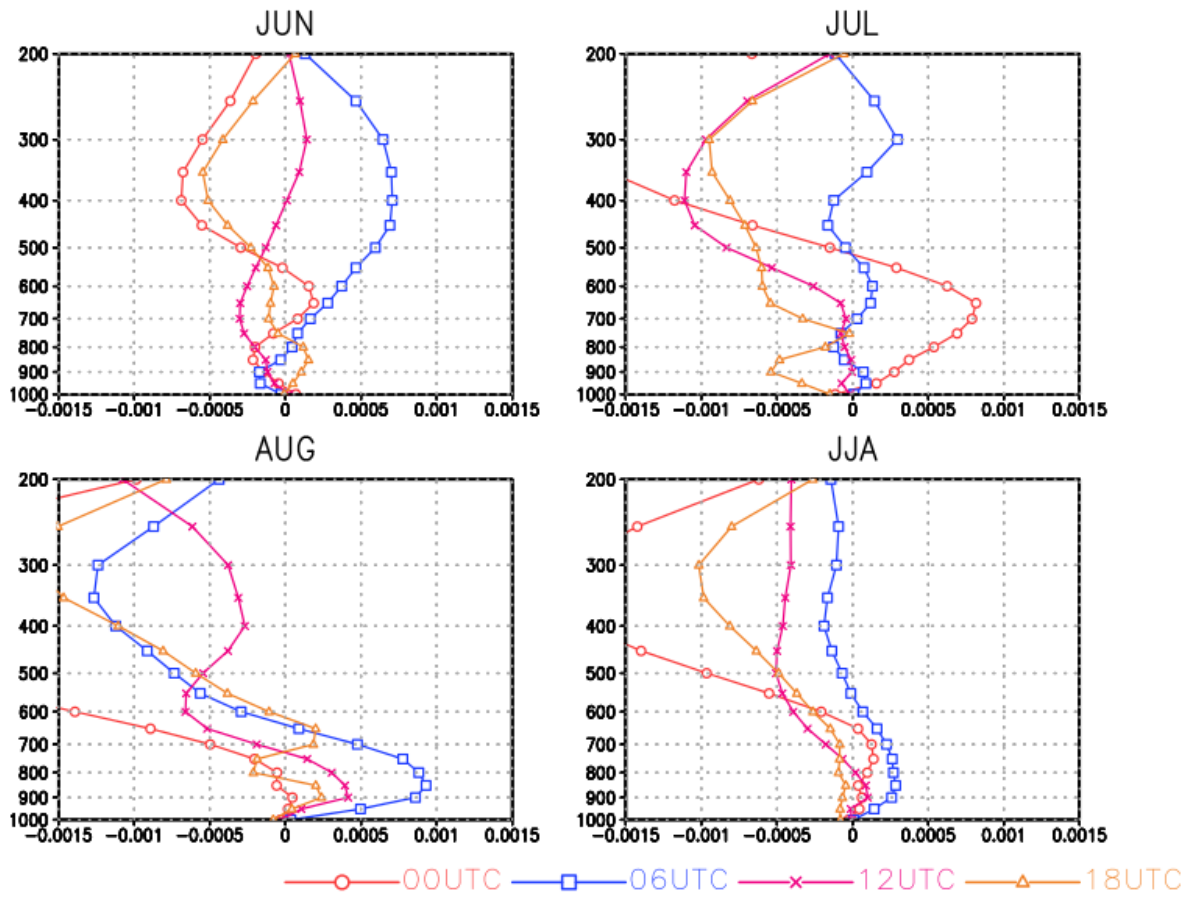


Figure 57. Mean vertical diurnal profiles of the w-wind component (m/s) difference (IRR-NOIR) over the Great Plains. Averaged for a box bounded between 105°W–94°W and 30°N–45°N.

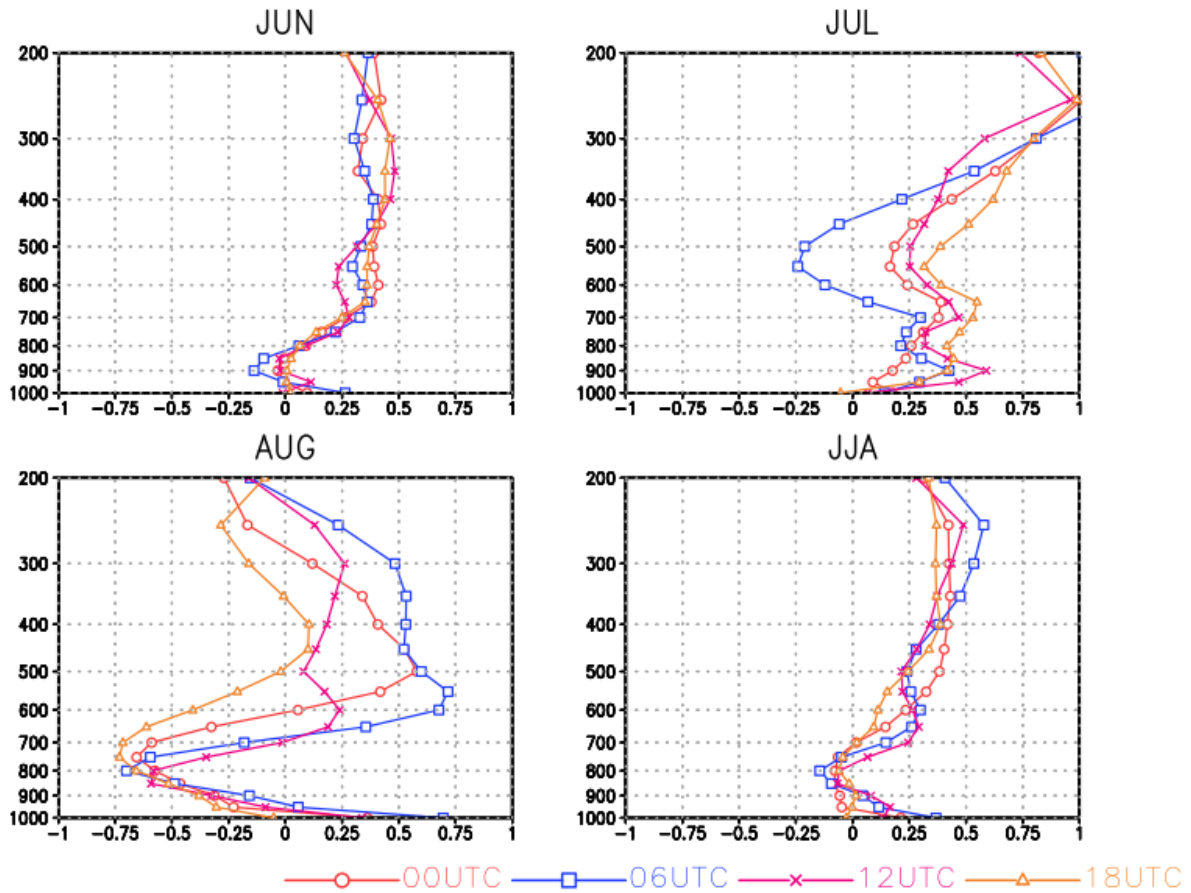


Figure 58. Mean vertical diurnal profiles of the overall wind speed (m/s) difference (IRR-NOIR) over the Great Plains. Averaged for a box bounded between 105°W–94°W and 30°N–45°N.

### *Great Plains Low-Level Jet Differences*

This section evaluates differences between the IRR and NOIR simulations LLJs across the GP. Monthly and diurnal means and differences are presented for all three months and all four hours of WRF output for the mean LLJ core height as well as speed. Broad patterns that show up across all of these LLJ figures are increased discontinuity during the afternoon hours (00 UTC and 18 UTC). LLJs which form during the day are much more variable and less common. This makes the evaluation of the differences more difficult than LLJs which occur at night when they are more homogenous over space and time.

LLJ heights for the month of June (Figures 59-63) show small variations around 400 m with the largest differences occurring along the northern edge of the Midwestern states and to the south near Louisiana away from areas of intense irrigation. This might suggest that larger scale atmospheric feedbacks are influencing the circulation in these areas even in the first month of the simulations. June LLJ speeds (Figures 64-68) also show only minor changes between the simulations diurnally with the largest differences in similar places as the LLJ heights. Note, that in those areas the frequency across the entire three-month simulation is quite small and even smaller for just a single month. July LLJ heights (Figures 69-73) as well as speed (Figures 74-78) have similar spatial differences as June, however, the differences are larger. The most notable changes to the LLJ height for JJA is over northern Wisconsin and Minnesota where the IRR simulation has mean LLJ heights over 200 m higher. Also, the LLJ speeds show relatively large decreases of around 4 m/s over a similar WI-MN area. More interestingly are the increases in LLJ speed over the central GP of up to 2 m/s nearly directly over the most irrigated regions. Both regions meet the criteria for statistical significance. In August, the LLJ height (Figures 79-83) differences become larger and more broadly spaced overnight, during the day there are very few cells which meet the LLJ criteria. LLJ speed (Figures 84-88) differences are slightly positive over the GP and irrigated region, and downstream unlike July there are also increases of nearly 2 m/s. Summing it up over JJA LLJ heights (Figures 89-92) during the day are much more variable and result in distributions that are statistically significant.

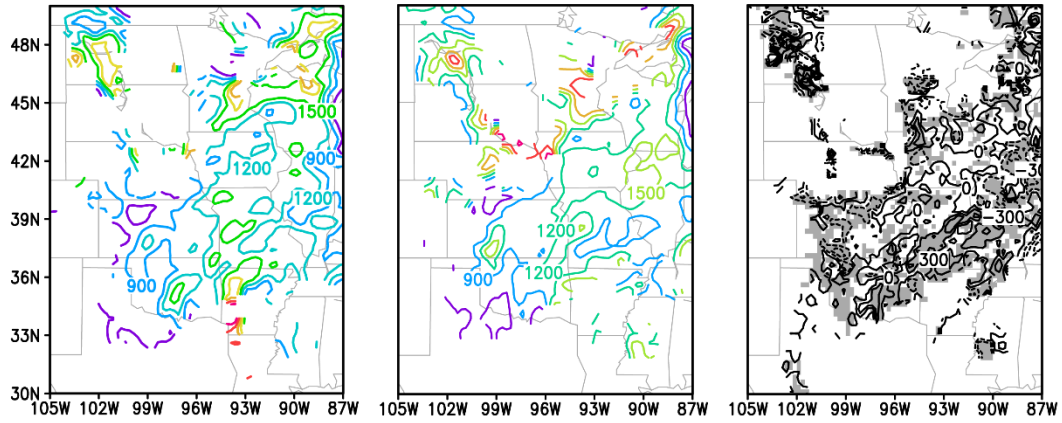


Figure 59. June 00 UTC Jet heights and differences (IRR-NOIR). The gray shading depicts statistical significance at the 95% confidence interval.

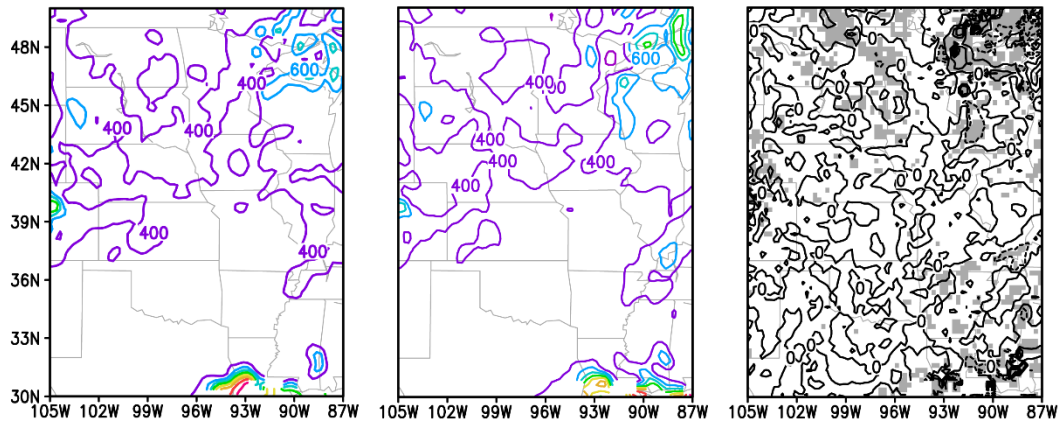


Figure 60. June 06 UTC Jet heights and differences (IRR-NOIR). The gray shading depicts statistical significance at the 95% confidence interval.

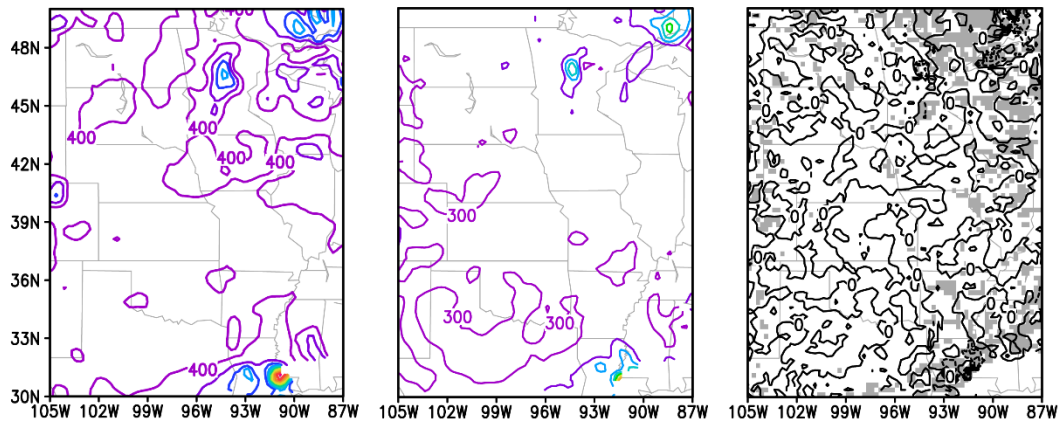


Figure 61. June 12 UTC Jet heights and differences (IRR-NOIR). The gray shading depicts statistical significance at the 95% confidence interval.

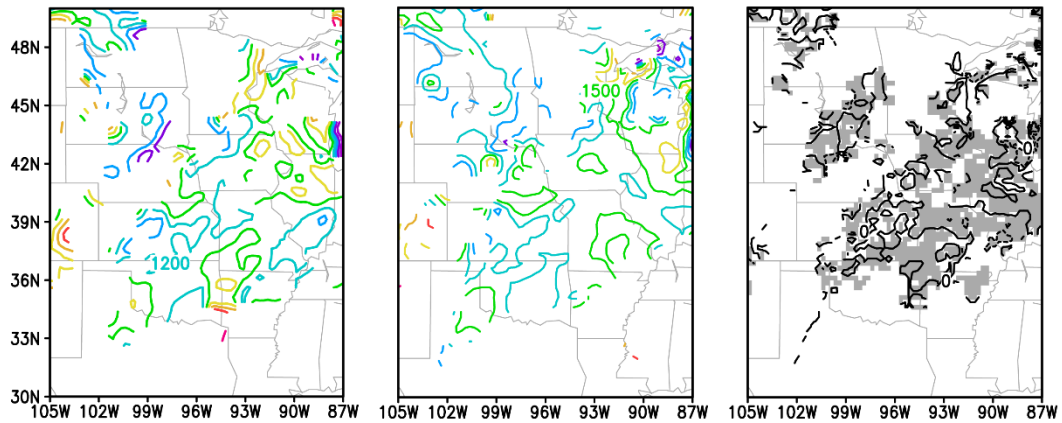


Figure 62. June 18 UTC Jet heights and differences (IRR-NOIR). The gray shading depicts statistical significance at the 95% confidence interval.

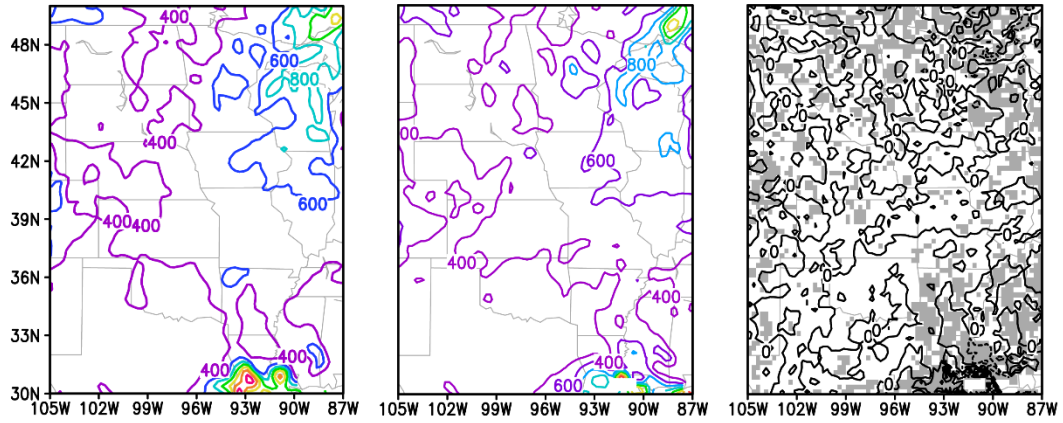


Figure 63. June LLJ All Hours height and differences (IRR-NOIR). The gray shading depicts statistical significance at the 95% confidence interval.

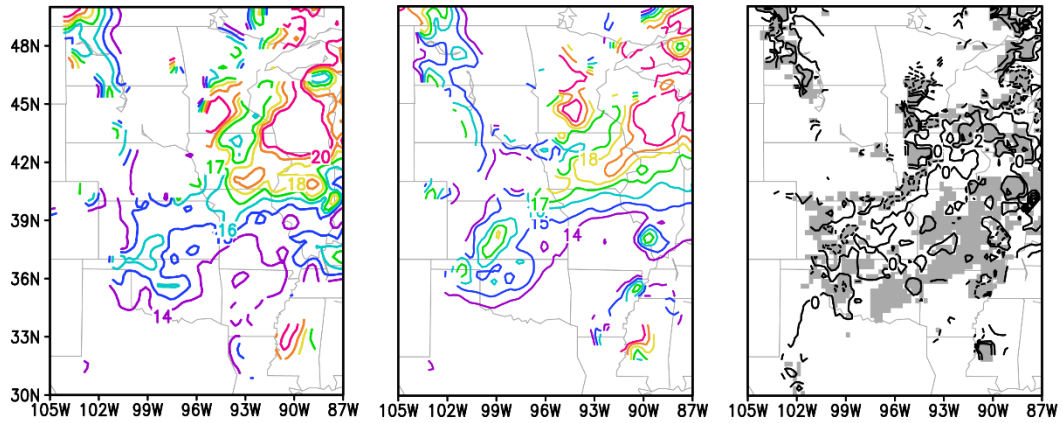


Figure 64. June 00 UTC Jet speed and differences (IRR-NOIR). The gray shading depicts statistical significance at the 95% confidence interval.

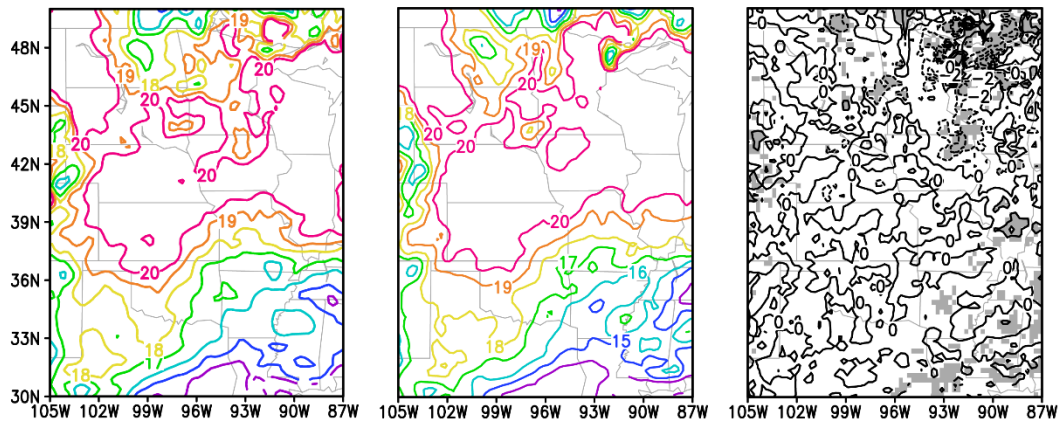


Figure 65. June 06 UTC Jet speed and differences (IRR-NOIR). The gray shading depicts statistical significance at the 95% confidence interval.

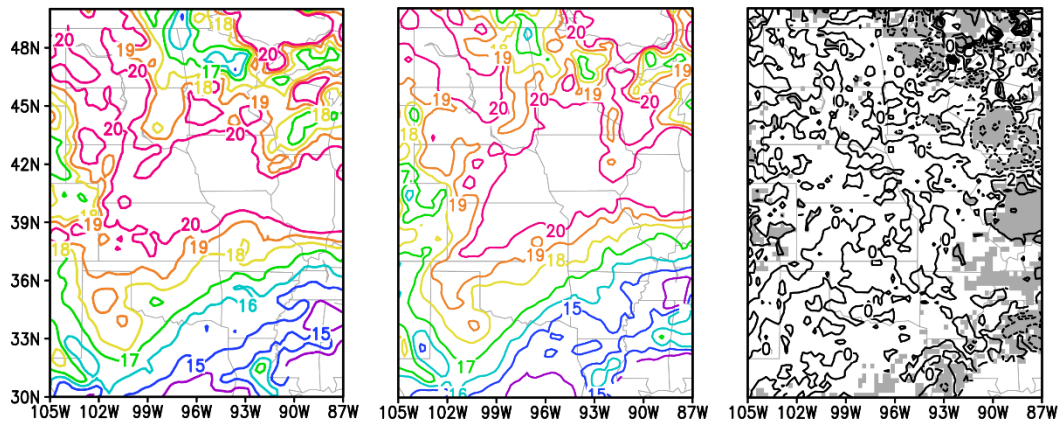


Figure 66. June 12 UTC Jet speed and differences (IRR-NOIR). The gray shading depicts statistical significance at the 95% confidence interval.

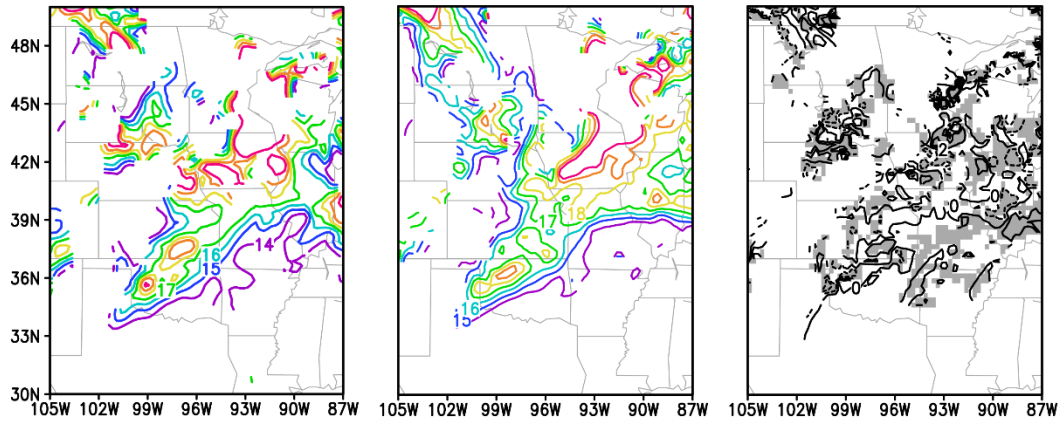


Figure 67. June 18 UTC LLJ speed and differences (IRR-NOIR). The gray shading depicts statistical significance at the 95% confidence interval.

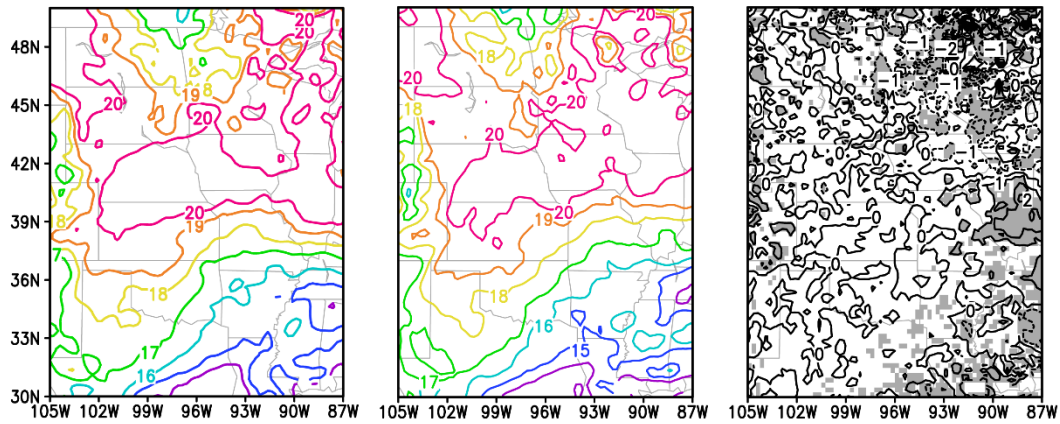


Figure 68. June all hours LLJ speed and differences (IRR-NOIR). The gray shading depicts statistical significance at the 95% confidence interval.

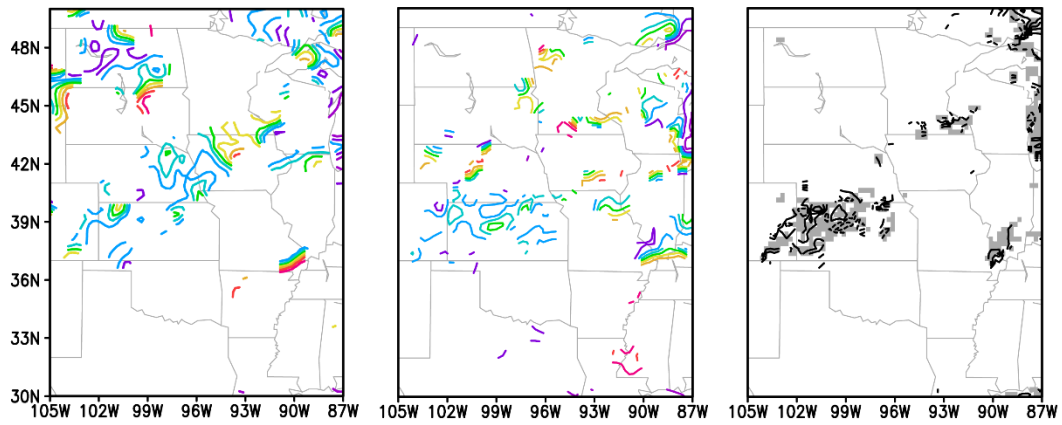


Figure 69. July 00 UTC LLJ height and differences (IRR-NOIR). The gray shading depicts statistical significance at the 95% confidence interval.

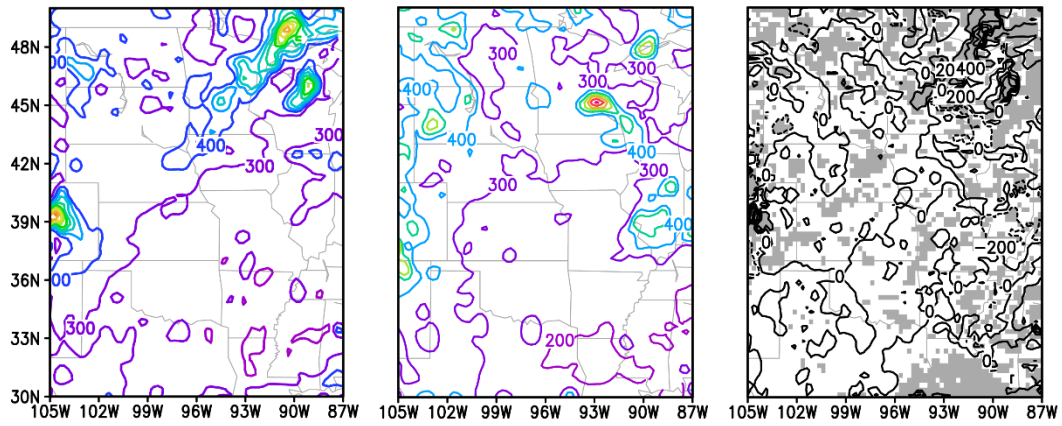


Figure 70. July 06 UTC LLJ height and differences (IRR-NOIR). The gray shading depicts statistical significance at the 95% confidence interval.

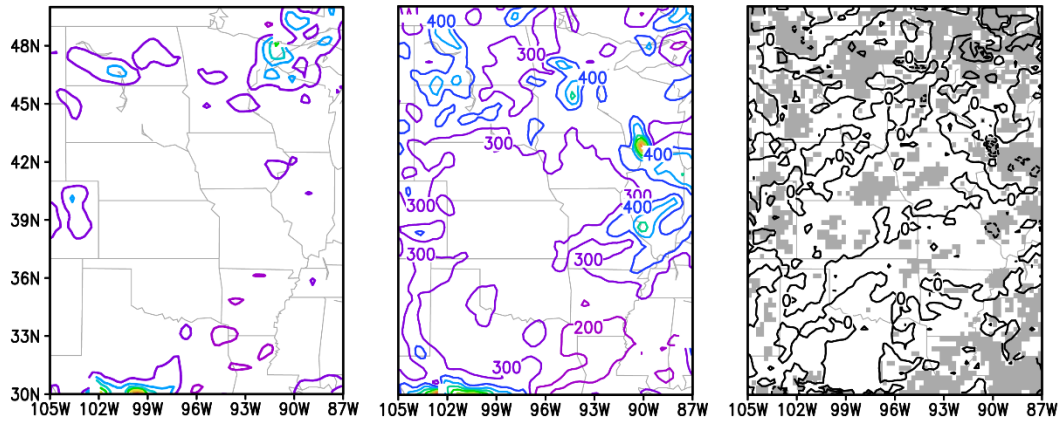


Figure 71. July 12 UTC LLJ height and differences (IRR-NOIR). The gray shading depicts statistical significance at the 95% confidence interval.

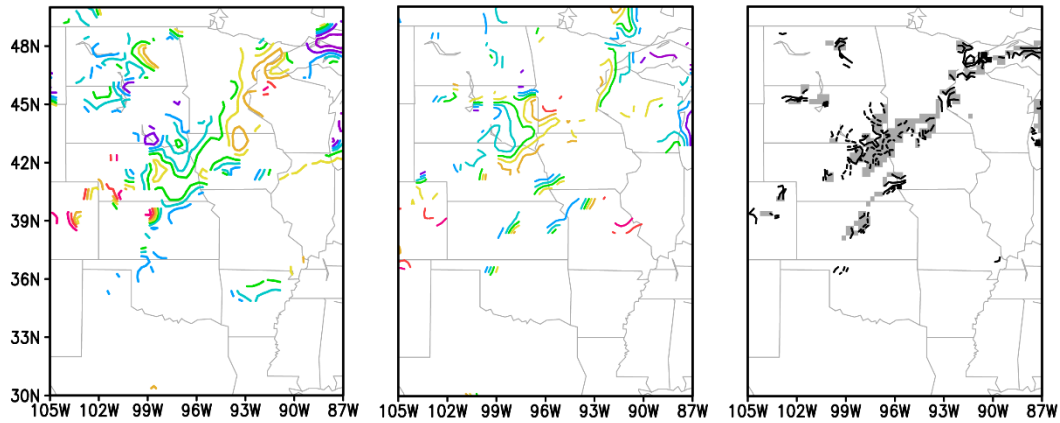


Figure 72. July 18 UTC LLJ height and differences (IRR-NOIR). The gray shading depicts statistical significance at the 95% confidence interval.

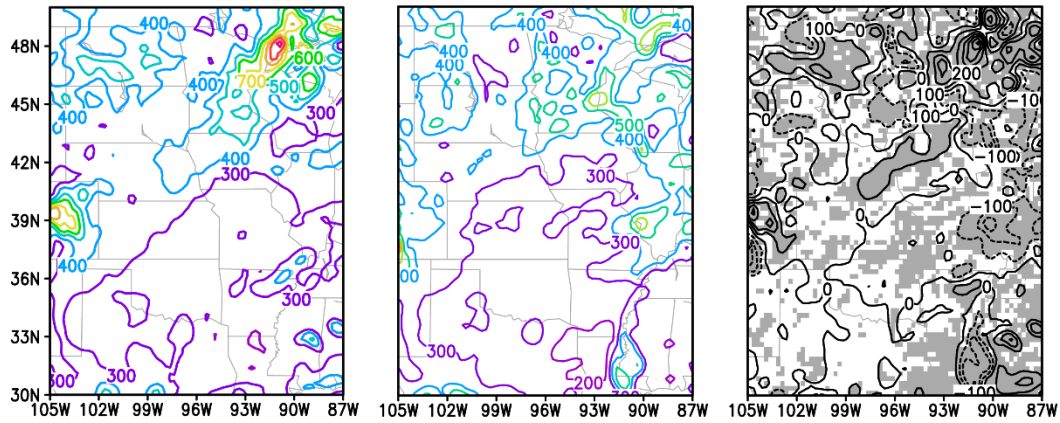


Figure 73. July all hours LLJ height and differences (IRR-NOIR). The gray shading depicts statistical significance at the 95% confidence interval.

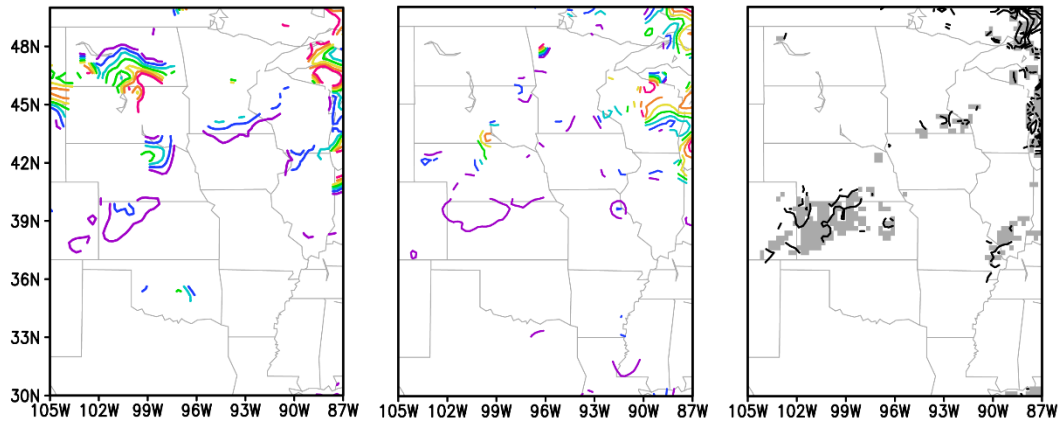


Figure 74. July 00 UTC LLJ speed and differences (IRR-NOIR). The gray shading depicts statistical significance at the 95% confidence interval.

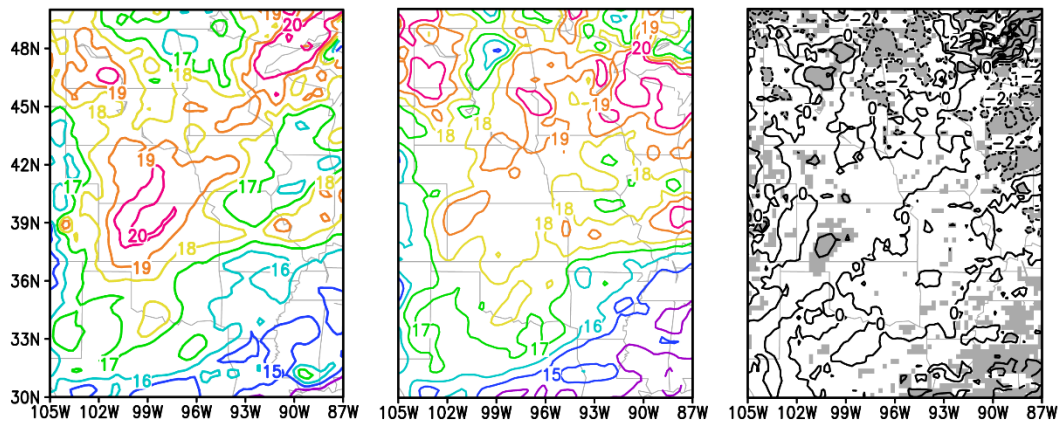


Figure 75. July 06 UTC LLJ speed and differences (IRR-NOIR). The gray shading depicts statistical significance at the 95% confidence interval.

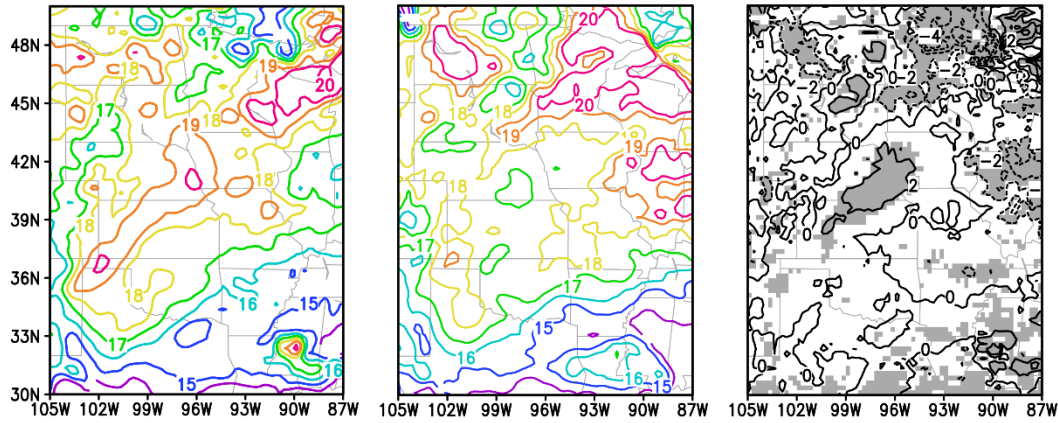


Figure 76. July 12 UTC LLJ speed and differences (IRR-NOIR). The gray shading depicts statistical significance at the 95% confidence interval.

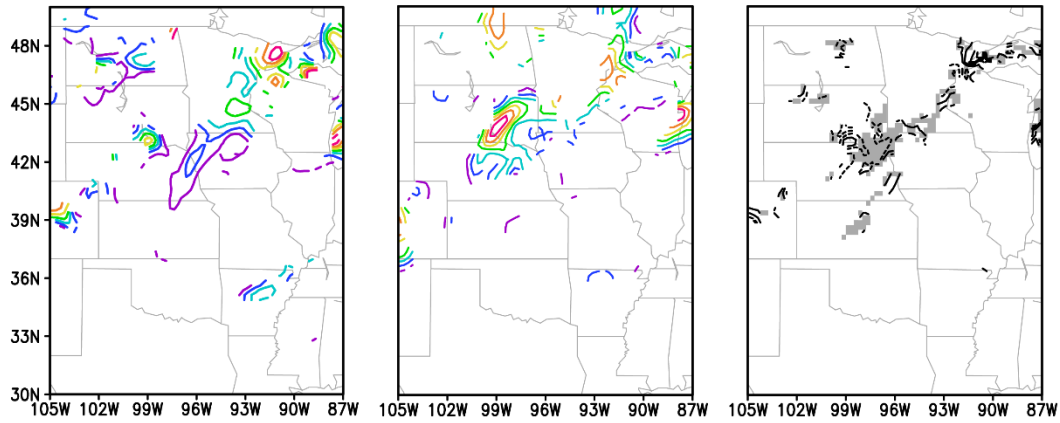


Figure 77. July 18 UTC LLJ speeds and differences (IRR-NOIR). The gray shading depicts statistical significance at the 95% confidence interval.

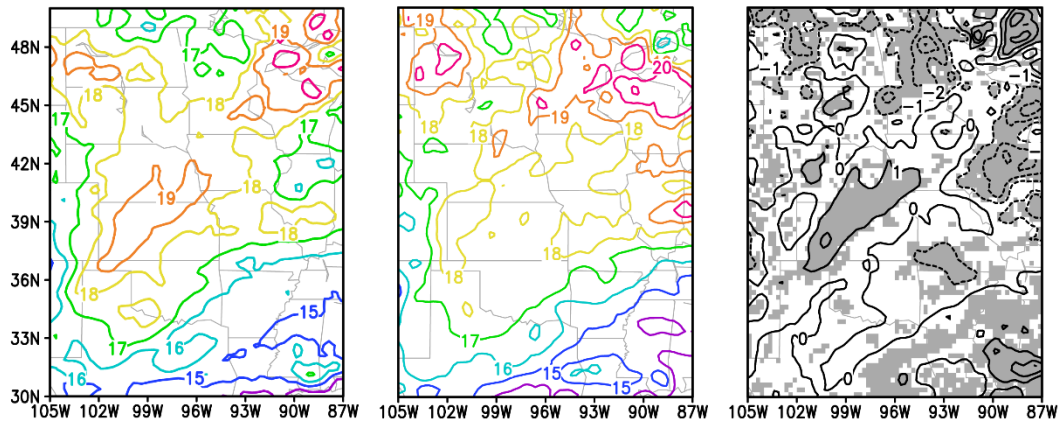


Figure 78. July all hours LLJ speed and differences (IRR-NOIR). The gray shading depicts statistical significance at the 95% confidence interval.

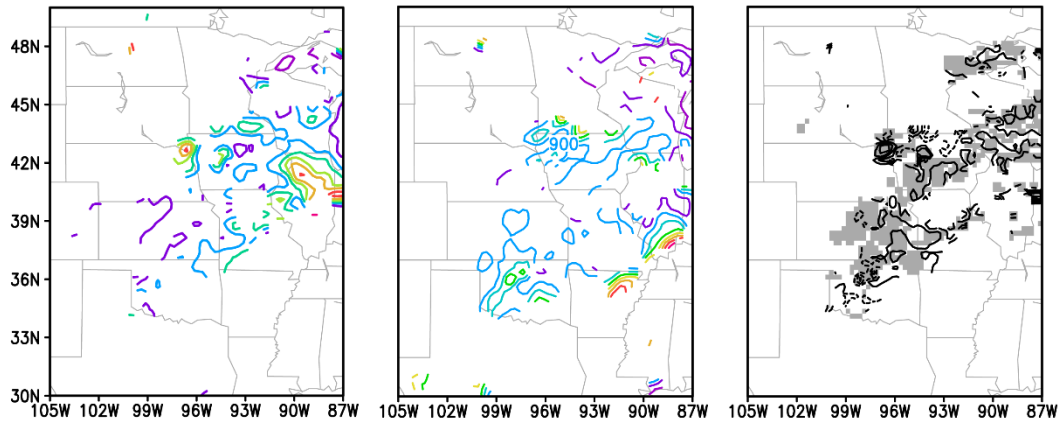


Figure 79. August 00 UTC LLJ height and differences (IRR-NOIR). The gray shading depicts statistical significance at the 95% confidence interval.

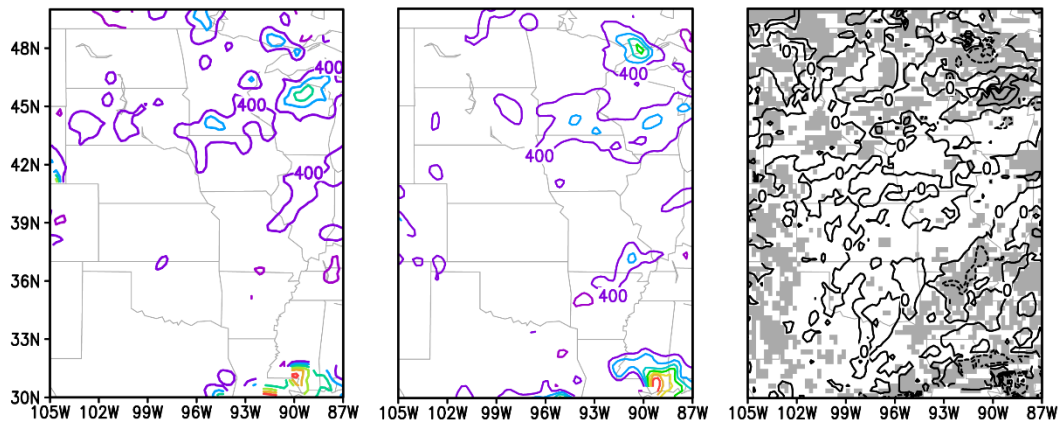


Figure 80. August 06 UTC LLJ height and differences (IRR-NOIR). The gray shading depicts statistical significance at the 95% confidence interval.

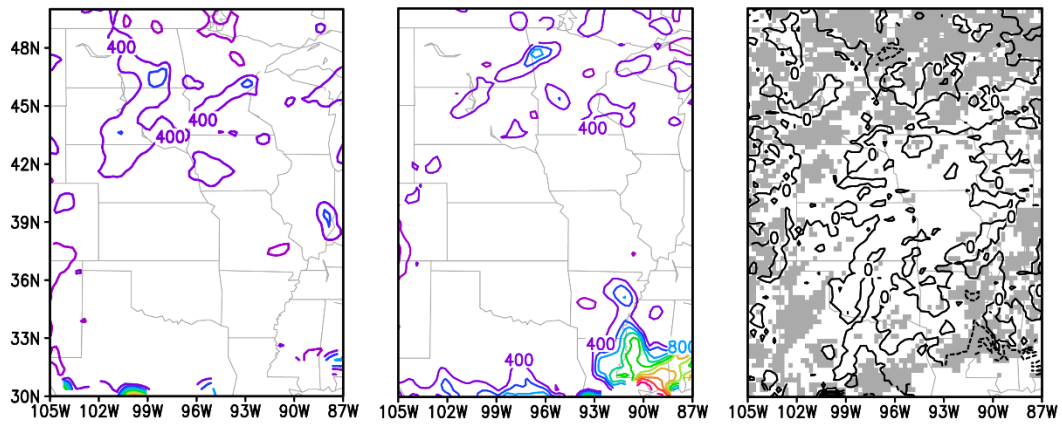


Figure 81. August 12 UTC LLJ height and differences (IRR-NOIR). The gray shading depicts statistical significance at the 95% confidence interval.

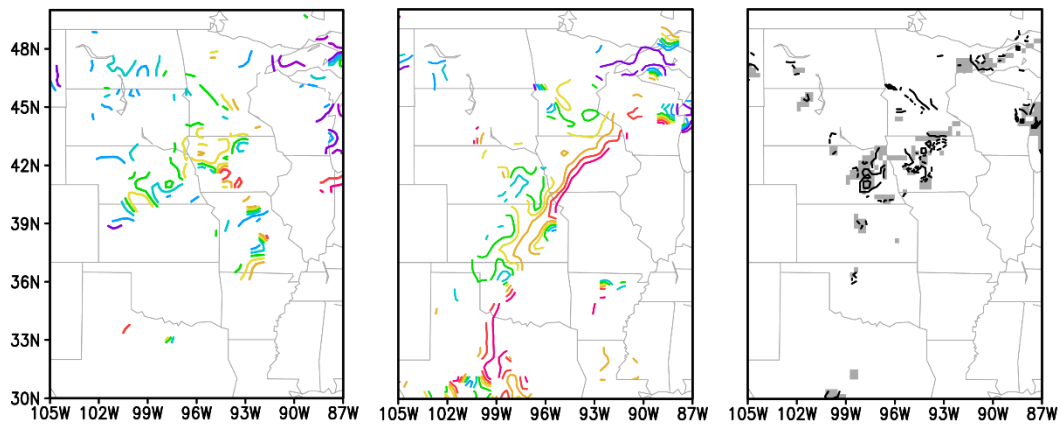


Figure 82. August 18 UTC LLJ height and differences (IRR-NOIR). The gray shading depicts statistical significance at the 95% confidence interval.

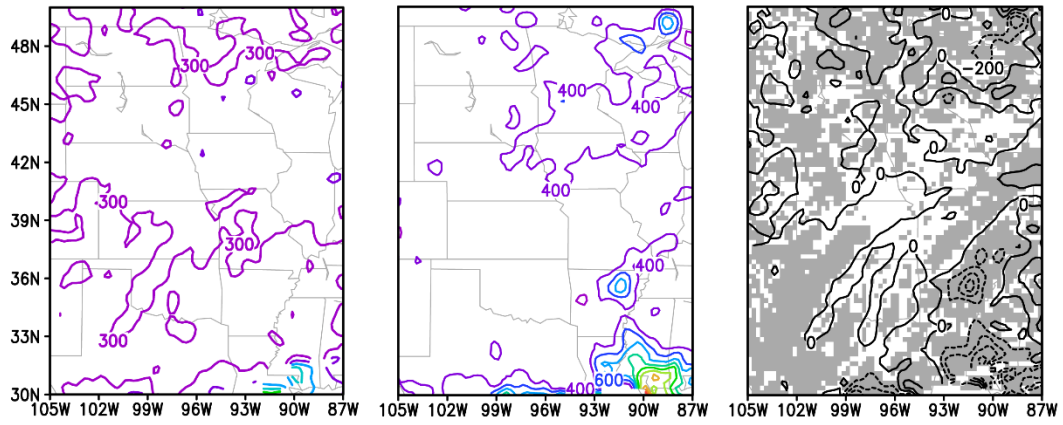


Figure 83. August all hours LLJ height and differences (IRR-NOIR). The gray shading depicts statistical significance at the 95% confidence interval.

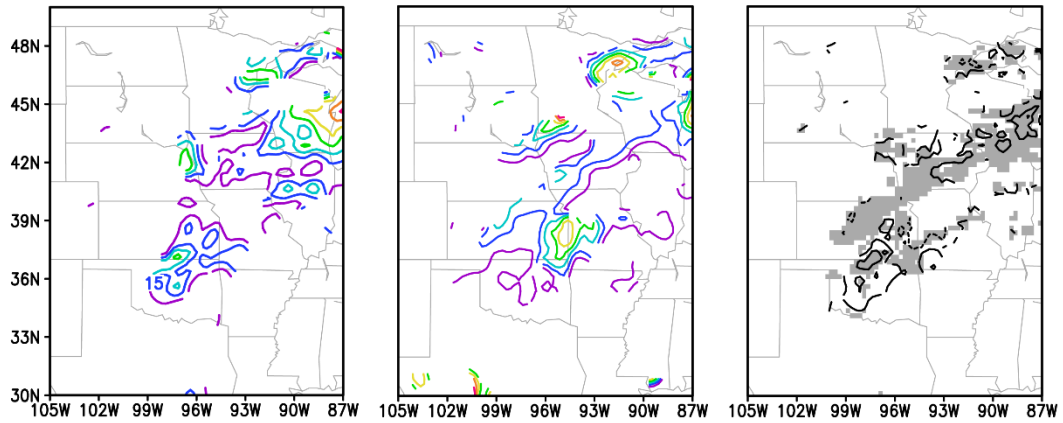


Figure 84. August 00 UTC LLJ speed and differences (IRR-NOIR). The gray shading depicts statistical significance at the 95% confidence interval.

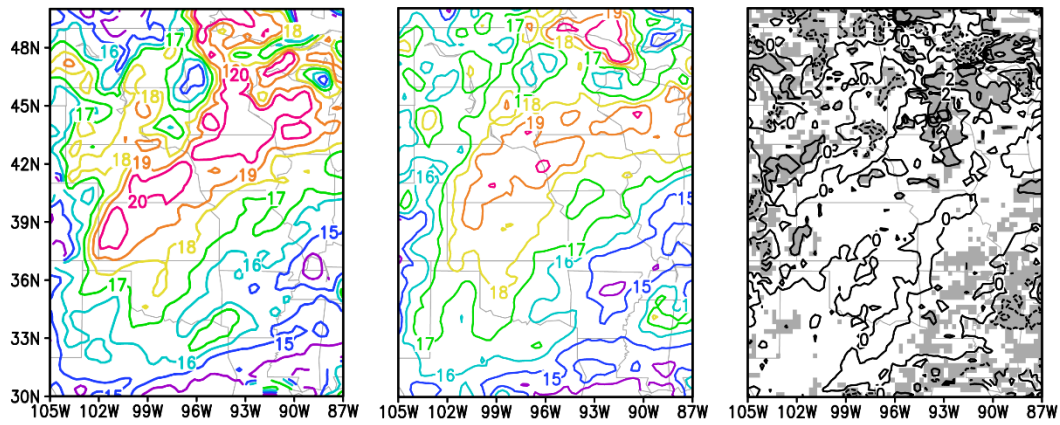


Figure 85. August 06 UTC LLJ speed and differences (IRR-NOIR). The gray shading depicts statistical significance at the 95% confidence interval.

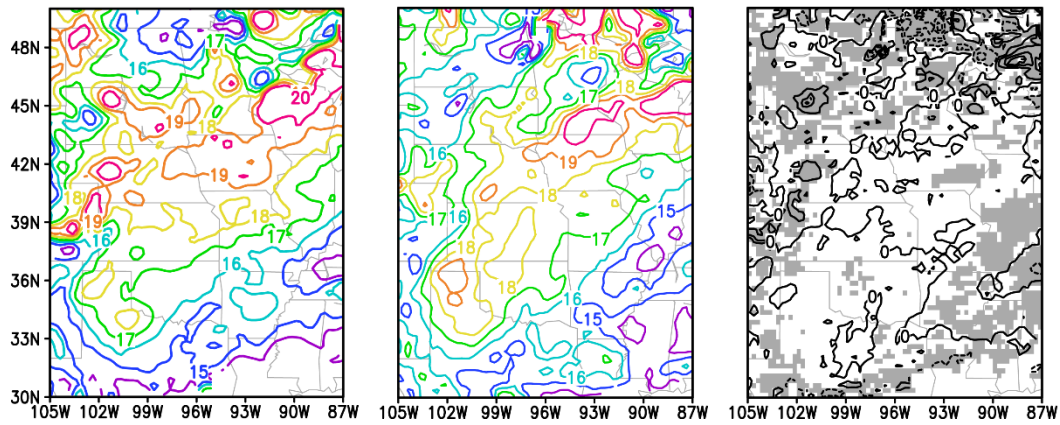


Figure 86. August 12 UTC LLJ speed and differences (IRR-NOIR). The gray shading depicts statistical significance at the 95% confidence interval.

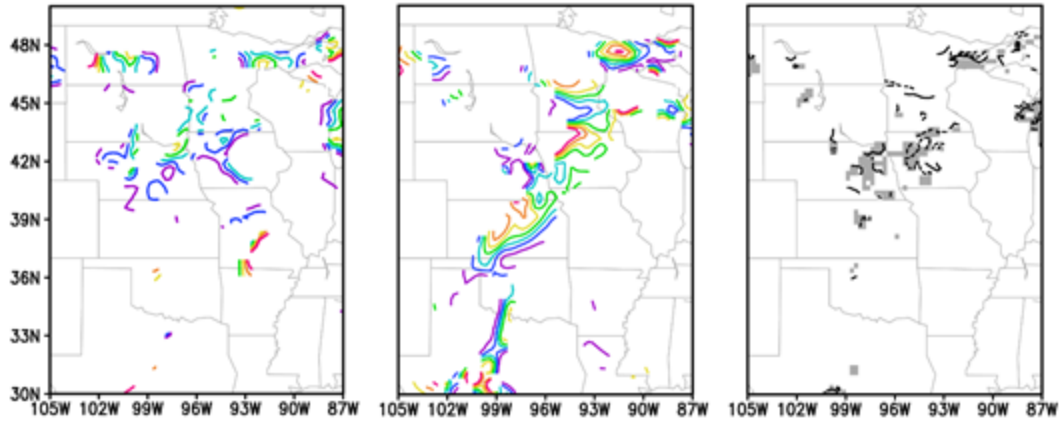


Figure 87. August 18 UTC LLJ speed and differences (IRR-NOIR). The gray shading depicts statistical significance at the 95% confidence interval.

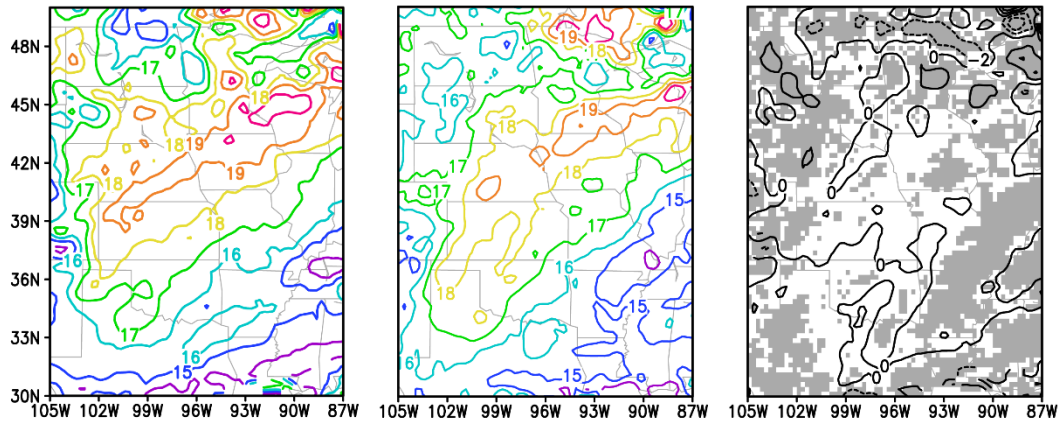


Figure 88. August all hours LLJ speed and differences (IRR-NOIR). The gray shading depicts statistical significance at the 95% confidence interval.

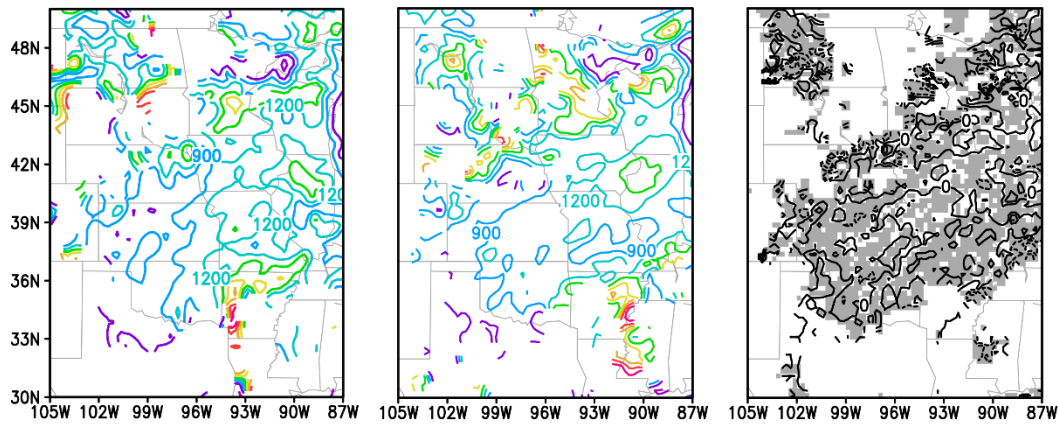


Figure 89. JJA 00 UTC LLJ height and differences (IRR-NOIR). The gray shading depicts statistical significance at the 95% confidence interval.

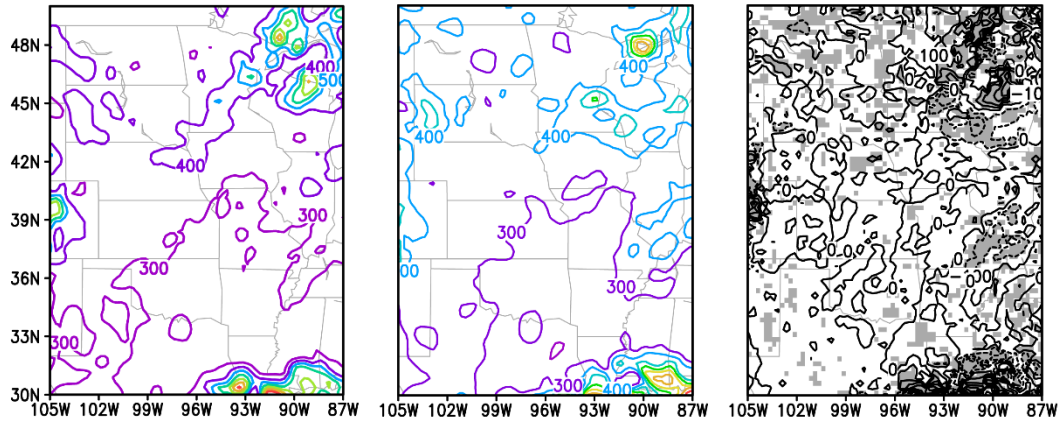


Figure 90. JJA 06 UTC LLJ height and differences (IRR-NOIR). The gray shading depicts statistical significance at the 95% confidence interval.

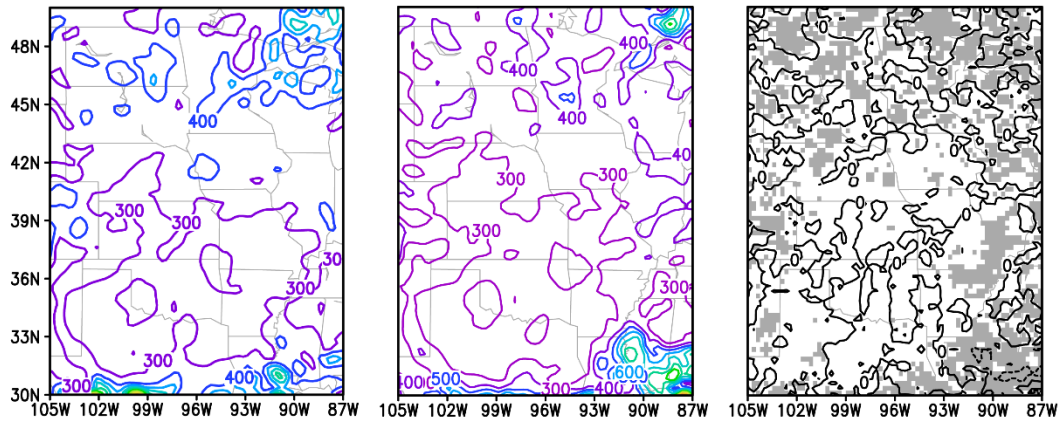


Figure 91. JJA 12 UTC LLJ height and differences (IRR-NOIR). The gray shading depicts statistical significance at the 95% confidence interval.

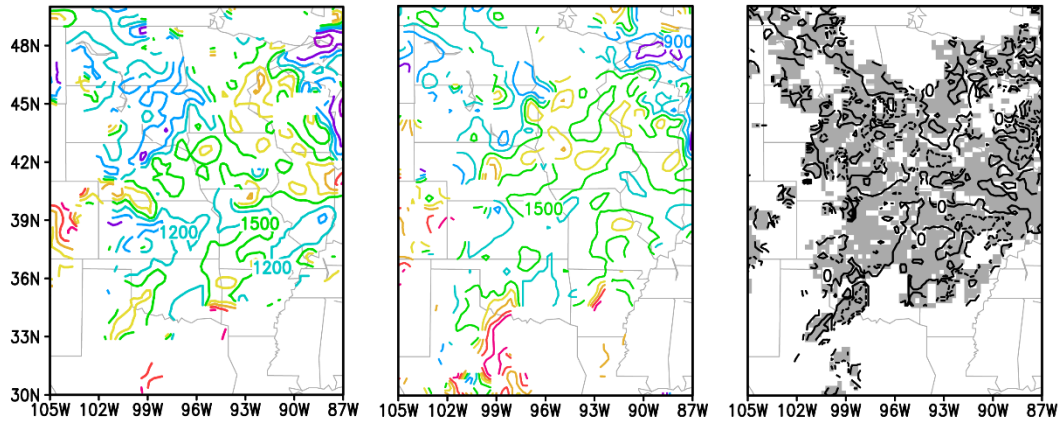


Figure 92. JJA 18 UTC LLJ height and differences (IRR-NOIR). The gray shading depicts statistical significance at the 95% confidence interval.

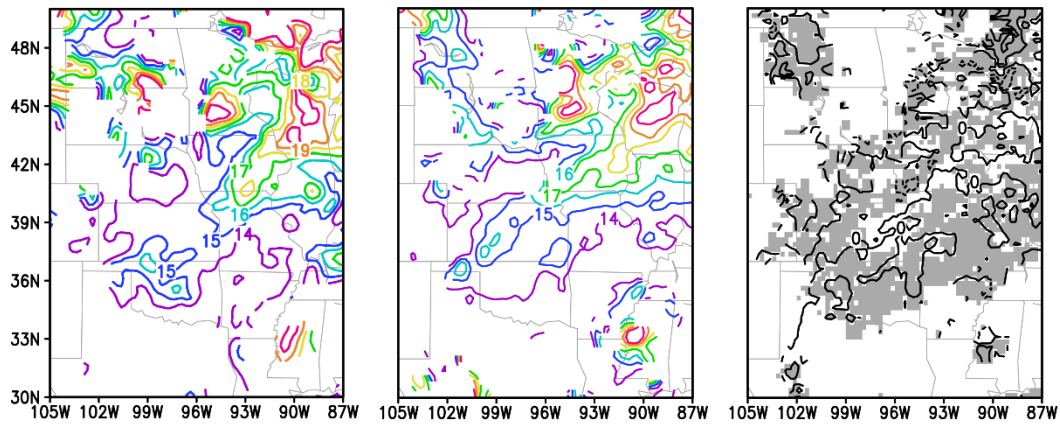


Figure 93. JJA 00 UTC LLJ speed and differences (IRR-NOIR). The gray shading depicts statistical significance at the 95% confidence interval.

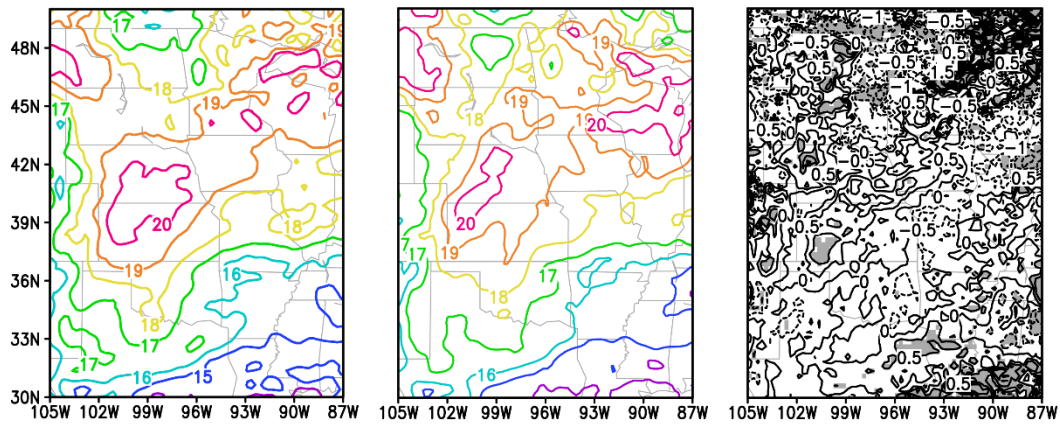


Figure 94. JJA 06 UTC LLJ speed and differences (IRR-NOIR). The gray shading depicts statistical significance at the 95% confidence interval.

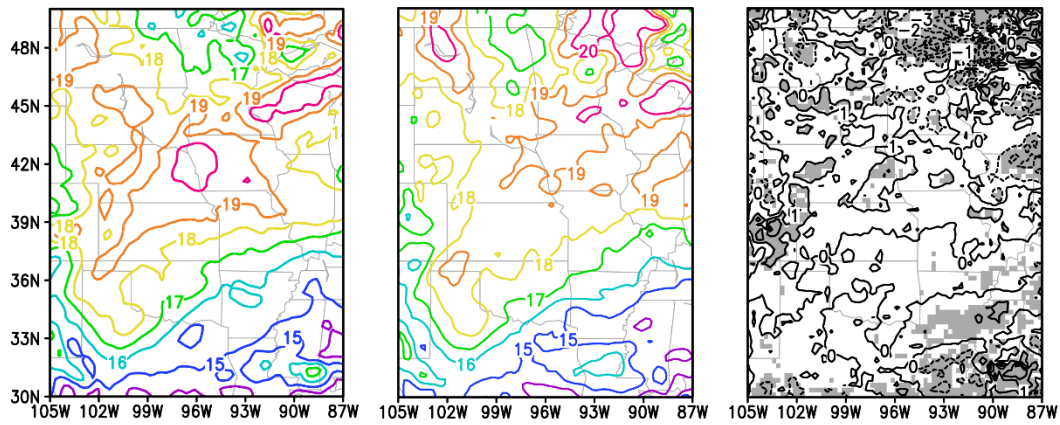


Figure 95. JJA 12 UTC LLJ speed and differences (IRR-NOIR). The gray shading depicts statistical significance at the 95% confidence interval.

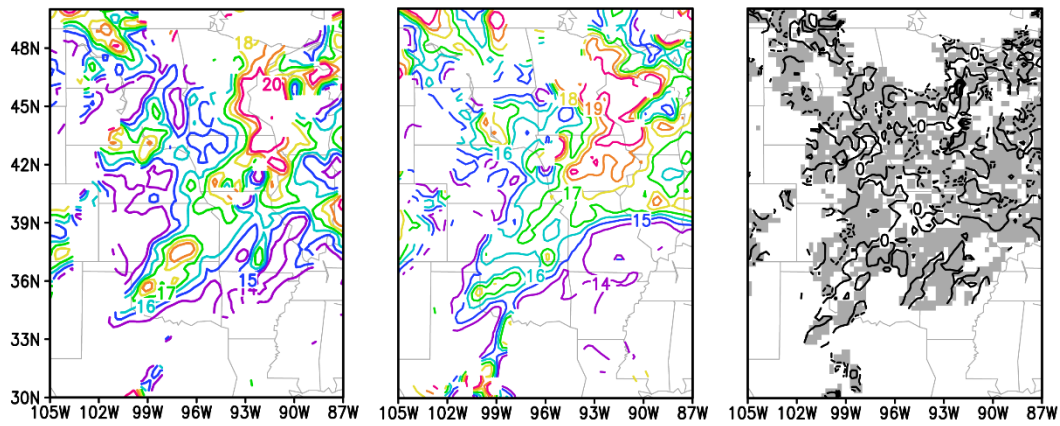


Figure 96. JJA 18 UTC LLJ speed and differences (IRR-NOIR). The gray shading depicts statistical significance at the 95% confidence interval.

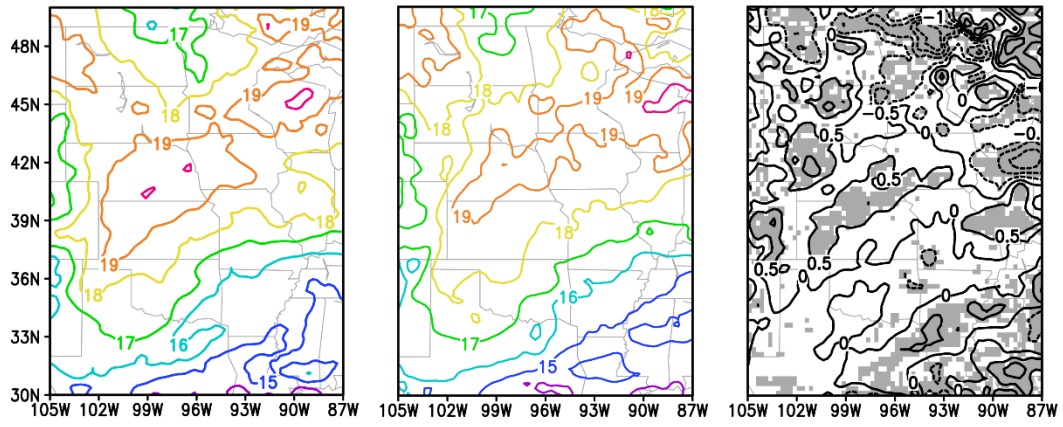


Figure 97. JJA all hours LLJ speed and differences (IRR-NOIR). The gray shading depicts statistical significance at the 95% confidence interval.

## **APPENDIX**

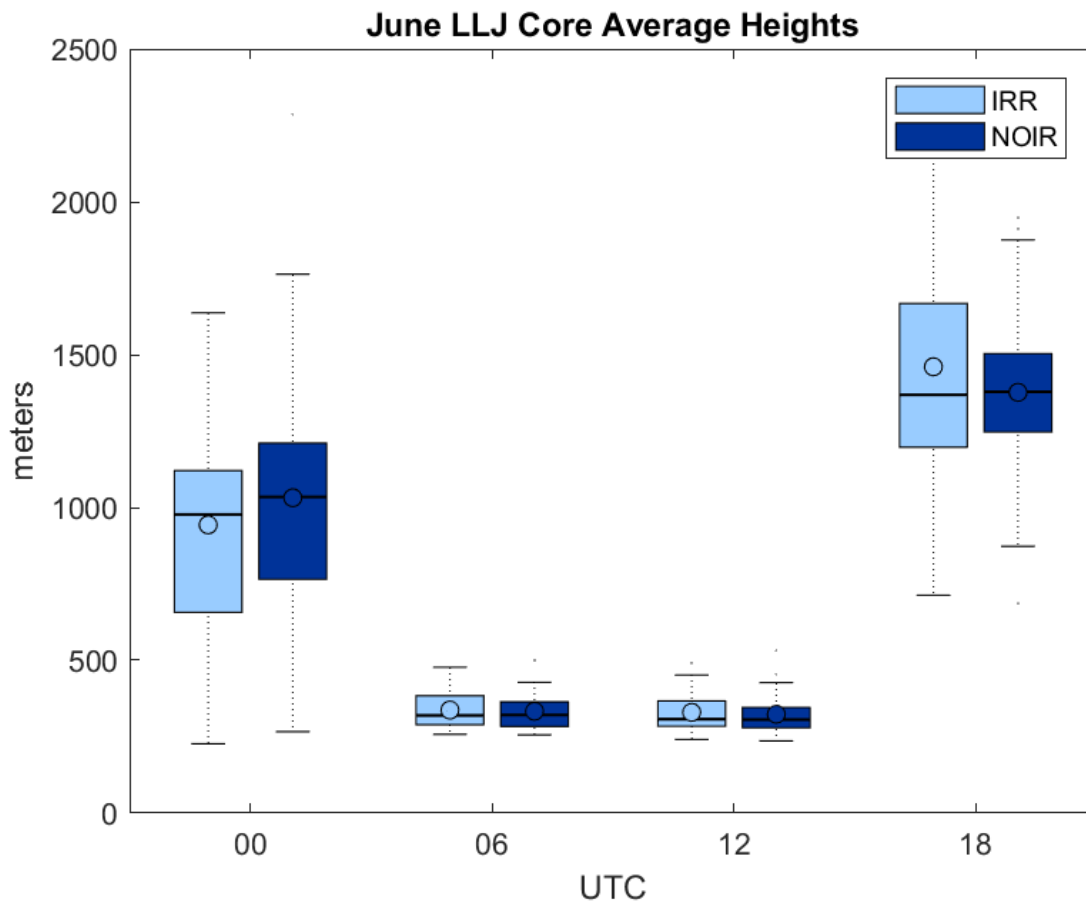


Figure 98. June LLJ height for 00, 06, 12, and 18 UTC. Averages are for a box between approximately 100°W – 90°W and 30°N – 43°N.

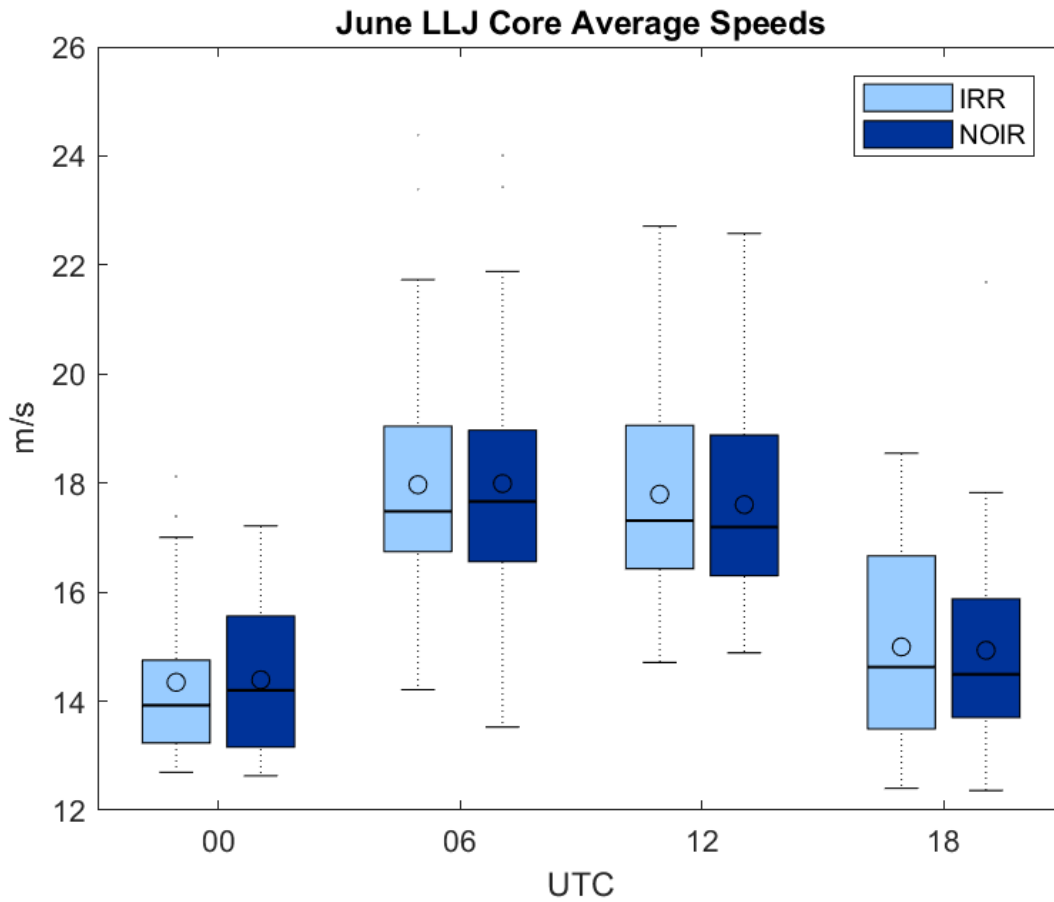


Figure 99. June LLJ speed for 00, 06, 12, and 18 UTC. Averages are for a box between approximately 100°W – 90°W and 30°N – 43°N.

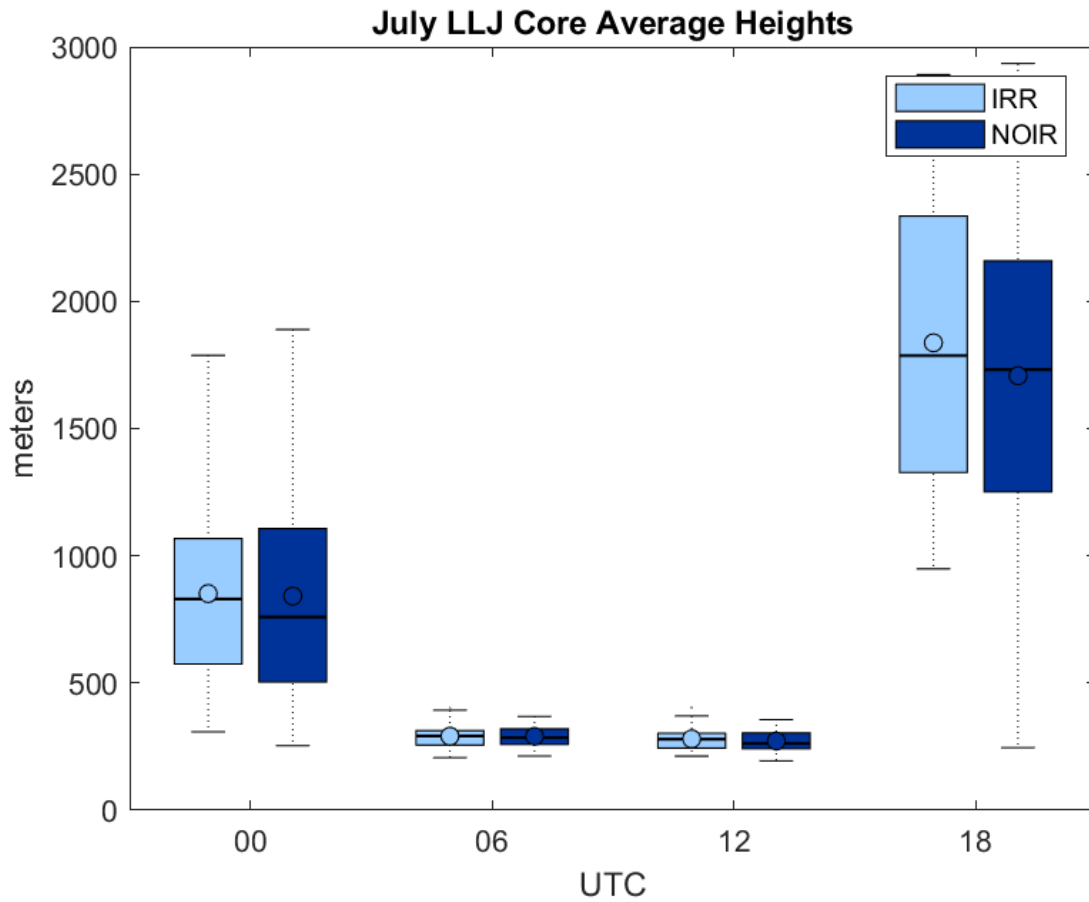


Figure 100. July LLJ height for 00, 06, 12, and 18 UTC. Averages are for a box between approximately 100°W – 90°W and 30°N – 43°N.

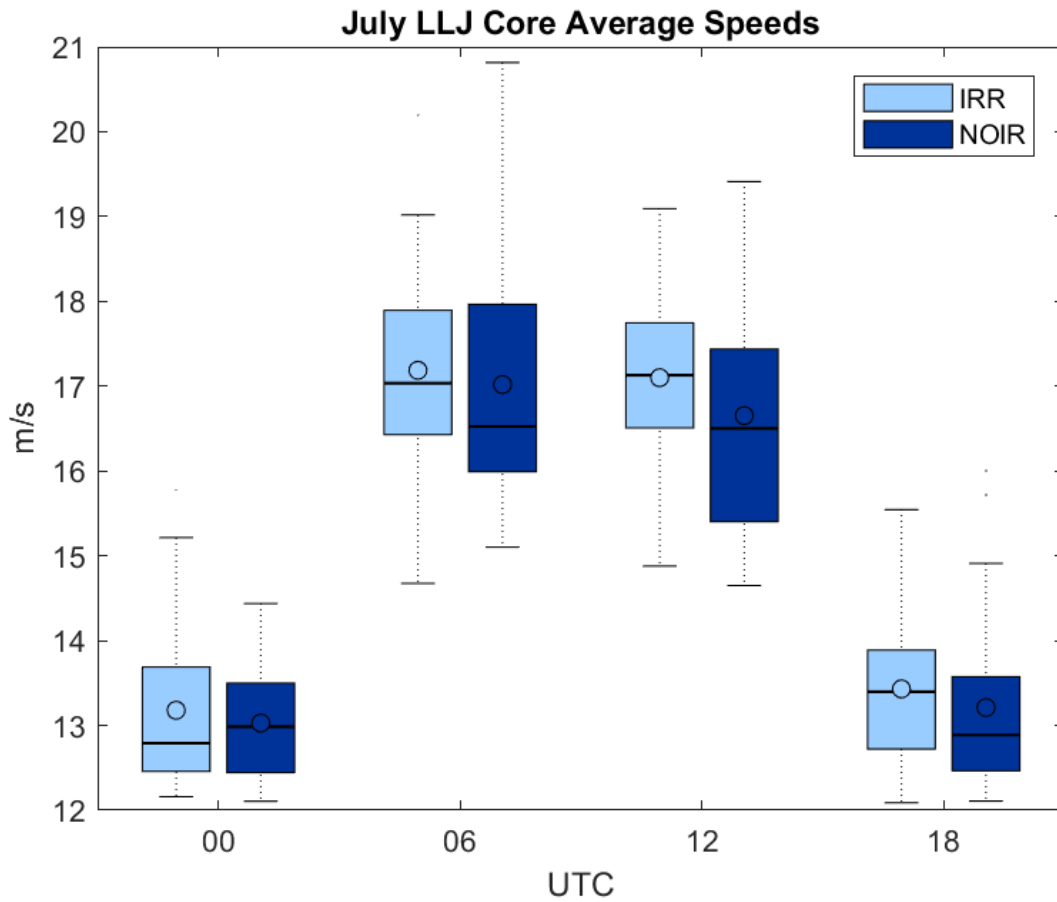


Figure 101. July LLJ speed for 00, 06, 12, and 18 UTC. Averages are for a box between approximately 100°W – 90°W and 30°N – 43°N.

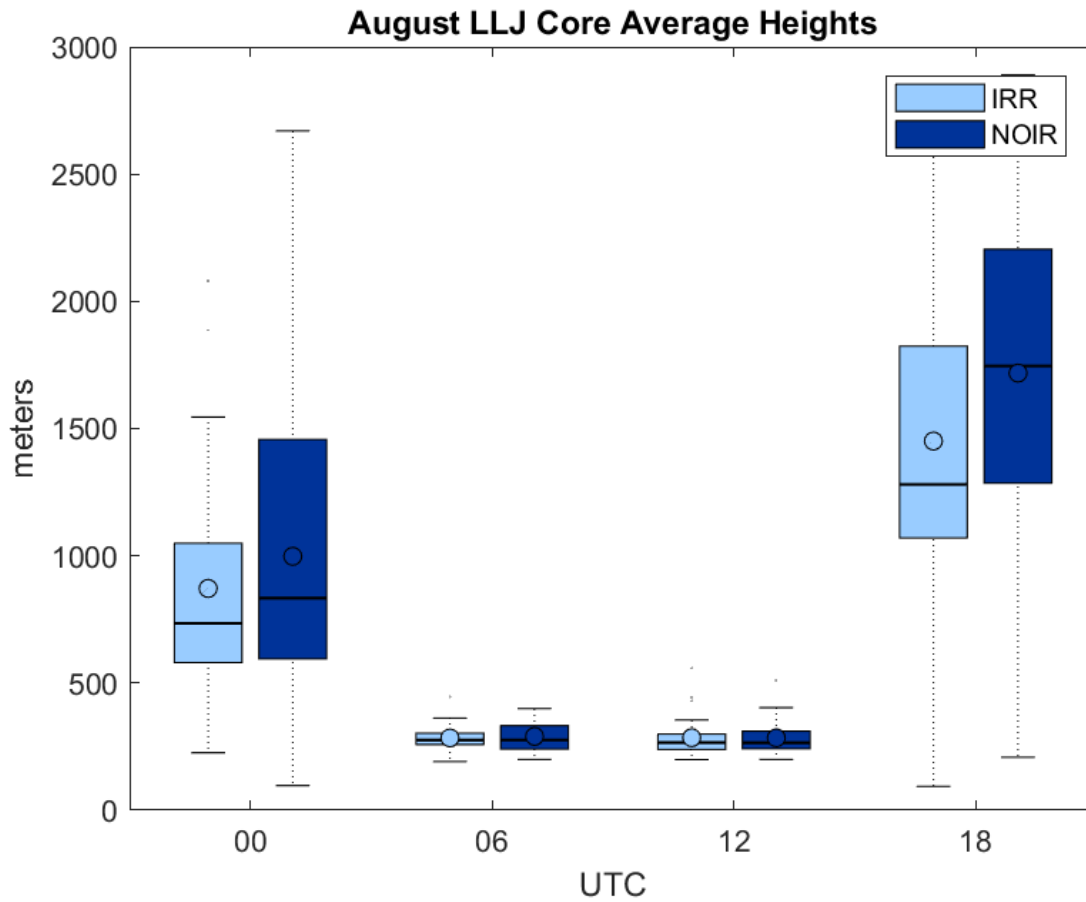


Figure 102. August LLJ height for 00, 06, 12, and 18 UTC. Averages are for a box between approximately 100°W – 90°W and 30°N – 43°N.

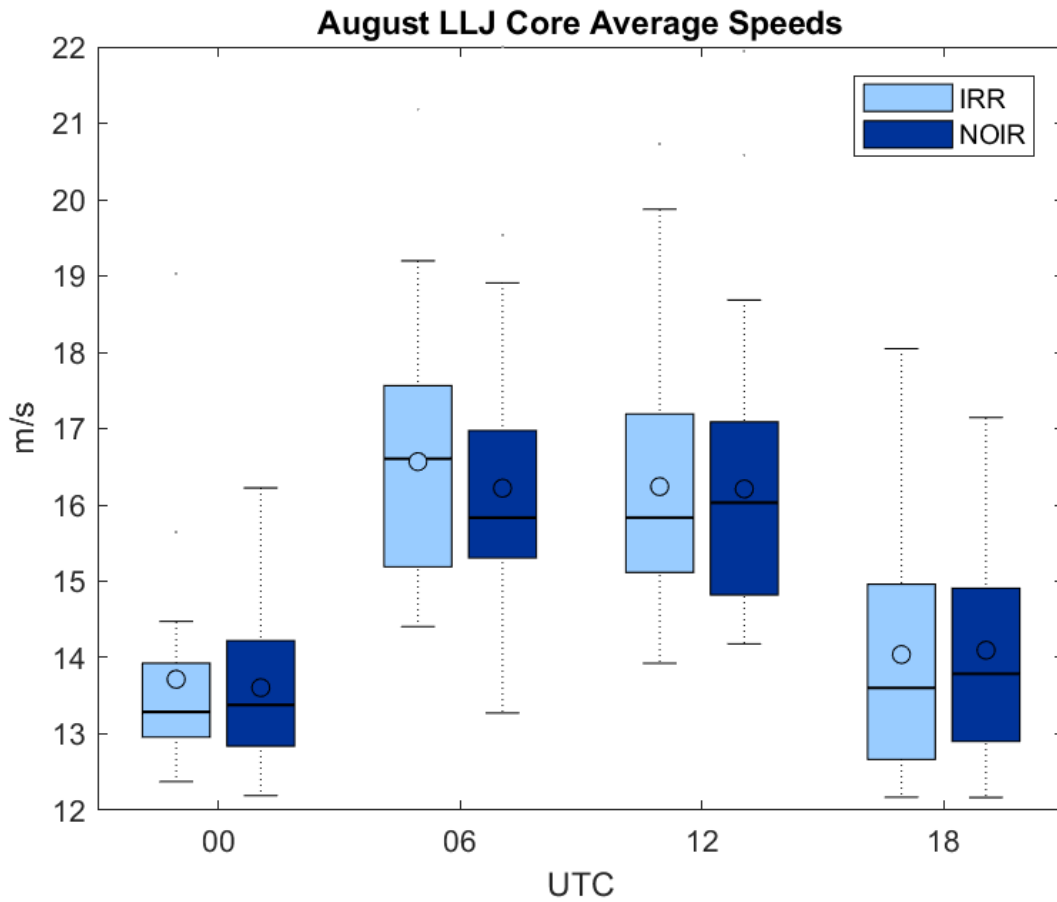


Figure 103. August LLJ speed for 00, 06, 12, and 18 UTC. Averages are for a box between approximately 100°W – 90°W and 30°N – 43°N.

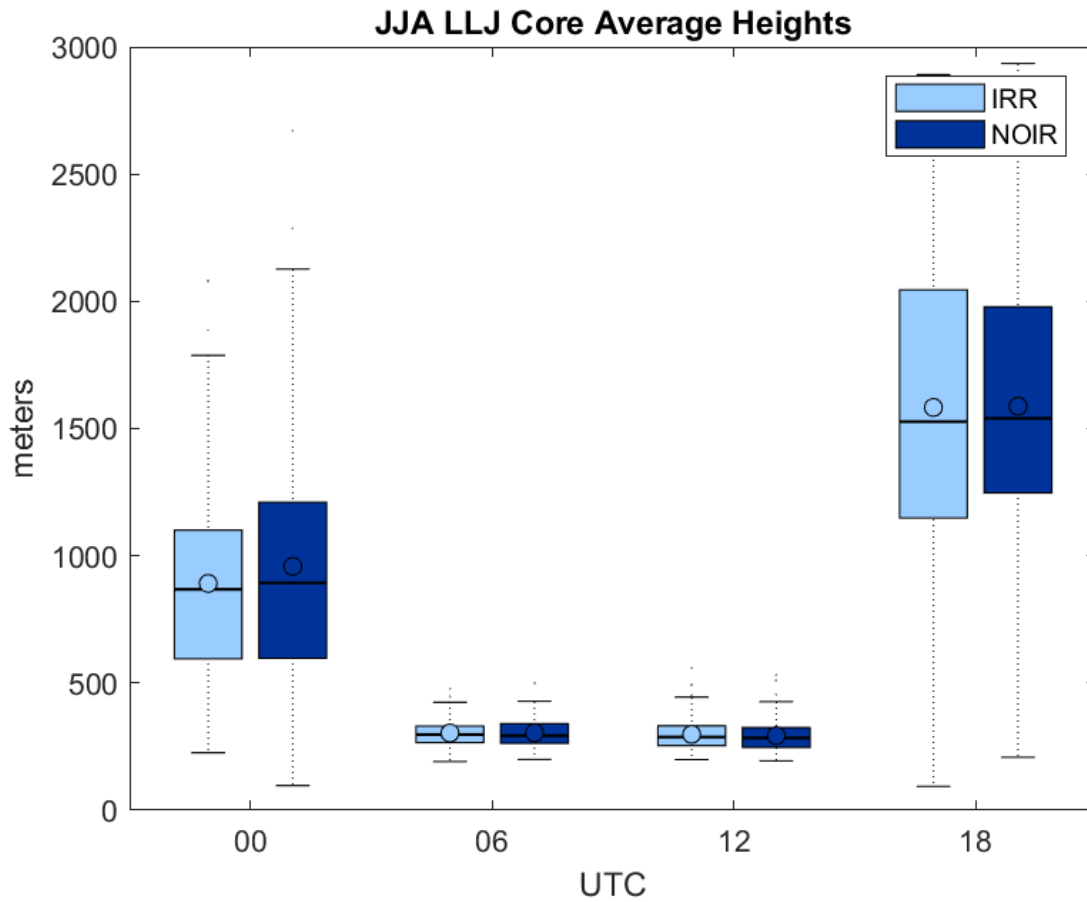


Figure 104. June, July, and August LLJ height for 00, 06, 12, and 18 UTC. Averages are for a box between approximately 100°W – 90°W and 30°N – 43°N.

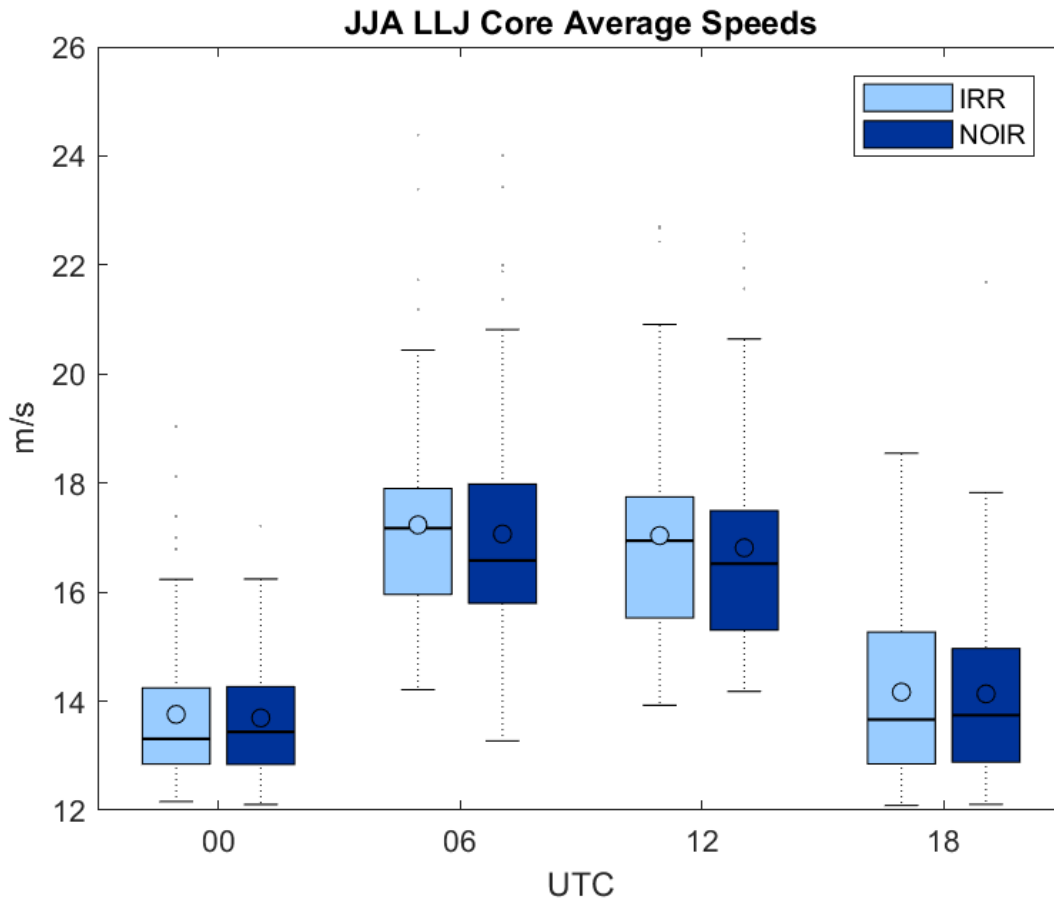


Figure 105. June, July, and August LLJ speed for 00, 06, 12, and 18 UTC. Averages are for a box between approximately 100°W – 90°W and 30°N – 43°N.

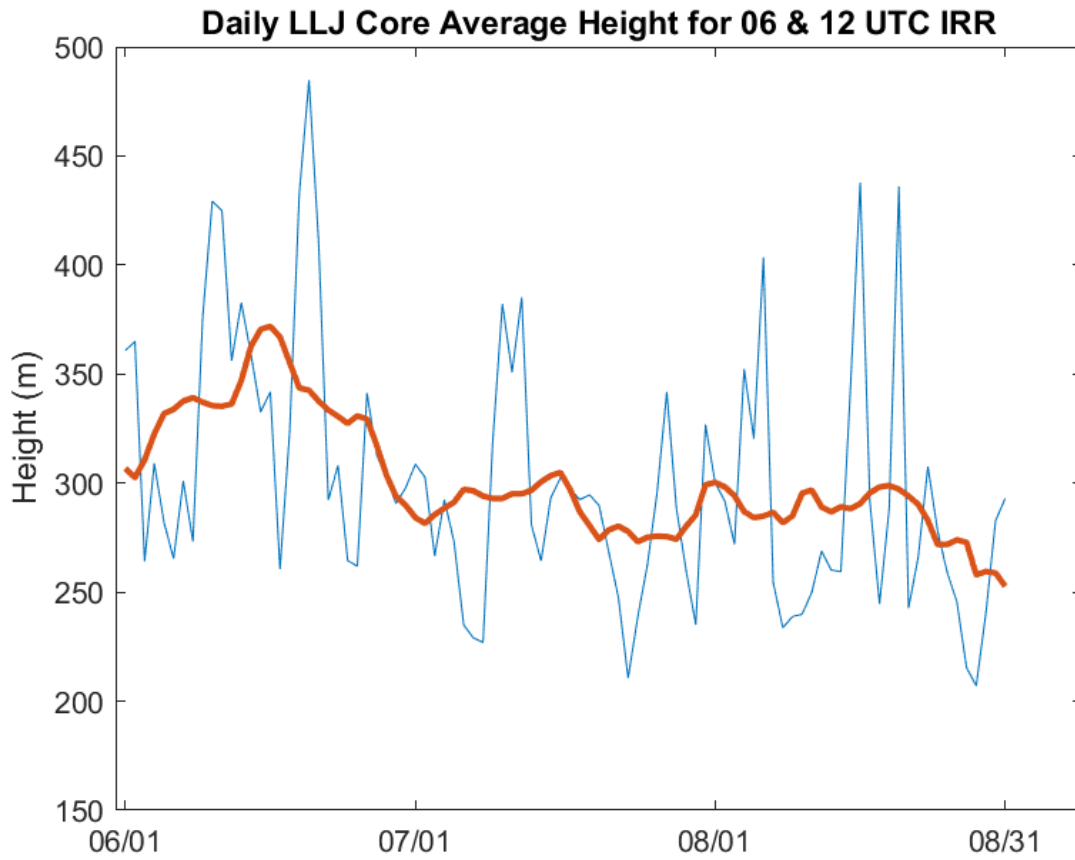


Figure 106. (Blue line) June, July, and August timeseries of daily mean LLJ height averaged across 06 and 12 UTC for the IRR simulation, and averaged for a box between approximately  $100^{\circ}\text{W} - 90^{\circ}\text{W}$  and  $30^{\circ}\text{N} - 43^{\circ}\text{N}$ . (Red line) 8 day moving average of LLJ height.

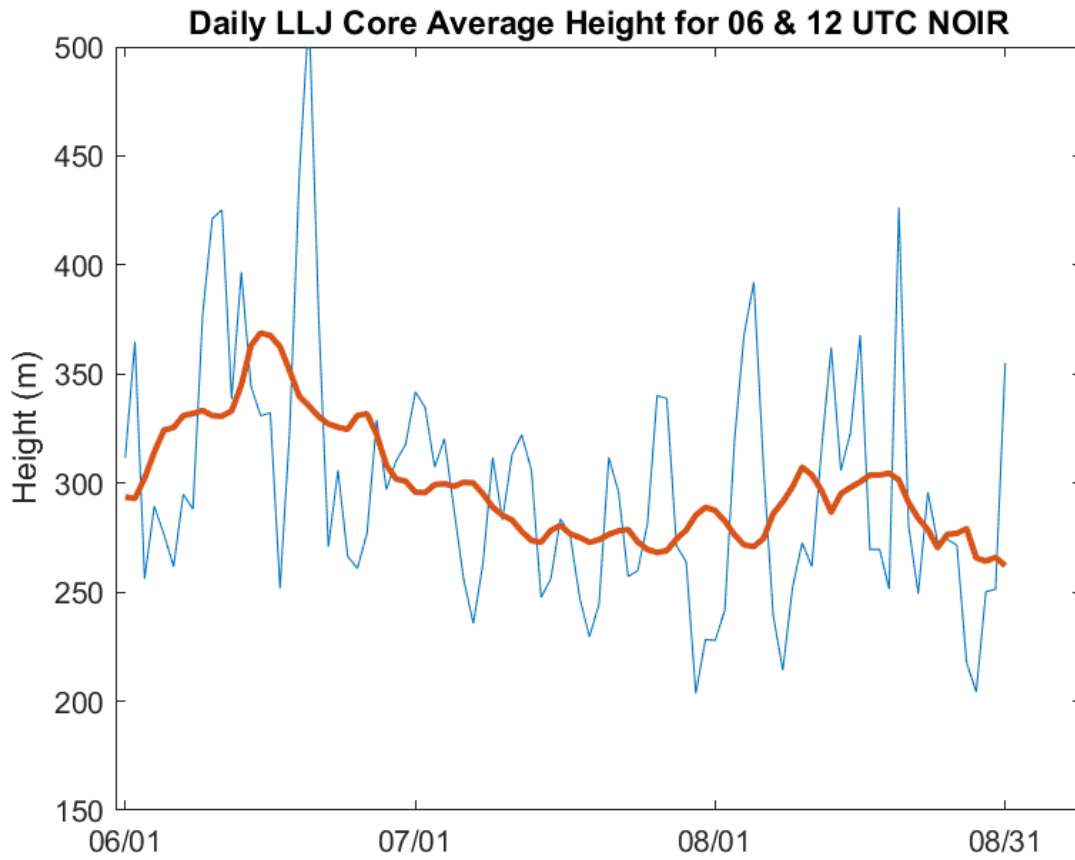


Figure 107. (Blue line) June, July, and August timeseries of daily mean LLJ height averaged across 06 and 12 UTC for the NOIR simulation, and averaged for a box between approximately 100°W – 90°W and 30°N – 43°N. (Red line) 8 day moving average of LLJ height.

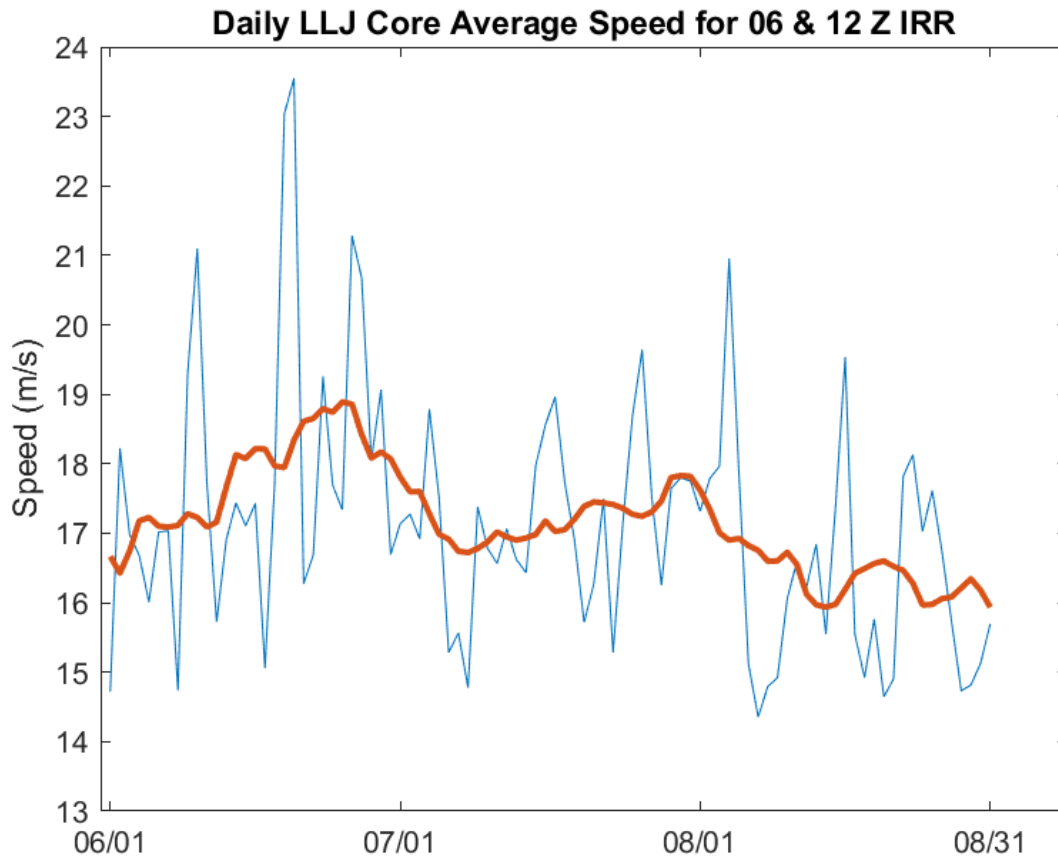


Figure 108. (Blue line) June, July, and August timeseries of daily mean LLJ speed averaged across 06 and 12 UTC for the IRR simulation, and averaged for a box between approximately 100°W – 90°W and 30°N – 43°N. (Red line) 8 day moving average of LLJ height.

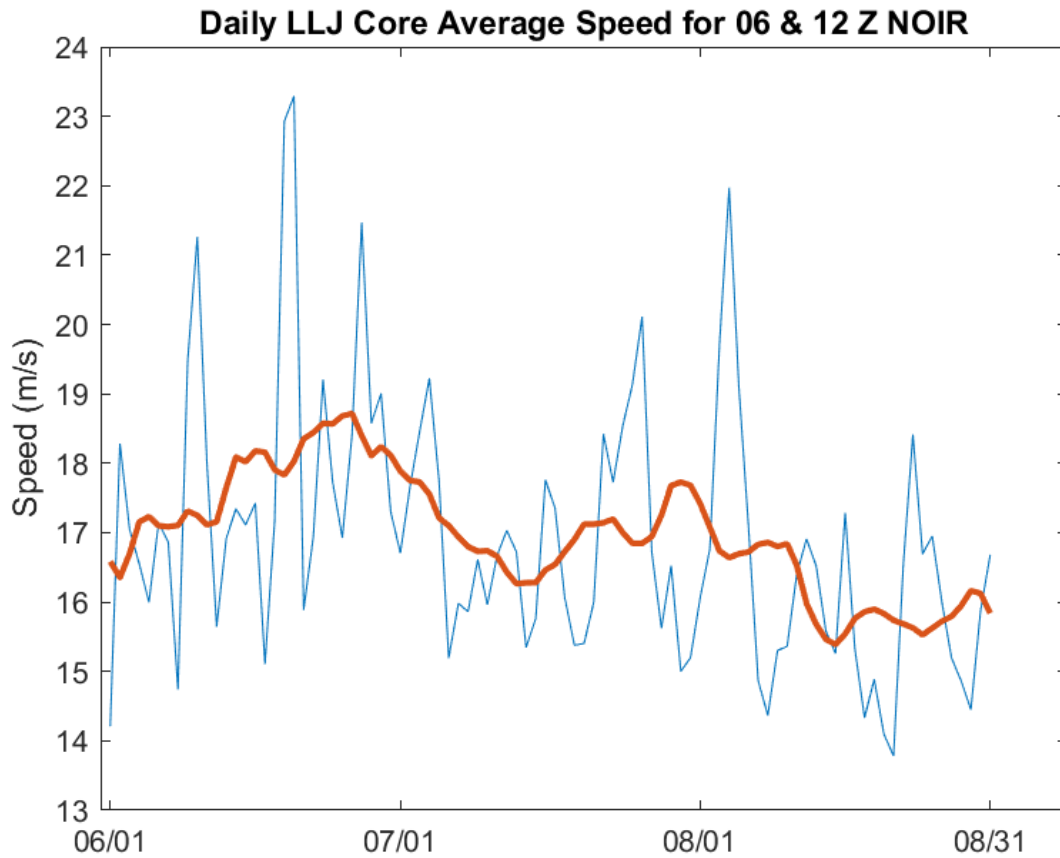


Figure 109. (Blue line) June, July, and August timeseries of daily mean LLJ speed averaged across 06 and 12 UTC for the NOIR simulation, and averaged for a box between approximately  $100^{\circ}\text{W} - 90^{\circ}\text{W}$  and  $30^{\circ}\text{N} - 43^{\circ}\text{N}$ . (Red line) 8 day moving average of LLJ height.

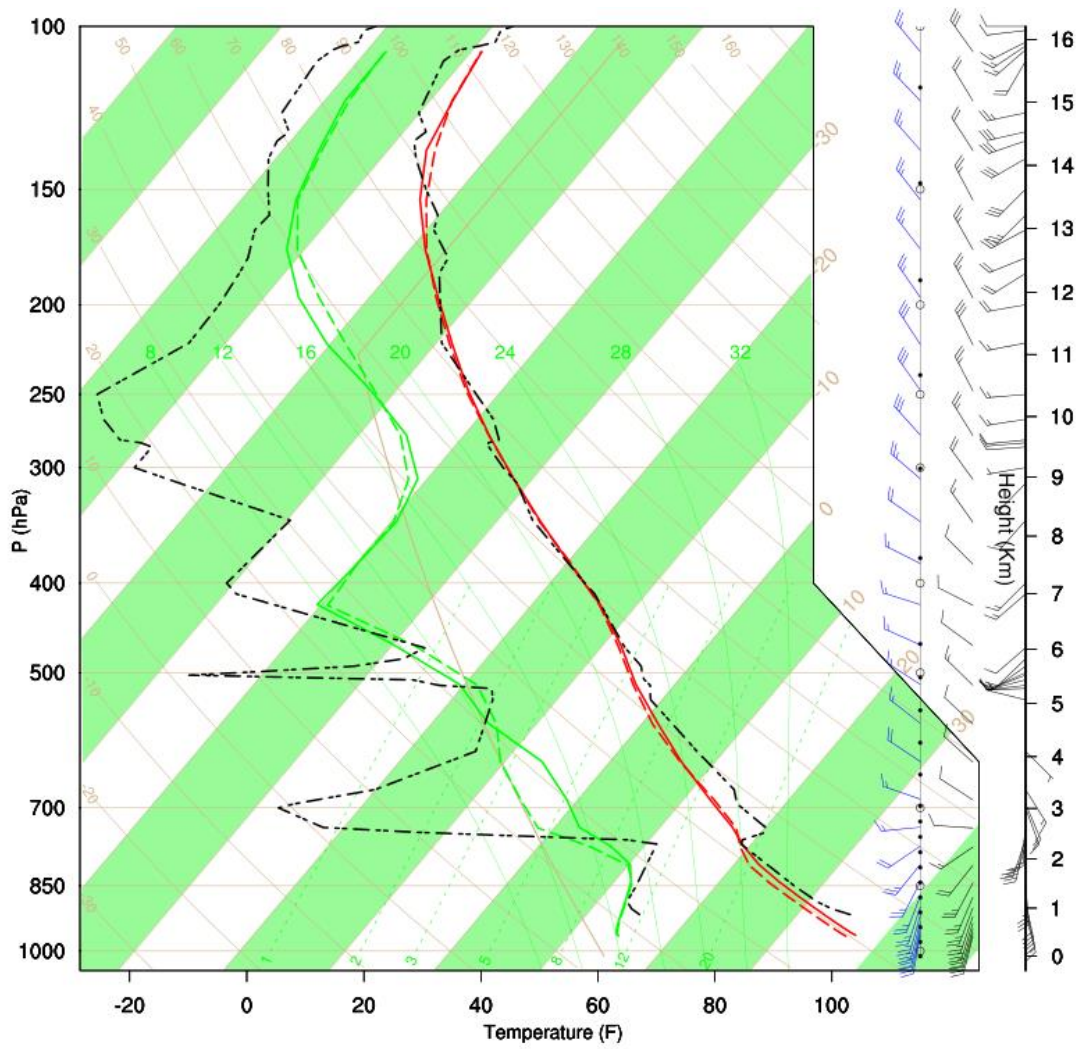


Figure 110. Skew-T Log-P diagram at 00 UTC, 19 June 2012 for Dodge City, KS. Shown are the IRR (red solid line), NOIR (red dashed line), and observed (black dot-dash line) temperature and mixing ratio profiles. The wind profiles from left to right are for the IRR, NOIR and observations.

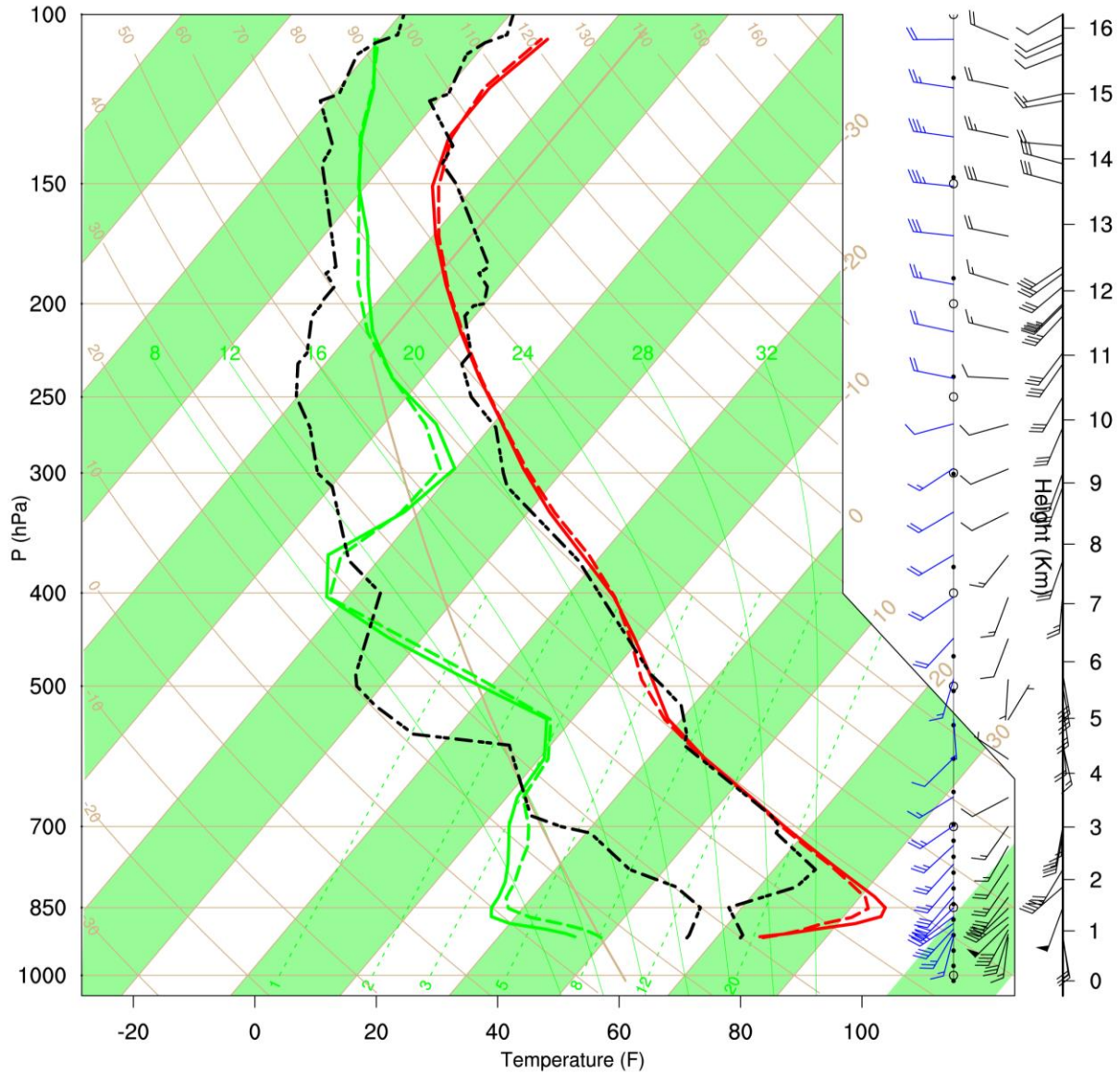


Figure 111. Skew-T Log-P diagram at 12 UTC, 19 June 2012 for Dodge City, KS. Shown are the IRR (red solid line), NOIR (red dashed line), and observed (black dot-dash line) temperature and mixing ratio profiles. The wind profiles from left to right are for the IRR, NOIR and observations.

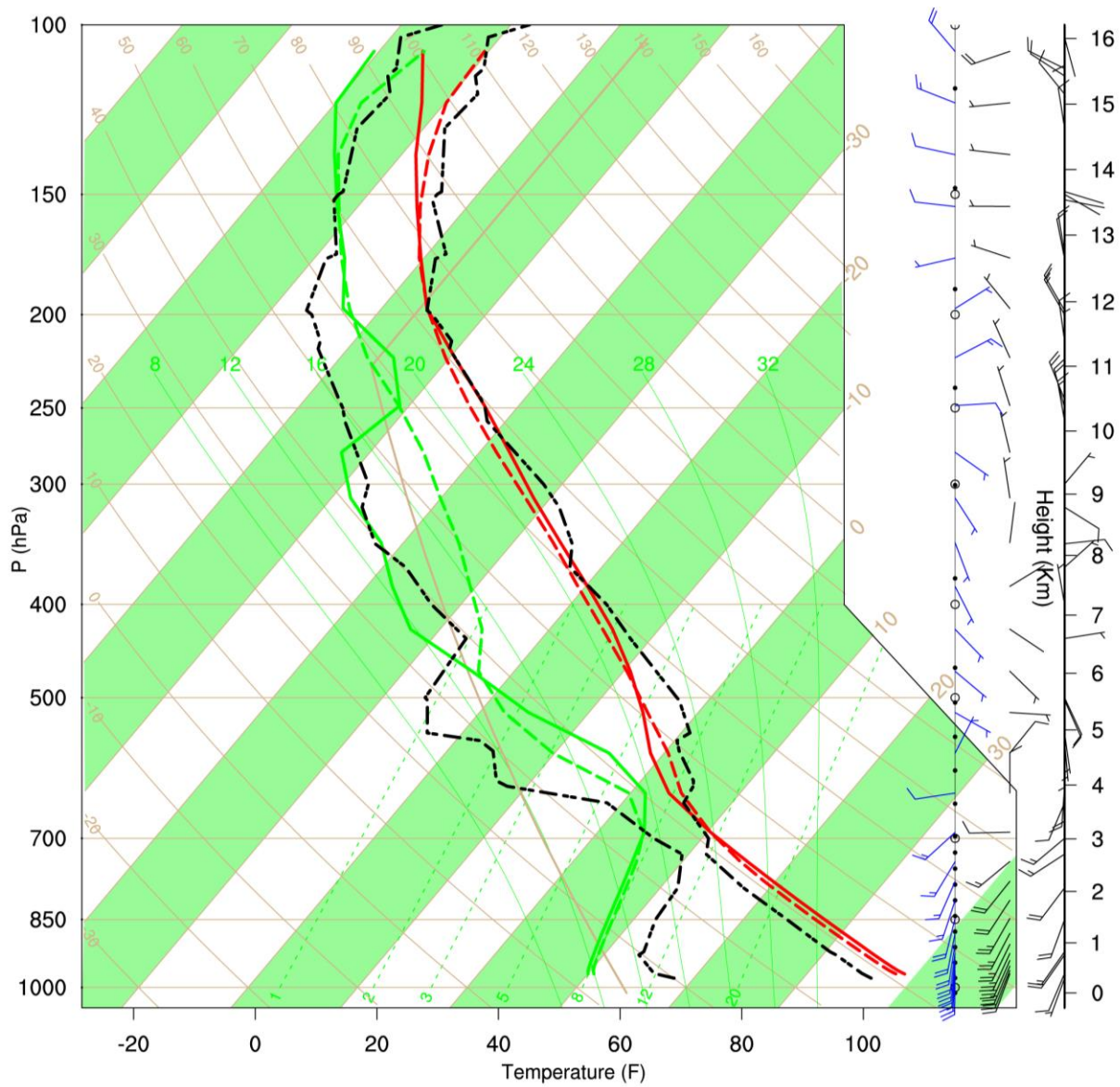


Figure 112. Skew-T Log-P diagram at 00 UTC, 4 July 2012 for Topeka, KS. Shown are the IRR (red solid line), NOIR (red dashed line), and observed (black dot-dash line) temperature and mixing ratio profiles. The wind profiles from left to right are for the IRR, NOIR and observations.

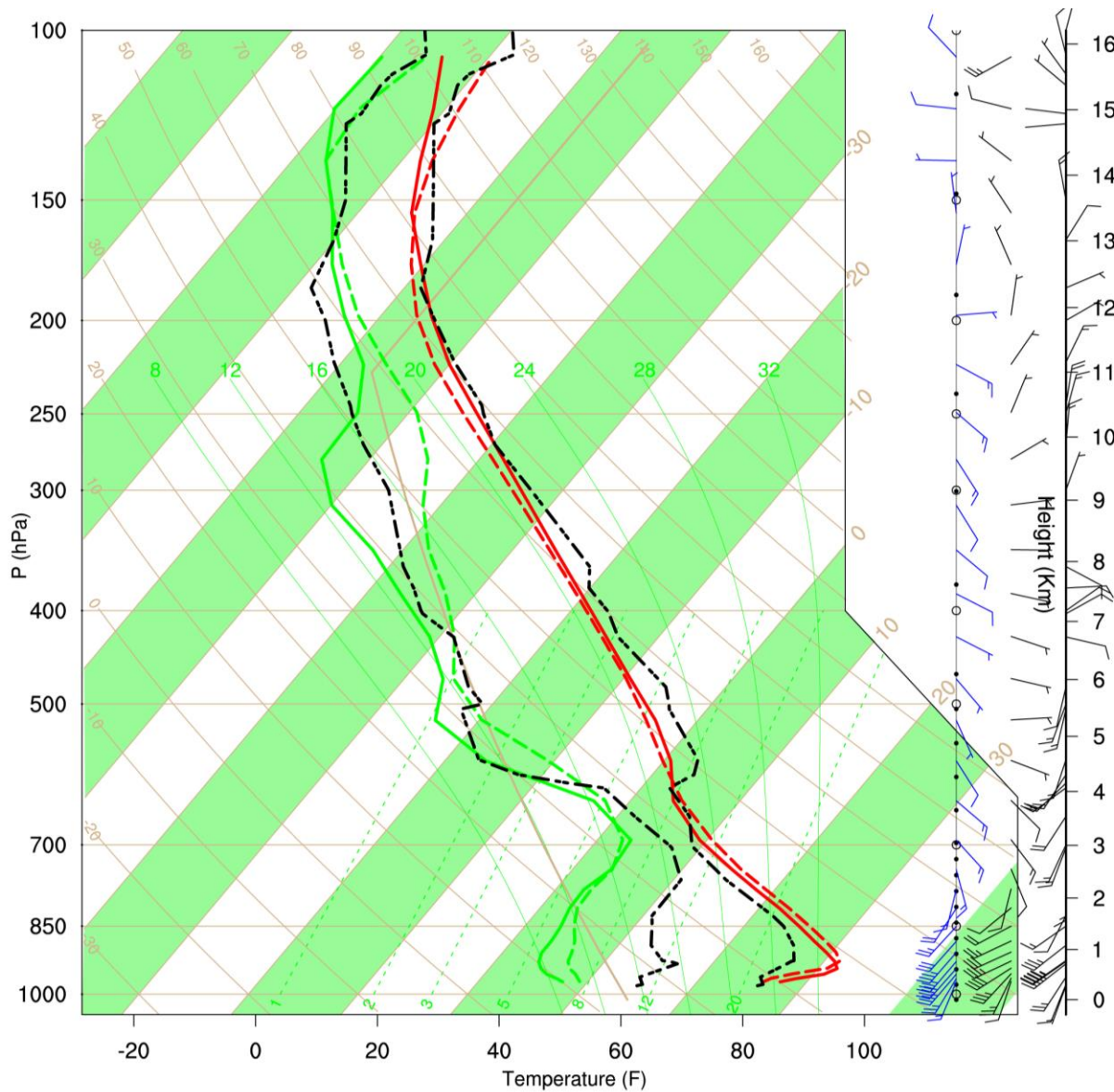


Figure 113. Skew-T Log-P diagram at 12 UTC, 4 July 2012 for Topeka, KS. Shown are the IRR (red solid line), NOIR (red dashed line), and observed (black dot-dash line) temperature and mixing ratio profiles. The wind profiles from left to right are for the IRR, NOIR and observations.

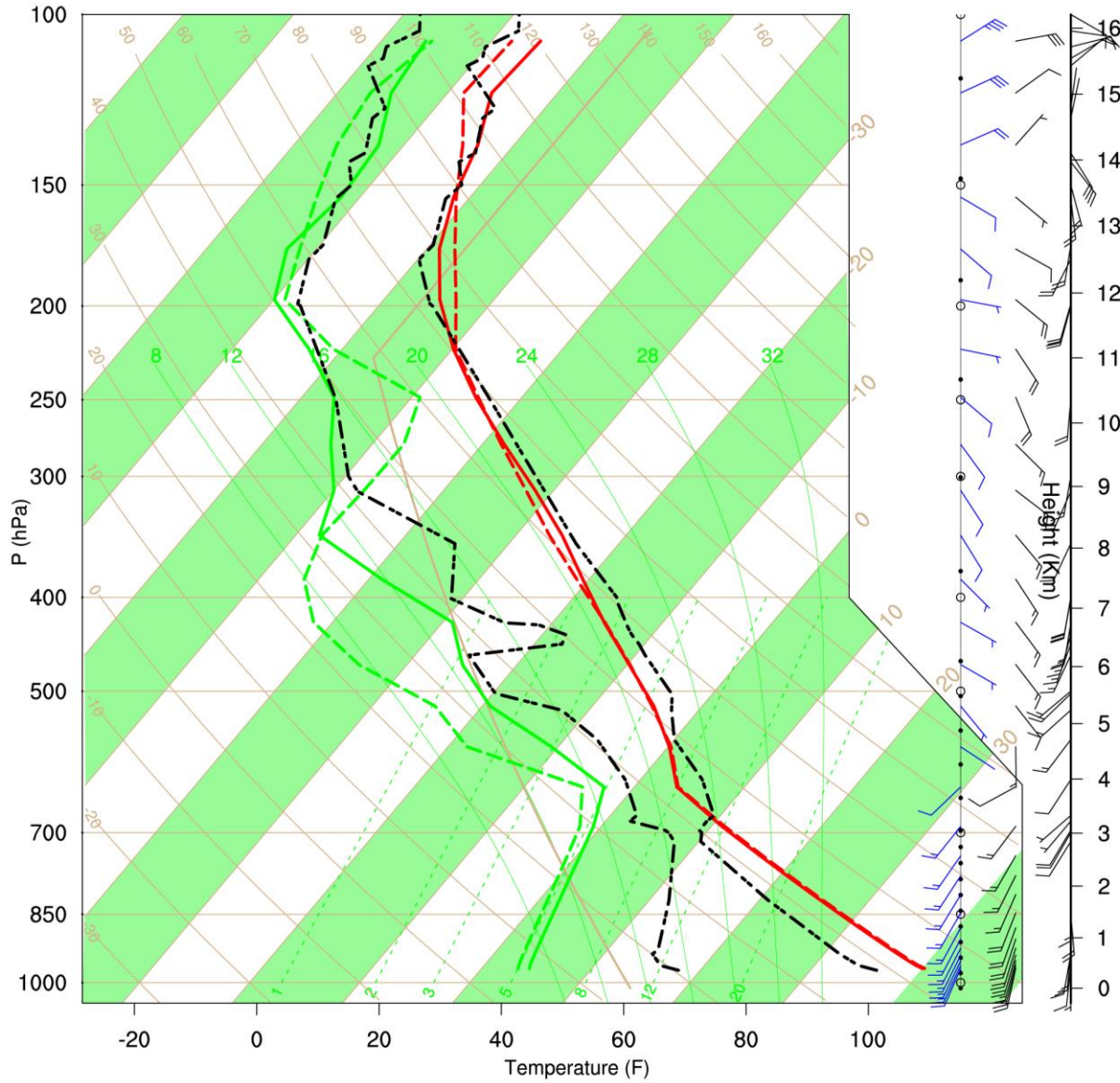


Figure 114. Skew-T Log-P diagram at 00 UTC, 25 July 2012 for Norman, OK. Shown are the IRR (red solid line), NOIR (red dashed line), and observed (black dot-dash line) temperature and mixing ratio profiles. The wind profiles from left to right are for the IRR, NOIR and observations.

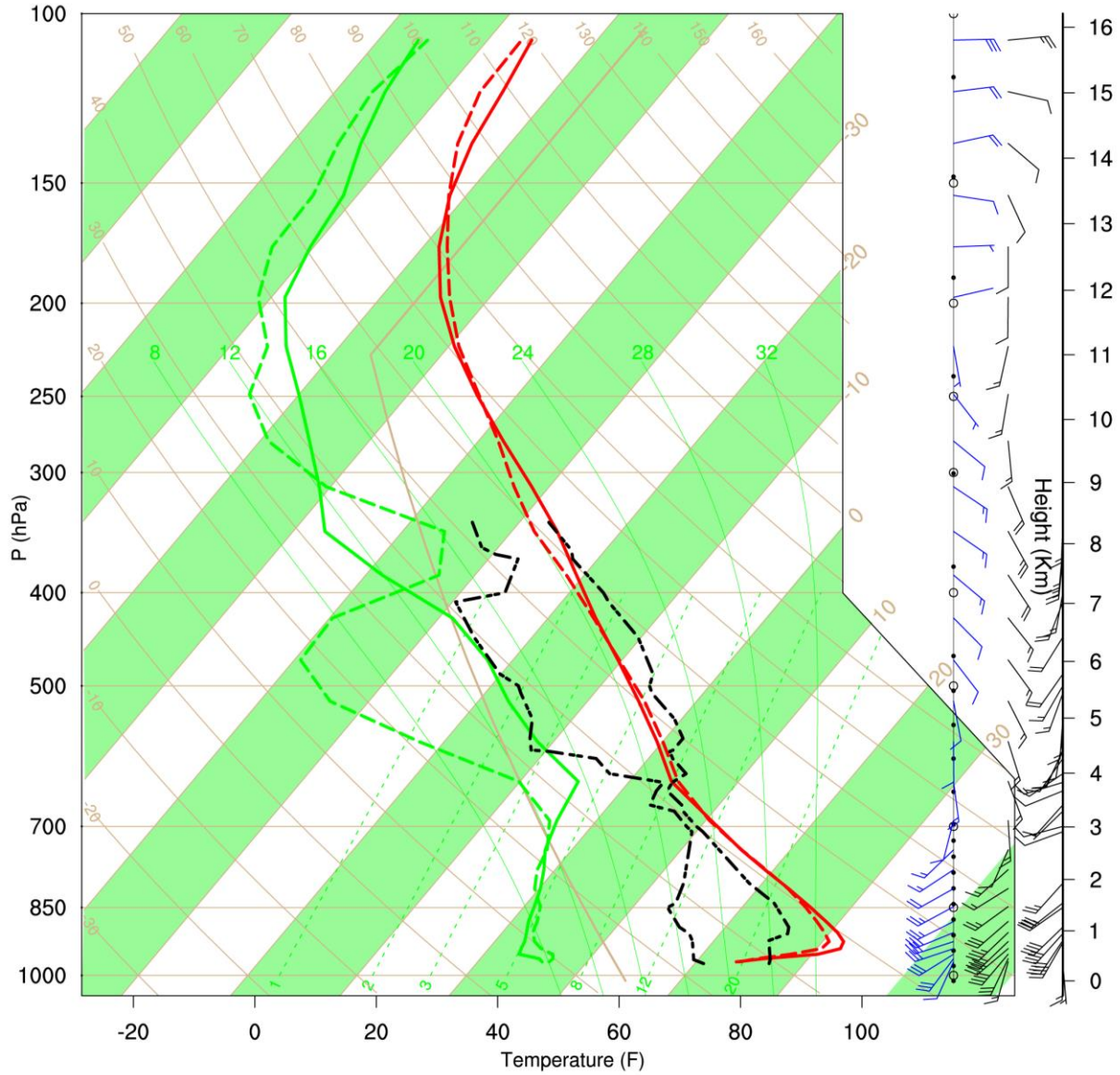


Figure 115. Skew-T Log-P diagram at 12 UTC, 25 July 2012 for Norman, OK. Shown are the IRR (red solid line), NOIR (red dashed line), and observed (black dot-dash line) temperature and mixing ratio profiles. The wind profiles from left to right are for the IRR, NOIR and observations.

## CHAPTER V - DISCUSSION AND CONCLUSION

This research set out to test the hypothesis that a realistic amount of irrigation would provide enough forcing to alter the LLJ across the GP. There have been many studies done on the LLJ, starting with the theory of LLJ formation (e.g., Blackadar 1957; Holton 1967), and then subsequent studies using numerical models and observations to test the theory (e.g., Zhong et al. 1996; Fast and McCorcle 1990; Shapiro et al 2016). A number of LLJ climatologies have been produced (e.g., Bonner 1968; Whiteman et al. 1997; Doubler et al. 2015) documenting the most frequent locations for LLJ formation as well as other notable jet features such as jet core height, velocity, and diurnal phase. This early research has led to the research done by McCorcle (1988) and Huber et al. (2014), both of which examined the role of soil moisture on lower atmosphere circulation. These two studies were conducted as sensitivity tests, and opened the door for the present research.

The results of this study have shown that with the addition of a realistic amount of irrigation there is enough forcing to affect the surface energy budget. By the end of the three-month simulation surface and low-level temperatures increase by around 1 degree Celsius. The temperature changes come alongside geopotential height differences on the order of a few meters. The changes in geopotential height show subtle increases to central high pressure through increased interior ridging. As well as decreased heights and east-coast troughing. These changes to geopotential height correspond to the decreased precipitation over the GP (irrigated region), as well as increased precipitation downwind due in part to a larger scale synoptic feedback as noted in Pei et al. (2016).

The changes noted between the two model simulations (IRR and NOIR) are admittedly small, however, this was expected with the only difference being the addition of irrigation. Also, the magnitude of the differences is on par with other studies (e.g., Huber et al. 2014; Cook et al. 2008). That said, there were still significant differences to both the LLJ core speed and height over and downwind of the most heavily irrigated regions. However, with small changes comes difficulty in attribution, and pinning down exactly what is causing the changes to the LLJ isn't clear. It's possible that the differences in low level geopotential height is enough to impact Holton's (1967) mechanism. If the height gradient across the sloping terrain is large enough the corresponding enhancement to the PGF across the gradient may increase the background geostrophic wind. Also, with increases to surface temperature there may be increases in PBL turbulent kinetic energy (TKE) and increased mixing. The increased mixing may increase the effects of friction within the boundary layer. This would increase the ageostrophic wind vector, thus magnifying Blackadar's (1957) inertial oscillation of the ageostrophic wind vector and increasing the LLJ speed.

The plans for future work all primarily address the current limitations of the above research. Firstly, confidence in all of the results and conclusion drawn from this study could be increased through simulations of additional years. Having only a single three-month summer season means the number of cases are limited, and all distributions are relatively short making significant statistical differences difficult to achieve. This also means interseasonal differences are ignored. The background conditions for 2012 were unusually hot and dry across the GP, and the response due to a realistic amount of irrigation may change with changing background conditions. For this reason, lengthening the simulations by adding additional years would not

only increase the number of events and distribution size, but also cover a wider range of background conditions providing a more robust response.

Some LLJ studies (e.g., Cook et al. 2008; Huber et al 2014) only examine LLJs on a single isobaric level, most commonly 850 hPa. This study instead employs a methodology proposed by Bonner (1968), and has been employed by additional studies (e.g., Walters et al. 2014; Doubler et al. 2015) which uses specified wind speed and shear thresholds. Each method comes with its own pros and cons, however, to achieve a more robust conclusion both methods could be used. This would include both isolated LLJ data and a description of the three-dimensional wind.

This study gives a simplified representation of the diurnal phase of the LLJ by only examining four different times per day at six hourly intervals. This is arguably too coarse to make any conclusions on diurnal shifts between the simulations. To add to this research, up to one hourly output would be useful in providing a more detailed description of the diurnal differences in LLJ development.

The irrigation scheme could also be refined. Currently, the irrigation scheme is calibrated for the GP. However, irrigation is also applied in relatively large amounts in both California's Central Valley and the Lower Mississippi River Valley. If the irrigation scheme were calibrated for other regions, then the effects that propagate downwind may differ in response. Finally, attempting to account for changes to agricultural and irrigation practices through mid-century may provide further insight into anthropogenic climate change. All of these avenues provide the potential for additional insight into the cause and effects of LLJs.

## **BIBLIOGRAPHY**

## BIBLIOGRAPHY

- Adegoke, J. O., R. a. Pielke, J. Eastman, R. Mahmood, and K. G. Hubbard, 2002: Impact of Irrigation on Midsummer Surface Fluxes and Temperature under Dry Synoptic Conditions: A Regional Atmospheric Model Study of the U.S. High Plains. *Mon. Weather Rev.*, **131**, 556–564, doi:10.1175/1520-0493(2003)131<0556:IOIOMS>2.0.CO;2.
- Arritt, R. W., T. D. Rink, M. Segal, D. P. Todey, C. a. Clark, M. J. Mitchell, and K. M. Labas, 1996: The Great Plains Low-Level Jet during the Warm Season of 1993. *Mon. Weather Rev.*, **125**, 2176–2192, doi:10.1175/1520-0493(1997)125<2176:TGPLLJ>2.0.CO;2.
- Barnston, A. G., and P. T. Schickedanz, 1984: The Effect of Irrigation on Warm Season Precipitation in the Southern Great Plains. *J. Clim. Appl. Meteorol.*, **23**, 865–888, doi:10.1175/1520-0450(1984)023<0865:TEOIEW>2.0.CO;2.
- Basara, J. B., and K. C. Crawford, 2002: Linear relationships between root-zone soil moisture and atmospheric processes in the planetary boundary layer. *J. Geophys. Res. Atmos.*, **107**, 1–18, doi:10.1029/2001JD000633.
- Beebe, R. C., 1974: Large scale irrigation and severe storm enhancement. Preprint, Symp. on Atmospheric Diffusion and Air Pollution, Santa Barbara, *Amer. Meteor. Soc.*, 392–395.
- Blackadar, A. K., 1957: Boundary Layer Wind Maxima and Their Significance for the Growth of Nocturnal Inversions. *Bull. Amer. Meteor. Soc.*, **38**, 283–290.
- Bleeker, W., and M. J. Andre, 1951: On diurnal variation of precipitation, particularly over central U.S.A., and its relation to large- scale orographic circulation systems. *Quart. J. Roy. Meteor. Soc.*, **77**, 260–271.
- Bonner, W. D., 1968: Climatology of the Low Level Jet. *Mon. Wea. Rev.*, **96**, 833–850, doi:10.1175/1520-0493(1968)096<0833:COTLLJ>2.0.CO;2.
- Bonner, W. D., and J. Paegle, 1970: Diurnal variations in boundary layer winds over the south-central united states in summer. *Mon. Wea Rev.*, **98**, 735–744, doi:10.1175/1520-0493(1970)098<0735:DVIBLW>2.3.CO;2.
- Buajitti, K., and A. K. Blackadar, 1957: Theoretical studies of diurnal wind-structure variations in the planetary boundary layer. *Quart. J. Roy. Meteor. Soc.*, **83**, 486–500, doi:10.1002/qj.49708335804.
- Chen, T. C., and J. A. Kpaeyeh, 1993: the Synoptic-Scale Environment Associated With the Low-Level Jet of the Great-Plains. *Mon. Wea. Rev.*, **121**, 416–420, doi:10.1175/1520-0493(1993)121<0416:TSSEAW>2.0.CO;2.

- Cook, B. I., S. P. Shukla, M. J. Puma, and L. S. Nazarenko, 2014: Irrigation as an historical climate forcing. *Clim. Dyn.*, **44**, 1715–1730, doi:10.1007/s00382-014-2204-7.
- Cook, K. H., E. K. Vizy, Z. S. Launer, and C. M. Patricola, 2008: Springtime intensification of the Great Plains low-level jet and Midwest precipitation in GCM simulations of the twenty-first century. *J. Climate*, **21**, 6321–6340, doi:10.1175/2008JCLI2355.1.
- Doubler, D. L., J. A. Winkler, X. Bian, C. K. Walters, and S. Zhong (2015), An NARR-derived climatology of southerly and northerly low-level jets over North America and coastal environs, *J. Appl. Meteor. Climatol.*, **54**, 1596–1619.
- Du, Y., and R. Rotunno, 2014: A Simple Analytical Model of the Nocturnal Low-Level Jet over the Great Plains of the United States. *J. Atmos. Sci.*, **71**, 3674–3683, doi:10.1175/JAS-D-14-0060.1.
- Dudhia, J., 1989: Numerical study of convection observed during the winter monsoon experiment using a mesoscale two-dimensional model. *J. Atmos. Sci.*, **46**, 3077–3107.
- Fast, J. D., and M. D. McCorcle, 1990: A Two-Dimensional Numerical Sensitivity Study of the Great Plains Low-Level Jet. *Mon. Wea. Rev.*, **118**, 151–164, doi:10.1175/1520-0493(1990)118<0151:ATDNSS>2.0.CO;2.
- Frisch, A. S., B. W. Orr, and B. E. Martner, 1991: Doppler Radar Observations of the Development of a Boundary-Layer Nocturnal Jet. *Mon. Wea. Rev.*, **120**, 3–16, doi:10.1175/1520-0493(1992)120<0003:DROOTD>2.0.CO;2.
- Frye, J. D., and T. L. Mote, 2010: The synergistic relationship between soil moisture and the low-level jet and its role on the prestorm environment in the southern Great Plains. *J. Appl. Meteor. Climatol.*, **49**, 775–791, doi:10.1175/2009JAMC2146.1.
- Harding, K. J., and P. K. Snyder, 2012a: Modeling the Atmospheric Response to Irrigation in the Great Plains. Part II: The Precipitation of Irrigated Water and Changes in Precipitation Recycling. *J. Hydrometeorol.*, **13**, 1687–1703, doi:10.1175/JHM-D-11-099.1.
- , and ———, 2012b: Modeling the Atmospheric Response to Irrigation in the Great Plains. Part II: The Precipitation of Irrigated Water and Changes in Precipitation Recycling. *J. Hydrometeorol.*, **13**, 1687–1703, doi:10.1175/JHM-D-11-099.1.
- Holton, J. R., 1967: The diurnal boundary layer wind oscillation above sloping terrain. *Tellus*, **19**, 199–205, doi:10.1111/j.2153-3490.1967.tb01473.x.
- Hong, S.-Y., and J.-O. J. Lim, 2006: The WRF single-moment 6-class microphysics scheme (WSM6). *J. Korean Meteor. Soc.*, **42**(2), 129–151.
- , Y. Noh, and J. Dudhia, 2006: A new vertical diffusion package with an explicit treatment of entrainment processes. *Mon. Wea. Rev.*, **134**, 2318–2341.

- Huber, D., D. Mechem, and N. Brunzell, 2014: The Effects of Great Plains Irrigation on the Surface Energy Balance, Regional Circulation, and Precipitation. *Climate*, **2**, 103–128, doi:10.3390/cli2020103.
- Kain, J. S., 2004: The Kain–Fritsch convective parameterization: An update. *J. Appl. Meteor.*, **43**, 170–181.
- , and J. M. Fritsch, 1993: Convective parameterization in mesoscale models: The Kain–Fritsch scheme, in the representation of cumulus convection in numerical models. *Meteorol. Monogr.*, **46**, 165–170.
- Klein, P. M., X. M. Hu, A. Shapiro, and M. Xue, 2015: Linkages Between Boundary-Layer Structure and the Development of Nocturnal Low-Level Jets in Central Oklahoma. *Boundary-Layer Meteorol.*, **158**, 383–408, doi:10.1007/s10546-015-0097-6.
- La Sorte, F. A., and Coauthors, 2014: The role of atmospheric conditions in the seasonal dynamics of North American migration flyways. *Journal of Biogeography*, **41**(9), 1685–1696.
- Lanicci, J. M., T. N. Carlson, and T. T. Warner, 1987: Sensitivity of the Great Plains Severe-Storm Environment to Soil-Moisture Distribution. *Mon. Wea. Rev.*, **115**, 2660–2673, doi:10.1175/1520-0493(1987)115<2660:SOTGPS>2.0.CO;2.
- Liechti, F. 2006: Birds: blowin’ by the wind?. *Journal of Ornithology*, **147**(2), 202–211.
- Mccorcle, M. D., 1988: Simulation of Surface-Moisture Effects on the Great Plains Low-Level Jet. *Mon. Wea. Rev.*, **116**, 1705–1720, doi:10.1175/1520-0493(1988)116<1705:SOSMEO>2.0.CO;2.
- Means, L. L., 1952: On Thunderstorm Forecasting in the Central United States. *Mon. Wea. Rev.*, **80**(10), 165–189.
- Mesinger, F., and Coauthors, 2006: North American Regional Reanalysis. *Bull. Amer. Meteor. Soc.*, **87**, 343–360.
- Mlawer, E. J., S. J. Taubman, P. D. Brown, M. J. Iacono, and S. A. Clough, 1997: Radiative transfer for inhomogeneous atmospheres: RRTM, a validated correlated-k model for the longwave. *J. Geophys. Res. Atmos.*, **102**, 16663–16682.
- Nunalee, C. G., and S., Basu, 2014: Mesoscale modeling of coastal low-level jets: implications for offshore wind resource estimation. *Wind Energy*, **17**(8), 1199–1216.
- Paegle, J., 1970: Studies of diurnally periodic Boundary Layer Winds. Technical Report, NSF Grant, GA-698, Dept. of Meteorology, University of California, Los Angeles.

- Parish, T., A. Rodi, and R. Clark, 1987: A Case Study of the Summertime Great Plains Low Level Jet. *Mon. Wea. Rev.*, **116**, 94–105, doi:10.1175/1520-0493(1988)116<0094:ACSOTS>2.0.CO;2.
- , and L. D. Oolman, 2010: On the Role of Sloping Terrain in the Forcing of the Great Plains Low-Level Jet. *J. Atmos. Sci.*, **67**, 2690–2699, doi:10.1175/2010JAS3368.1.
- Pei, L., Moore, N., Zhong, S., Kendall, A. D., Gao, Z., and Hyndman, D. W. 2016: Effects of Irrigation on Summer Precipitation over the United States. *J. Climate*, **29**, 3541–3558, doi:10.1175/JCLI-D-15-0337.1.
- Pielke, R. A., 2001: Influence of the spatial distribution of vegetation and soils on the prediction of cumulus convective rainfall. *Rev. of Geophys.*, **39**, 151.
- Schickedanz, P. T., 1976: The effect of irrigation on precipitation in the Great Plains. Illinois State Water Survey.
- Shapiro, A., E. Fedorovich, and S. Rahimi, 2016: A unified theory for the Great Plains nocturnal low-level jet. *J. Atmos. Sci. J. Atmos. Sci.*, **73**, 3037–3057, doi:10.1175/JAS-D-15-0307.1.
- Storwam, B., J. Dudhia, S. Basu, A. Swift, and I. Giammanco, 2009: Evaluation of the Weather Research and Forecasting model on forecasting low-level jets: Implication for wind energy. *Wind Energy*, **12**, 81–90.
- Uccellini, L. W., 1980: On the Role of Upper Tropospheric Jet Streaks and Leaside Cyclogenesis in the Development of Low-Level Jets in the Great Plains. *Mon. Wea. Rev.*, **108**, 1689–1696, doi:10.1175/1520-0493(1980)108<1689:OTROUT>2.0.CO;2.
- , and D. R. Johnson, 1979: The coupling of upper and lower tropospheric streaks and implications for the development of severe convective storms. *Mon. Wea. Rev.*, **107**, 682–703.
- Van de Wiel, B. J.H., A. Moene, G. Steeneveld, P. Baas, F. Bosveld, and A. Holtslag, 2010: A conceptual view on inertial oscillations and nocturnal low-level jets. *J. Atmos. Sci.*, **67**, 2679–2689, doi:10.1175/2010JAS3289.1.
- Wagner, A., 1939: Concerning the daily wind in the free atmosphere. *Beitrag Zur Physik der freien Atmosphere*, **25**, 145-170.
- Walters, C. K., J. A. Winkler, S. Husseini, R. Keeling, J. Nikolic, and S. Zhong, 2014: Low-level jets in the North American Regional Reanalysis (NARR): A comparison with rawinsonde observations. *J. Appl. Meteor. Climatol.*, **53**, 2093–2113, doi:10.1175/JAMC-D-13-0364.1.

Whiteman, C. D., X. Bian, and S. Zhong, 1997: Low-Level Jet Climatology from Enhanced Rawinsonde Observations at a Site in the Southern Great Plains. *J. Appl. Meteor.*, **36**, 1363–1376.

Zhong, S., J. D. Fast, and X. Bian, 1996: A Case Study of the Great Plains Low-Level Jet Using Wind Profiler Network Data and a High-Resolution Mesoscale Model. *Mon. Wea. Rev.*, **124**, 785–806, doi:10.1175/1520-0493(1996)124<0785:ACSOTG>2.0.CO;2.

——, and J. C. Doran, 1997: An Evaluation of the Importance of Surface Flux Variability on GCM-Scale Boundary-Layer Characteristics Using Realistic Meteorological and Surface Forcing. *J. Climate*, **11**, 2774–2788.